Induced Pluripotent Stem Cell-derived Brain Endothelial Cells as a Cellular Model to Study *Neisseria meningitidis* Infection

Induziert pluripotente Stammzellen-basierte Hirnendothelzellen als zelluläres Modell zur Untersuchung der Infektion mit *Neisseria meningitidis*

Dissertation

for a doctoral degree at the Graduate School of Life Sciences,

Julius-Maximilians-Universität Würzburg,

Section Infection and Immunity

submitted by

Sara Ferreira Martins Gomes

From Lisbon, Portugal

Würzburg, 2019

Submitted on: ……..……..

Members of the *Promotionskomitee*:

Chairperson: Prof. Dr. Thomas Müller

Primary Supervisor: Prof. Dr. Alexandra Schubert-Unkmeir

Supervisor (Second): Prof. Dr. Roy Gross

Supervisor (Third): Dr. Maria Steinke

Supervisor (Fourth): Dr. rer. nat. Kay Johswich

Date of Public Defence: ……..……

Date of Receipt of Certificates: ……

I dedicate this Dissertation to the memory of
my Mother, Maria Paula Pina Antunes Ferreira (1958-2017), and
my Grandfather, José Nuno Ferreira (1928-2019)

Zusammenfassung

Eine bakterielle Meningitis tritt auf, wenn durch Blut übertragene Bakterien hochspezialisierte Hirnendothelzellen (BEC) durchdringen und Zugang zu den Meningen erhalten. *Neisseria meningitidis* (*Nm)* ist ein human-exklusiver Erreger, für dessen Untersuchung es an geeigneten In-vitro-Modellen mangelt. Bis vor kurzem war die Modellierung von BEC-*Nm*-Wechselwirkungen fast ausschließlich auf immortalisierte humane Zellen beschränkt, denen wichtige BEC-Phänotypen fehlen. Besonders hervorzuheben sind das Fehlen physiologischer Barriereeigenschaften durch unkontinuierliche dichte Zell-Zell-Verbindungen. Als alternative Modellorganismen können humanisierte Mäuse verwendet werden, die sich jedoch auf bekannte Wirt-Erreger-Wechselwirkungen stützen und durch Speziesunterschiede eine eingeschränkte Übersetzbarkeit aufweisen. Dies begründet die Notwendigkeit, neuartige humane In-vitro-BEC-Modelle zu etablieren, die physiologische Barrierephänotypen aufweisen, um *Nm*-BEC-Wechselwirkungen zu untersuchen. Kürzlich wurde ein humanes Modell entwickelt, welches auf aus induziert pluripotenten Stammzellen (iPSCs) abgeleiteten humanen BECs basiert und sich durch einen physiologischen Blut-Hirn-Schranken-Phänotyp auszeichnet.

Die iPSC-BECs wurden in dieser Arbeit als neuartiges zelluläres Modell getestet, um *Nm*-Wirt-Pathogen-Wechselwirkungen zu untersuchen, wobei der Schwerpunkt auf Wirtsreaktionen auf *Nm*-Infektionen lag. Zwei Wildtypstämme und drei Mutantenstämme von *Nm* wurden verwendet, um zu bestätigen, dass diese ähnlichen Phänotypen wie in zuvor beschriebenen Modellen folgten. Hervorzuheben ist, dass die Rekrutierung des kürzlich veröffentlichten Pilus-Adhäsin-Rezeptors CD147 unter Meningokokken-Mikrokolonien in iPSC-BECs verifiziert werden konnte. Es wurde auch beobachtet, dass *Nm* die Expression der entzündungsfördernden und neutrophilen spezifischen Chemokine *IL6, CXCL1, CXCL2, CXCL8* und *CCL20* zu bestimmten Zeitpunkten der Infektion sowie die Sekretion von IFN-γ und RANTES durch iPSC-BECs signifikant erhöht. Es wurde zudem beobachtet, dass *Nm* die Tight Junction-Proteine ZO-1, Occludin und Claudin-5 zu späten Zeitpunkten der Infektion zerstört, verursacht durch die Infektion wurde ein ausgefranster und/oder diskontinuierlicher Tight Junction-Phänotyp beobachtet. Dieser Zerstörung geht die SNAI1-Aktivierung (ein Transkriptionsrepressor für Tight Junction-Proteine) voraus und könnte von ihr abhängig sein. In Übereinstimmung mit dem Verlust der Tight Junctions wurde zu späten Infektionszeitpunkten ein starker Verlust des transendothelialen elektrischen Widerstands und eine

Zunahme der Natriumfluoreszein-Permeabilität beobachtet. Bemerkenswerterweise korrelierte die bakterielle Transmigration mit dem Verlust der Tight Junctions, was darauf hinweist, dass der parazelluläre Weg zur bakteriellen Überwindung von BECs eine entscheidende Rolle spielt. Schließlich wurde die RNA-Sequencing (RNA-Seq) von sortierten, infizierten iPSC-BECs durch die Verwendung von fluoreszenzaktivierten Zellsortiertechniken (FACS) nach der Infektion durchgeführt. Dies ermöglichte erstmalig den Nachweis von Expressionsdaten von *Nm*-responsiven Wirtsgenen, welche bei der Meningitidis eine Rolle zu spielen scheinen.

Zusammenfassend konnte im Rahmen der vorliegenden Arbeit der Nutzen von iPSC-BECs *In-Vitro*-Modellen zur Untersuchung von *Nm*-Infektionen gezeigt werden. Dies ist das erste BEC-*In-vitro*-Modell, das alle wichtigen BEC-Tight Junctions exprimiert und ein hohes Barrierepotential aufweist. Insgesamt liefert das eingesetzte Modell neue Einblicke in die *Nm*-Pathogenese, einschließlich der Beeinflussung der Barriereeigenschaften und der Tight Junction-Komplexe durch *Nm*, und gibt erste Hinweise darauf, dass die parazelluläre Route zum *Nm*-Übertritt von BEC-Barrieren eine entscheidende Rolle spielt.

Abstract

Bacterial meningitis occurs when blood-borne bacteria are able to penetrate highly specialized brain endothelial cells (BECs) and gain access to the meninges. *Neisseria meningitidis* (*Nm*) is a human-exclusive pathogen for which suitable *in vitro* models are severely lacking. Until recently, modeling BEC-*Nm* interactions has been almost exclusively limited to immortalized human cells that lack proper BEC phenotypes. Specifically, these *in vitro* models lack barrier properties, and continuous tight junctions. Alternatively, humanized mice have been used, but these must rely on known interactions and have limited translatability. This motivates the need to establish novel human-based *in vitro* BEC models that have barrier phenotypes to research *Nm*-BEC interactions. Recently, a human induced pluripotent stem cell (iPSC) model of BECs has been developed that possesses superior BEC phenotypes and closely mimics the *in vivo* blood vessels present at the blood-meningeal barrier.

Here, iPSC-BECs were tested as a novel cellular model to study *Nm*-host pathogen interactions, with focus on host responses to *Nm* infection. Two wild type strains and three mutant strains of *Nm* were used to confirm that these followed similar phenotypes to previously described models. Importantly, the recruitment of the recently published pilus adhesin receptor CD147 underneath meningococcal microcolonies could be verified in iPSC-BECs. *Nm* was also observed to significantly increase the expression of pro-inflammatory and neutrophil-specific chemokines *IL6*, *CXCL1*, *CXCL2*, *CXCL8*, and *CCL20*, at distinct time points of infection, and the secretion of IFN-γ and RANTES by iPSC-BECs. *Nm* was directly observed to disrupt tight junction proteins ZO-1, Occludin, and Claudin-5 at late time points of infection, which became frayed and/or discontinuous upon infection. This destruction is preceded by, and might be dependent on, *SNAI1* activation (a transcriptional repressor of tight junction proteins). In accordance with tight junction loss, a sharp loss in trans-endothelial electrical resistance, and an increase in sodium fluorescein permeability was observed at late infection time points. Notably, bacterial transmigration correlated with junctional disruption, indicating that the paracellular route contributes for bacterial crossing of BECs. Finally, RNA-Sequencing (RNA-Seq) of sorted, infected iPSC-BECs was established through the use of fluorescence-activated cell sorting (FACS) techniques following infection. This allowed the detection of expression data of *Nm*-responsive host genes not previously described thus far to play a role during meningitidis.

In conclusion, here the utility of iPSC-BECs *in vitro* to study *Nm* infection could be demonstrated. This is the first BEC *in vitro* model to express all major BEC tight junctions and to display high barrier potential. Altogether, here this model provides novel insights into *Nm* pathogenesis, including an impact of *Nm* on barrier properties and tight junction complexes and suggests that the paracellular route contributes to *Nm* traversal of BECs.

Table of Contents

List of Figures

List of Tables

Abbreviation Index

ADAM	A Disintegrin And Metalloproteinase
ADM	Adrenomedullin
AJ	Adherent Junction
β2AR	β2-adrenergic receptor
BBB	Blood-Brain Barrier
b-CSF	Blood-Cerebrospinal Fluid
BEC	Blood Endothelial Cell
bFGF	Basic Fibroblast Growth Factor
BSA	Bovine Serum Albumin
PE	Phycoerythrin
CC	Clonal Complex
CD	Cluster of Differentiation
CD147	Basigin or Extracellular Matrix Metalloproteinase Inducer
CD31	Platelet Endothelial Cell Adhesion Molecule (PECAM-1)
CDH5	Cadherin 5 (VE-Cadherin)
cDNA	Complementary DNA
CEACAM	Carcinoembryonic Antigen-related Cell Adhesion Molecule
CFH	Complement Factor H
CLDN	Claudin
CNS	Central Nervous System
CO_2	Carbon Dioxide
COX IV	Cytochrome c Oxidase Subunit IV
CSF	Cerebrospinal Fluid
DAPI	4′,6-diamidino-2-phenylindole
DMEM	Dulbecco's Modified Eagle's Medium
DMEM/F-12	Dulbecco's Modified Eagle Medium/nutrient mixture F-12
DNA	Deoxyribonucleic Acid
dNTP	Nucleoside Triphosphate
EC	Endothelial Cell

ECM	Extracellular Matrix
EDTA	Ethylenediaminetetraacetic Acid
ESC	Embryonic Stem Cell
EtOH	Ethanol
FACS	Fluorescence-Activated Cell Sorting
FCS	Fetal Calf Serum
fHBP	Factor H-binding Protein
GAPDH	Glyceraldehyde 3-Phosphate Dehydrogenase
GFP	Green Fluorescent Protein
Glut1	Glucose Transporter 1
GM-CSF	Granulocyte-Macrophage Colony-Stimulating Factor
GO	Gene Ontology
GRO	Growth-Regulated Oncogene
HBMEC	Human Brain Microvascular Endothelial Cell
HIV	Human Immunodeficiency Virus
HRP	Horseradish Peroxidase
HS	Human Serum
HSPG	Heparan Sulfate Proteoglycans
ICAM-1	Intercellular Adhesion Molecule 1
IgG	Immunoglobulin G
IL	Interleukin
iPSC	Induced Pluripotent Stem Cells
iPSC-BEC	Induced Pluripotent Stem Cell-derived Brain Endothelial Cell
JAM	Junctional Adhesion Molecule
KO	Kock Out
LOS	Lipo-oligosaccharide
LPS	Lipopolysaccharide
MCP-1	Monocyte Chemoattractant Protein 1
MEM NEAA	Minimum Essential Medium Non-Essential Amino Acids
MG	Matrigel
$MgCl_2$	Magnesium Chloride

MLST	Multilocus Sequence Typing
MMP	Matrix Metalloproteinase
MOI	Multiplicity of Infection
mRNA	Messenger RNA
MRP	Multidrug Resistance Protein
NaCl	Sodium Chloride
$NaHCO_3$	Sodium Bicarbonate
Na-Fluorescein	Sodium Fluorescein
Nm	*Neisseria meningitidis*
OCLN	Occludin
Opa	Colony Opacity-Associated Proteins
PBS	Phosphate-Buffered Saline
PCR	Polymerase Chain Reaction
PDS	Platelet-Poor Plasma Derived Serum
PFA	Paraformaldehyde
P-gp	P-glycoprotein
qRT-PCR	Quantitative Realtime-PCR
RA	Retinoic Acid
RANTES	Regulated on Activation, Normal T Cell Expressed and Secreted
RNA	Ribonucleic Acid
rRNA	Ribosomal RNA
RT	Room Temperature
SAS	Subarachnoid Space
SDS	Sodium Dodecyl Sulfate
Sg	Serogroup
SNAI1	Snail Family Transcriptional Repressor 1
St	Sequence Type
TEER	Trans-endothelial Electrical Resistance
Tfp	Type IV pili
TLR	Toll-like Receptor
TNF-α	Tumor Necrosis Factor-alpha

TNFAIP2	TNF Alpha Induced Protein 2
tRNA	Transfer RNA
UM	Unconditioned Medium
VE-Cadherin	Vascular Endothelial Cadherin
VEGFA	Vascular Endothelial Growth Factor A
vWF	von-Willebrand Factor
ZO	*Zonula Occludens*

1. Introduction

1.1. Meningococcal Infection

Bacterial meningitis is a leading cause of central nervous system (CNS) infections, caused by only a handful of pathogens: *Escherichia coli K1* and *Streptococcus agalactiae* (Group B *Streptococcus*), in the newborn, and *Neisseria meningitidis (Nm), Haemophilus influenzae* type b and *Streptococcus pneumoniae* in children and adults (Huang et al., 2000; Pong and Bradley, 1999; van de Beek et al., 2006). *Nm* or meningococcus is a Gram-negative, aerobic diplococci and human-exclusive pathogen that asymptomatically colonizes the upper respiratory tract of 10–40 % of the world population (Caugant & Maiden, 2009; Rouphael & Stephens, 2012). In susceptible individuals, *Nm* infection is a leading cause of purpura fulminans and meningitis. Purpura fulminans is a frequent complication of *Nm* invasive infection associated with a high mortality rate, and characterized by thrombosis of dermal microvessels that rapidly develops to hemorrhagic skin necrosis (Lécuyer et al., 2017). Meningitis is a disease that is still associated to high mortality despite current administration of modern antibiotic treatments (Rouphael and Stephens, 2012). Reports of illness resembling meningococcal disease date back to the 16th century, though the first time that the disease was identified dates to 1805 (Rosenstein et al., 2001). The disease was reported by Vieusseux when an outbreak swept through Geneva (Vieusseux, 1805). The causative agent, the meningococcus, was first isolated and identified in 1887 (Weichselbaum, 1887).

Currently, meningococci strains are classified into serogroups (Sg) according to the immunologic reactivity of their capsule (Gotschlich et al., 1969). Sg A, B, C, Y, and W, are closely related to meningococcal invasive diseases, although 13 meningococcal Sg have been identified (Hill et al., 2010; Read, 2014). Vaccines against Sg A, C, Y, and W meningococci targeting the capsule's polysaccharides have been developed (Pace and Pollard, 2007), while the recently developed vaccine 4CMenB was reverse engineered using whole-genome sequencing strategies, allowing the identification of new protein antigens able to induce bactericidal antibodies (Serruto et al., 2012a). Further classification of *Nm* is based on: a) major outer membrane porins into serotypes and serosubtypes, b) lipopolysaccharide (LPS, also referred to as lipo-oligosaccharide (LOS) in meningococci) into immunotypes, and c) multi-locus sequence typing (MLST) classifies strains into sequence types (STs) (Hill et al., 2010).

An important step in the pathogenesis of *Nm* is the ability to cross two cellular barriers, one in the nasopharynx and one in the brain. Here, focus will be placed into the brain barrier that this pathogen must cross in order to invade the meninges.

1.1.1. Barriers of the Central Nervous System

The human adult brain is endowed with five main interfaces acting as barriers between the parenchyma CNS and surrounding fluids: (a) the arachnoid barrier, containing the meningeal blood-cerebrospinal fluid (b-CSF) barrier, (b) the blood–brain barrier (BBB), (c) the choroid plexus b-CSF barrier, (d) the circumventricular organs barrier, and (e) Ependyma in the adult brain (Saunders et al., 2016; Weller et al., 2018). Additionally, during embryonic development, a sixth interface is present: (f) the interface between the CSF and the embryonic brain, existing only in the fetus (**Figure 1**) (Møllgård et al., 2017; Saunders et al., 2016).

The BBB is by far the most studied brain barrier, localized at the level of brain endothelial cells (BECs) within the microvessels that irrigate the CNS. The work of Friedrich in 1875 provided first evidence of the existence of this barrier. Upon injecting tracer dyes into the bloodstream of rodents, he observed that these dyes stained all organs except the brain and spinal cord (Ehrlich, 1885). The work of Goldmann corroborated the existence a barrier separating the brain from the circulation. By applying trypan blue into the CSF, he observed staining of the brain but not of the blood circulation and structures on the periphery of the brain (Goldmann, 1913). However, the term "BBB", often miscited, was only coined in 1921 by Lena Stern ("*barrière hémato-encéphalique*") (Saunders et al., 2016; Stern and Gautier, 1921). Only with the development of electron microscopy techniques was it possible to localize the BBB at the level of BECs and identify tight junctions as the structures responsible for preventing brain permeability to exogenous substances (Reese and Karnovsky, 1967).

The BBB surface area is estimated at roughly 20 m^2 with a total length of around 600,000 m (Pardridge, 2002). The main barrier function of the BBB is attributed to the microvascular BECs of brain capillaries, which differ in their properties from blood vessel ECs from the peripheral circulation (see Section 1.1.2.). These highly specialized ECs depend on adjacent cellular and acellular layers, which are prerequisites for proper maintenance of barrier function. The so-called

neurovascular unit (NVU) consists of acellular extracellular matrix (ECM) components such as basal membrane, BECs, and the cellular network that supports them: pericytes, astrocytes, microglia, and neurons (Weiss et al., 2009).

The meningeal b-CSF barrier, detailed in Section 1.1.1.1. , contains BECs similar to those of the BBB (Allt and Lawrenson, 1997). The remaining barriers present in the brain lack BBB-like endothelia and are irrigated with fenestrated capillaries, allowing free diffusion of proteins and solutes with the blood circulation (Saunders et al., 2016). The choroid plexus, localized in the ventricles of the brain, is composed by a single layer of sealed cuboidal epithelial cells responsible for producing CSF, which enclose a network of permeable capillaries (Engelhardt and Sorokin, 2009). The circumventricular organs are structures located in the midline of the ventricular system composed by specialized ependymal cells called tanycytes (depicted as TC, **Figure 1**), connected by tight junctions between their apices (Krisch et al., 1978). Non-specialized ependymal cells, in contrast, form a physical barrier separating the interstitial space of the brain from the CSF, but are linked by gap junctions that do not restrict exchange of large molecules (Møllgård et al., 1987).

1.1.1.1. Meningeal Blood-Cerebrospinal Fluid Barrier

The site for bacterial crossing into the CSF has been under debate over the last decades, with earlier publications often referring to the BBB as the barrier limiting access of *Nm* to the CSF (Pron et al., 1997; Taha et al., 1998), which is anatomically incorrect (see **Figure 1**). Post-mortem studies of a meningococcal meningitis patient revealed bacteria closely attached to the apical surface of the ECs in the choroid plexus capillaries and in the meningeal vessels (Pron et al., 1997). However, no colonies could be detected adhering or invading choroidal epithelial cells. *In vivo* studies have further confirmed meningococcal tropism for microvascular ECs, where adhesion was restricted to capillaries located in low blood flow regions (Mairey et al., 2006). Thus, it has been hypothesized that meningococci probably do not traverse the b-CSF barrier located at the choroid plexus, but at the level of the meninges – particularly, the vessels that irrigate the subarachnoid space (SAS) (**Figure 2**) (Weller et al., 2018).

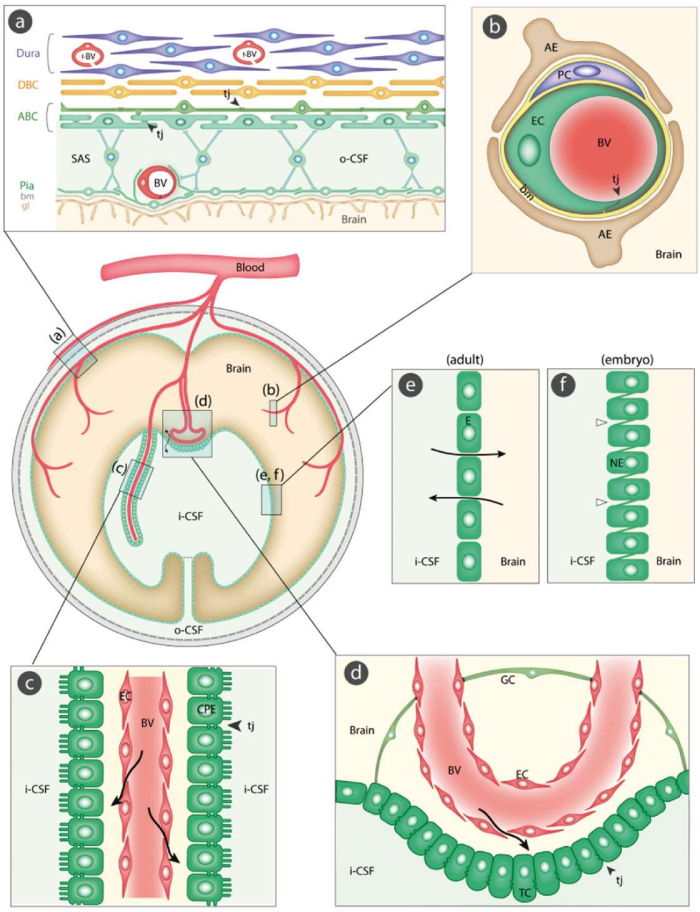

Figure 1. Schematic diagram of the barriers and interfaces of the brain.

Barrier systems in the adult brain (a-e) and an additional one found in the fetus (f). Barrier-forming cellular layers are colored in green. (A) The meningeal barrier, containing barrier-forming cells in (1) the outer layer of the arachnoid membrane (arachnoid barrier cells [ABC]) and (2) the blood vessels (BV) of the subarachnoid space (SAS), which contain tight junctions (tj, arrowheads). By contrast, blood vessels within the dura mater are fenestrated (f-BV). Outer cerebrospinal fluid (o-CSF); dural border cells (DBC); bm = basement membrane; gl = glia limitans. (B) The endothelial cells (ECs) of the BBB form a barrier between cerebral capillaries and the brain parenchyma, forming the NVU with the support of astrocyte end-feet (AE) and pericytes (PC). The CSF-brain barriers form a third group of interfaces. These include (C) the choroid plexus epithelial cells (CPE) that maintain a barrier between the internal CSF (i-CSF) and blood vessels, (D) the circumventricular organs barrier formed by sealed tanycytes (TC) and astroglial cells (GC), and (E) Ependymal barrier in adults, formed by non-specialized fenestrated ependymal cells. Lastly, the embryonic CSF-brain barrier formed by strap junctions (open arrowheads) present between adjacent neuroepithelial cells (NE). Adapted from (Saunders et al., 2016).

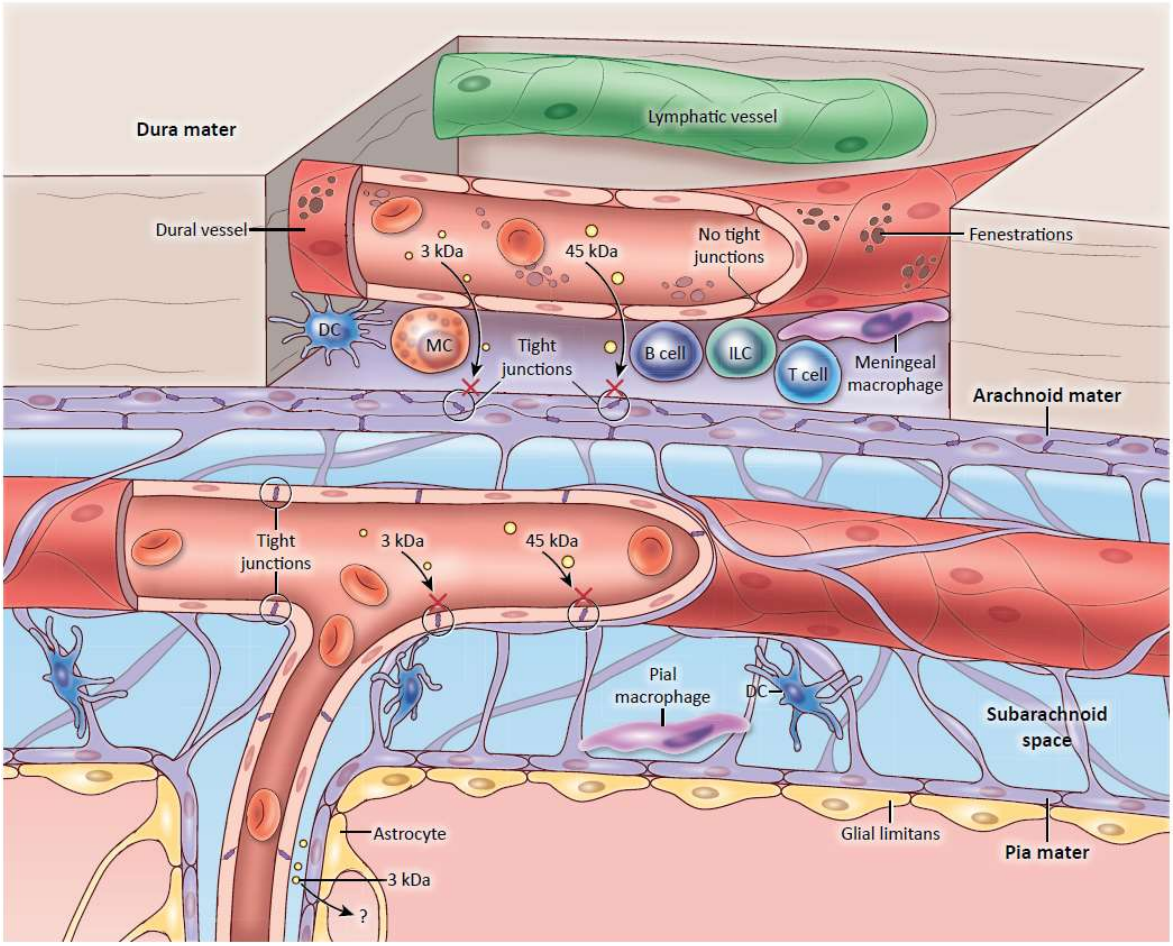

Figure 2. Schematic illustration of the structural composition of the meninges.

The meninges are divided into three layers: dura, arachnoid and pia mater. The dura mater is the layer most adjacent to the skull and is rigid, highly innervated, and irrigated by lymphatic vessels and fenestrated blood vessels. Immune cells residing in the dura layer include dendritic cells (DC), mast cells (MC), innate lymphoid cells (ILCs), meningeal macrophages, T cells, and B cells. The arachnoid is the first impermeable barrier to the CNS parenchyma, followed by the pial vessels that also contain tight junctions. The pia mater and glia limitans are the last physical barrier before the parenchyma. Pial vessels are surrounded by leptomeningeal cells lying in the SAS, filled with CSF. Some immune cells also reside in the pia, namely macrophages and DCs. Diffusion of small molecules (3 kDa) is restricted to the superficial layers of the parenchyma. Adapted from (Rua and McGavern, 2018).

The meninges are membranes that cover and protect the brain and spinal cord, that are anatomically divided into three layers: dura mater (adjacent to the skull), arachnoid mater, and pia mater (above the brain and spinal cord parenchyma) (**Figure 2**) (Rua and McGavern, 2018). The dura mater is composed by a dense collagenous membrane that contains lymphatic as well as fenestrated blood

vessels (Absinta et al., 2017; Protasoni et al., 2011). These blood vessels allow the passage of relatively large molecules (e.g. 43–45 kDa) injected into the blood (Balin et al., 1986; Rua and McGavern, 2018). For this reason, the first impermeable barrier in the meninges consists of arachnoid cells on the outer layer membrane of the arachnoid, forming a physical barrier between the CSF and the dura mater (Saunders et al., 2016).

The arachnoid and pial membranes are structurally continuous and together form the leptomeninges, between which circulates the CSF. In the SAS, pial vessels form a barrier to the free passage of pathogens and blood-derived materials into the CSF, due to the presence of tight junctions with similar characteristics as BBB endothelia, although lacking the surrounding pericytes and astrocytic end-feet (Cassella et al., 1997; Nabeshima et al., 1975; Rua and McGavern, 2018; Saunders et al., 2016; Weller et al., 2018). However, pial vessels are separated from the CSF by a layer of leptomeningeal cells, which have been identified as meningeal fibroblasts and meningeal macrophages by light and electron microscopy (Mercier et al., 2002). Underlying these leptomeningeal cells are astrocytes and astrocytic end-feet, which form the final meningeal barrier before the brain parenchyma, referred to as the glia limitans. Pial vessels branch into smaller arteries that eventually penetrate into the brain tissue, becoming progressively smaller and enclosed by astrocytic end-feet, giving rise to BBB capillaries (Iadecola, 2004).

1.1.2. Properties of Brain Endothelial Cells

BECs lining the BBB and pial vessels are highly specialized cells that maintain cerebral homeostasis and protect the brain from toxic compounds and pathogens (van Sorge and Doran, 2012; Weller et al., 2018). BECs accomplish this through their selectively permeable and barrier-forming phenotype that arises from the presence of complex tight junctions, efflux transporters and highly regulated receptor-mediated transcytosis (Engelhardt and Sorokin, 2009). Additionally, BECs are extremely thin cells (0.3 to 0.5 μm) (Fagerholm, 2007) that differ from peripheral ECs through their increased mitochondrial content (Oldendorf et al., 1977), lack of fenestration (Fenstermacher et al., 1988) and minimal pinocytotic activity (Sedlakova et al., 1999). These characteristics make BECs not only a physical barrier to the diffusion of substances across the BBB, but also contribute to their function as transport and metabolic barriers.

As a physical barrier, free passage of substances into the parenchyma is prevented by the presence of complex cell-cell junctions, referred to as tight junctions, between adjacent BECs. These junctions are responsible for the low paracellular permeability and high trans-endothelial electrical resistance (TEER) of brain microvessels (Butt et al., 1990; Crone and Olesen, 1982). Tight junctions are elaborate transmembrane protein structures that seal the intercellular space between ECs, but are also present between epithelial cells. By functioning as a zipper-like complex, these junctions affect endothelial polarization and separation of the apical and basolateral cell membranes (facing the vessel lumen and the perivascular space, respectively), and the asymmetrical distribution of plasma membrane proteins (Hawkins, 2005). Notably, the junctions themselves are asymmetrically distributed and accumulate near the apical side of lateral cell membranes. Their transmembrane components in BECs include Occludin, Claudins, and junctional adhesion molecules (JAMs) (**Figure 3**). These proteins become anchored to the cellular actin cytoskeleton by associating with membrane proteins such as Zona Occludens 1 (ZO-1), which are located on the intracellular side of the plasma membrane (Coureuil et al., 2017). Claudins 1, 3, 5, 12 and 18 have been described to be present in BECs (Krause et al., 2008), although increasing importance has been recently given to the role of Claudin-5 in barrier function (Greene et al., 2019; Helms et al., 2015). Additionally, adherens junctions also provide important adhesive contacts near the basolateral side of neighboring ECs. The most important adherens junction found in BECs is vascular endothelial cadherin (VE-cadherin), an endothelium-specific member of the cadherin family of adhesion proteins, which associates with p120, β-catenin and plakoglobin proteins (Dejana et al., 2008).

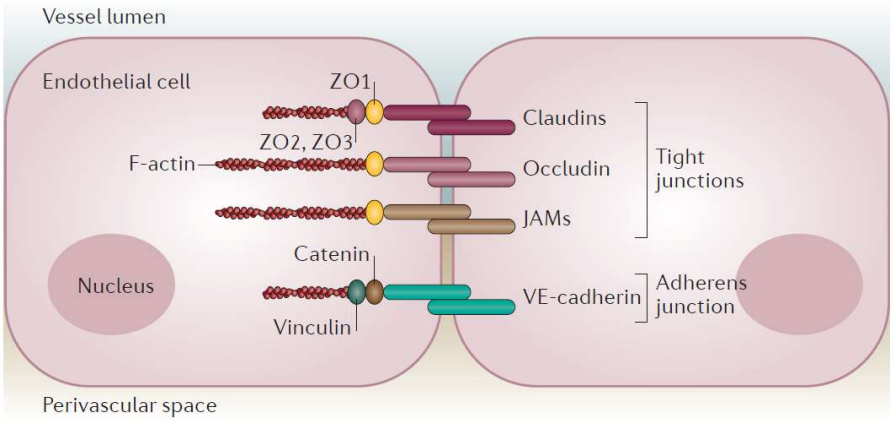

Figure 3. Cell-cell junctions of sealed BECs from the BBB and meningeal b-CSF barrier.

BECs are connected through tight and adherens junctions. Tight junctions in ECs are composed by Claudins, Occludin and JAMs, while the most prevalent adherent junction is VE-cadherin. Membrane-associated cytoplasmic proteins bind these proteins to scaffolding (such as filamentous actin (F-actin)) and signaling proteins. Adapted from (Coureuil et al., 2017).

BECs act as transport barriers in the sense that the transport of large molecules and even nutrients is under tight regulation at the BBB level. The expression of efflux pumps limits brain uptake of metabolites, neurotoxic substances and pharmaceuticals. These pumps include P-glycoprotein (P-gp, or multidrug resistance protein 1 (MDR1), the encoded product of the *ABCB1* gene) (Leslie et al., 2005; Regina et al., 2010; Tsuji et al., 1992), multidrug resistance related proteins (MRPs) (Leslie et al., 2005; Regina et al., 2010; Zhang et al., 2000), and breast cancer resistance protein (BCRP) (Cooray et al., 2002; Eisenblätter et al., 2003; Leslie et al., 2005). Traffic of molecules allowed into the CNS, such as amino acids and glucose, takes places through carrier-mediated transport. Endothelial polarity and the presence of abluminal (perivascular side) and luminal (blood side) membranes is crucial for the active transport of molecules across the BBB (Bauer et al., 2014; Betz et al., 1980; Betz and Goldstein, 1978). For example, glucose uptake and transport occurs primarily through the action of glucose transporter 1 (Glut-1), which asymmetrically accumulates at the abluminal side (Cornford et al., 1994; Farrell and Pardridge, 1991). The expression of the Par6/Par3/PKCz polarity complex by BECs has been shown to be important for the establishment of endothelial polarity and lumen formation in general (Zovein et al., 2010). Interestingly, hijacking

of the polarity complex in BECs is one of the mechanisms believed to lead to opening of a paracellular route for bacterial traffic during meningoccocal infection (Section 1.1.4.3.).

1.1.3. The Blood Phase of Meningococcal Infection

Prior to reaching the CNS and causing meningitis, meningococci must reach and survive in the blood (known as bacteraemia or blood phase). In order to cause infectious meningococcal disease, *Nm* must cross the epithelium of the nasopharynx to reach the bloodstream, where it is able to resist complement-mediated killing, survive and proliferate (Quagliarello and Scheld, 1992). Most adults are resistant to infection through acquired immunity and the mechanisms that trigger the crossing of the nasopharynx from asymptomatic carriage remain mostly unexplained (Virji, 2009). Specific human genetic polymorphisms were found to be associated with mortality and severity in meningococcal disease, particularly regarding the risk of developing purpura fulminans (Brouwer et al., 2009, 2010). Blood-borne meningococci can either cause deadly septic shock leading to purpura fulminans and/or meningitis, by crossing the meningeal b-CSF barrier and invading the meninges. It has been speculated that these clinical forms of meningococcal disease may reflect the level of bacteremia of the human host (i.e. low or high bacteremia) (Coureuil et al., 2013). Although pathogenic *Neisseria* do not seem to produce small molecular iron chelators known as siderophores, they are endowed with iron chelation systems (e.g. lactoferrin- and transferrin-binding proteins) that allow acquisition of host iron *in vivo* during blood dissemination (Schryvers and Stojiljkovic, 1999; West and Sparling, 1985). In cases of high bacteremia, extensive colonization of peripheral blood vessels may result in vascular leakage, leading to extensive thrombosis and purpura symptoms before the development of signs of meningitis. By contrast, when low or moderate numbers of meningococci circulate the bloodstream, it is likely that limited vascular colonization and few purpuric lesions develop (Coureuil et al., 2013). In this case, the prominent clinical manifestation of infection will likely be meningitis due to breaching of the b-CSF barrier and colonization of the CNS. Notably, as infections are very often discovered at this stage, it becomes crucial that meningococci possess factors that promote host immune evasion and allow the blood phase to be totally asymptomatic.

1.1.3.1. Host Evasion Mechanisms

In order to overcome immune detection, *Neisseria* is capable of surface modulation mechanisms that allow it to change its surface components. These include phase variation and structural or antigenic variation mechanisms. Phase variation consists on the ability to reversibly switch genes that code for surface antigens on and off, while structural/antigenic variation depends on allelic exchange of genes or gene fragments from imported neisserial DNA (Virji, 2009). Moreover, *Neisseria´*s genome contains multiple copies of certain genes (e.g. *pil* and *opa)*, allowing intragenomic recombination that can result in surface structural variation (Segal et al., 1986; Stern et al., 1986).

Protection against the host immune system during bacteremia is granted additionally by the expression of the polysaccharide capsule, the sialylation of LOS, and binding to human complement factor-H (CFH). The production of the capsule prevents bacterial phagocytosis or complement-mediated lysis (Mook-Kanamori et al., 2011). The production of sialylated LOS by Sg B, C, W and Y enables meningococci to mimic host cell surfaces that also express sialic acid, contributing for evasion from the host (Hung and Christodoulides, 2013; Mandrell et al., 1988). Factor-H binding protein (fHBP) was recently identified as a virulence factor that contributes to immune evasion during the blood phase. This 28 kDa surface-exposed lipoprotein hijacks host CFH, a key immune regulator of the immune response that protects host cells from being attacked by other complement proteins. Binding of *Nm* to host CFH therefore enhances the ability of meningococci to evade complement-dependent killing (Welsch and Ram, 2008). The importance of this mechanism is highlighted by the fact that individuals carrying polymorphisms in the *CFH* gene are associated with increased susceptibility to meningococcal disease (Brouwer et al., 2009; Davila et al., 2010). Importantly, fHBP is expressed by all invasive *Nm* isolates studied to date, although the level of expression varies between strains (Welsch and Ram, 2008). The recently developed vaccine 4CMenB contains this surface-exposed protein as main antigen for protection against Sg B strains (Serruto et al., 2012b). Serum protein CFH related-3 (CFHR3) was found to compete with and function as an antagonist of CFH for binding to neisserial fHBP (Caesar et al., 2014). As CFHR3 binding does not elicit immune protection from the host, the levels of both factors in an individual can potentially determine whether or not infection develops into meningitis or remains asymptomatic (Caesar et al., 2014).

Temperature was recently found to be an important environmental cue for the activation of mechanisms of immune evasion by *Nm* (Loh et al., 2013a). In particular, meningococcal genes *cssA*, *fHbp*, and *lst*, which encode factors contributing to capsule biosynthesis, fHBP expression, and LOS sialylation, respectively, are subject to thermoregulation (Loh et al., 2013b). The authors hypothesized that increases in temperature, which occur during inflammation, act as a 'danger signal' for *Nm* to enhance microbial defense mechanisms.

Lastly, the manipulation of binding strength and affinity to toll like receptor 4 (TLR4) on mammalian host cells might represent a mechanism of host evasion. TLR4 is the receptor for meningococcal LPS and its activation leads to signaling events that promote proinflammatory responses such as the release of cytokines. TLR4 recognizes the lipid A moiety of the LPS molecule, and the chemical composition of the lipid A determines how well it is recognized by TLR4 (Fransen et al., 2009). *Nm* was reported to produce lipid A with six acyl chains, the optimal number for TLR4 recognition (Munford and Varley, 2006). Strikingly, however, *Nm* strains isolated from patients with attenuated inflammatory responses were found to harbor a mutation in the *lpxl1* gene that lead to the formation of penta-acylated lipid A moieties (Fransen et al., 2009). This mutation was present in about 9 % of disease isolates, and was associated with less coagulopathy in patients and significantly diminished inflammatory responses in macrophages, suggesting that the low-activity LPS may have an important role in virulence by aiding the bacteria to evade the innate immune system (Fransen et al., 2009).

1.1.4. Invasion and Breaching of the Blood-Cerebrospinal Fluid Barrier

Meningitis occurs when the leptomeninges become inflamed in response to bacterial infection. Binding of *Nm* to the endothelium of brain microvessels that compose the meningeal b-CSF barrier and BBB is a crucial step in disease progression into meningitis (Mairey et al., 2006; Weller et al., 2018). As previously mentioned, *Nm* is able to bind to BECs only at shear stress levels close to the ones observed in capillaries (Mairey et al., 2006). However, once adhesion occurs, meningococci are very resistant to detachment and are able to resist high blood velocities, multiply and form colonies on the apical side of BECs (Mairey et al., 2006). This ability to resist shear stress and grow at the luminal surface of BECs highlights the efficacy of the interaction between *Nm* and BECs, for which *Nm* has developed key strategies.

1.1.4.1. Type IV Pili

Type IV pili (Tfp) are the structures responsible for initial attachment and promotion of further *Nm*-BEC interactions. Tfp are hair-like appendages found on the surface of many bacteria, composed of heteromultimeric pilin subunits, which are assembled into helical fibers (Craig and Li, 2008). The major pilin subunit that composes the neisserial pilus structure is PilE, which is subject to antigenic variation following recombination with the silent loci *pilS* (Seifert et al., 1988). The crystal structure of the meningococcal PilE pilin and an atomic model of the intact pilus filament were recently reported (Kolappan et al., 2016). Other pilin-like proteins regulate additional Tfp functions such as aggregation (PilX), adhesion/signaling (PilV), and competence (ComP) (Hélaine et al., 2005; Mikaty et al., 2009; Wolfgang et al., 1999). These are called minor pilins as they structurally resemble PilE and therefore are assumed to be assembled within the filaments in a similar way (Craig and Li, 2008). However, one study found that PilX and PilV locate in the bacterial periplasm and not along the pilus fiber, as previous studies had proposed (Imhaus and Dumenil, 2014).

The PilC proteins, PilC1 and PilC2, are additional components of the pilus machinery with a less defined role during infection. PilC proteins seem to play a key part in Tfp biogenesis since PilC-null mutants appear defective for fiber expression, and lack the ability for transformation competence (Morand et al., 2004). They act as pilus tip adhesins in *Neisseria gonorrhoeae* (gonococcus) (Rudel et al., 1995), however, only PilC1 seems to be required for adhesion in meningococcus (Nassif et al., 1994). Finally, the cytoplasmic PilT protein controls pilus retraction, a phenomenon that produces a form of movement known as 'twitching motility' (Mattick, 2002). Pilus retraction has been shown to play a central role in the interactions of pathogenic *Neisseria* with human cells (Pujol et al., 1999). This process requires *de novo* protein synthesis and depends on the ATPase activity of PilT, causing pilus retraction via depolymerization of Tfp, and the opposite role of PilF for pilus elongation (Coureuil et al., 2014). Currently, it is thought that PilC and PilT interact as antagonists. The fact that PilC-null strains are poorly piliated suggests that lack of PilC allows fiber retraction as soon as pili are formed, supporting the role of PilC as counteracting PilT-mediated retraction. Deletion of PilT in a PilC-null background restores piliation, presumably by blocking pilus retraction, suggesting that PilC acts as an antagonist of PilT (Morand et al., 2004; Wolfgang et al., 1998). Additionally, PilT was shown to negatively influence gene regulation of PilC1. In a PilT-null background, PilC1 is upregulated, while the presence of

PilT downregulates the transcription of the *pilC1* gene (Yasukawa et al., 2006). The currently accepted model for Tfp-mediated meningococcal adhesion to host cells is based on a two-step process. First, localized adhesion is characterized by the upregulation of the PilC1 protein (Taha et al., 1998). Following this stage, pili are retracted, and attached non-piliated bacteria re-organize as monolayers covering the apical surface of the cells (Pujol et al., 1999). Recently, targeting Tfp has been explored as a potential therapeutic strategy against invasive meningococcal disease by using compounds to block Tpf functions and cause its retraction (Denis et al., 2019).

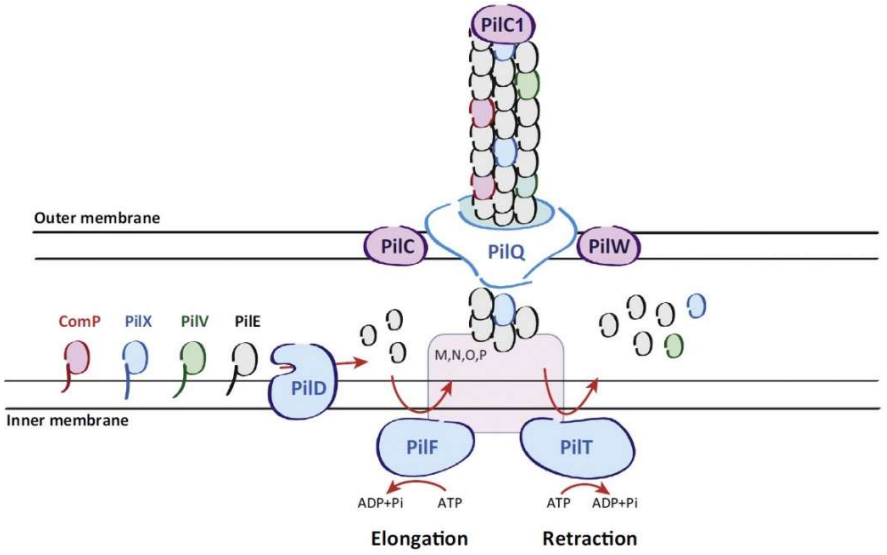

Figure 4. Components of the meningococcal pilus machinery and their presumed function.

The main pilus fiber is composed by major pilin PilE and minor pilins ComP, PilX, and PilV, with PilC1 on the tip mediating adhesion. The location of PilX and PilV is currently controversial and under debate. Pilus assembly from pilin subunits located in the cytoplasmic membrane is presumed to be induced by ATPase PilF (elongation), from a platform complex comprising PilD, PilF, PilM, PilN, PilO, and PilP. Retraction is induced by ATPase PilT via depolymerization of Tfp. The newly formed fiber is extruded to the cell surface through a pore formed by the PilQ secretin. PilW is an outer membrane protein that is necessary for PilQ stability. Adapted and modified from (Coureuil et al., 2014).

1.1.4.2. Other Virulence Factors

Though initial host-pathogen contact is thought to be Tfp-dependent, the interaction and invasion of the b-CSF barrier is greatly supported by other virulence factors, namely outer membrane

proteins. Of particular importance are colony opacity-associated (Opa) proteins Opa and OpcA (Virji et al.,1993), the most abundant protein adhesins in the outer membrane (Hung & Christodoulides, 2013). Opa and OpcA bind to host receptors carcinoembryonic antigen-related cell adhesion molecule-1 (CEACAM-1) and heparan sulfate proteoglycans (HSPG), respectively, to components of the ECM, and serum proteins such as vitronectin or fibronectin (Chen et al., 1995; Unkmeir et al., 2002). Though these proteins are thought to be partially masked by the capsule, Opa engages in cellular interactions that influence bacterial adhesion and invasion, especially in cells expressing high densities of CEACAM-1 receptor (Bradley et al., 2005). Complete genome sequencing has revealed that meningococci strains can harbour 3–4 *opa* genes (*opaA*, *opaB*, *opaD* and *opaJ*) (Parkhill et al., 2000; Tettelin et al., 2000). Opa is subject to phase variation regulated by translational control mechanisms common to both gonococci and meningococci (Stern and Meyer, 1987). By contrast, OpcA is expressed only in meningococci and by a single gene, *opcA*, although its levels of protein expression are also phase variable (Zhu et al., 1999). Other recently identified minor adhesion and adhesion-like proteins are reviewed in Hung & Christodoulides, 2013.

1.1.4.3. *N. meningitidis*-Brain Endothelial Cell Interactions: Cortical Plate Formation

The mechanisms that promote and result in breaching of the b-CSF barrier by *Nm* have been subject to extensive research over the past decades, although they are still not fully understood. Initial attachment of *Nm* to host cells induces the formation of host cellular protrusions around the bacteria that promote more intimate binding and internalization into vacuoles (Eugène et al., 2002). These cellular projections that mimic epithelial microvilli structures are likely to allow resistance of growing bacterial microcolonies to the high shear stress levels of the bloodstream (Mairey et al., 2006). Importantly, post mortem analysis of brain sections of a pediatric patient who died from fulminant meningitis revealed similar protrusion formation in BECs (Nassif et al., 2002). These protrusions are associated with the formation of membrane domains enriched with receptors and structural proteins at sites of bacterial binding, known as “cortical plaques” (Merz et al., 1999). Cortical plaques are generated following initial adhesion of Tfp (via PilE and PilV) to host receptor CD147, a member of the immunoglobulin superfamily (Bernard et al., 2014). Blocking of the Tfp:CD147 interaction inhibits the adhesion of meningococci to human BECs *in vitro* and the colonization of vessels in *ex vivo* human brain tissue explants (Bernard et al., 2014). Interestingly, PilE and PilV are also required to interact with the extracellular N-terminal region of the

β2-adrenergic receptor (β2AR), a member of the G protein-coupled receptor family. This receptor is responsible for transducing a signal inside cells, although β2AR is dispensable for adhesion (Coureuil et al., 2010; Lécuyer et al., 2012). Thus, pilus-mediated interaction with ECs relies on pilus binding to two cooperating but independent receptors: CD147 promotes initial attachment and adhesion, while β2AR induces signal transduction events. A recent report has shown that CD147 and β2ARs form hetero-oligomeric complexes, allowing for β2AR activation immediately after the initial interaction of bacterial pili with CD147 (Maïssa et al., 2017). Moreover, the scaffolding protein α-actinin-4 directly binds to the cytosolic tail of CD147 and governs the assembly of these complexes, a process that seems to increase the binding strength of meningococci to BECs under shear stress (Maïssa et al., 2017).

Activation of β2AR by Tfp is believed to modify the conformation of this receptor, resulting in biased activation of β-arrestin-mediated signaling pathways without activating G protein-mediated signal transduction (Coureuil et al., 2010). Following its activation, β2AR sequesters a) β-arrestins and β-arrestin-binding molecules (e.g. sarcoma (Src) tyrosine kinase, p120-catenin, and VE-cadherin) (Coureuil et al., 2009, 2010; Hoffmann et al., 2001), and b) ezrin and ezrin-binding proteins (Doulet et al., 2006; Lambotin, 2005). Recruitment of β-arrestins activates Src kinase, which induces active actin polymerization, and the recruitment of the polarity complex (i.e., Par6/Par3/PKCz) to sites of bacterial adhesion (Coureuil et al., 2009, 2010; Hoffmann et al., 2001). Ezrin-binding factors recruited to the site of meningococcal adhesion include CD44, intercellular adhesion molecule 1 (ICAM-1), and ErbB2 tyrosine kinase receptor, a second regulator of Src activity (Hoffmann et al., 2001). ErbB2 recruitment is particularly strong in ceramide-enriched platforms, induced by the transient increase of acid sphingomyelinase activity elicited by OpcA-expressing meningococci (Simonis et al., 2014). Activated Src phosphorylates cortactin (also known as cortical actin-binding protein), leading to anchoring of actin to the site of bacterial adhesion, promoting the cytoskeletal re-arrangements that result in cortical plaque formation (Lambotin et al., 2005; Uruno et al., 2001).

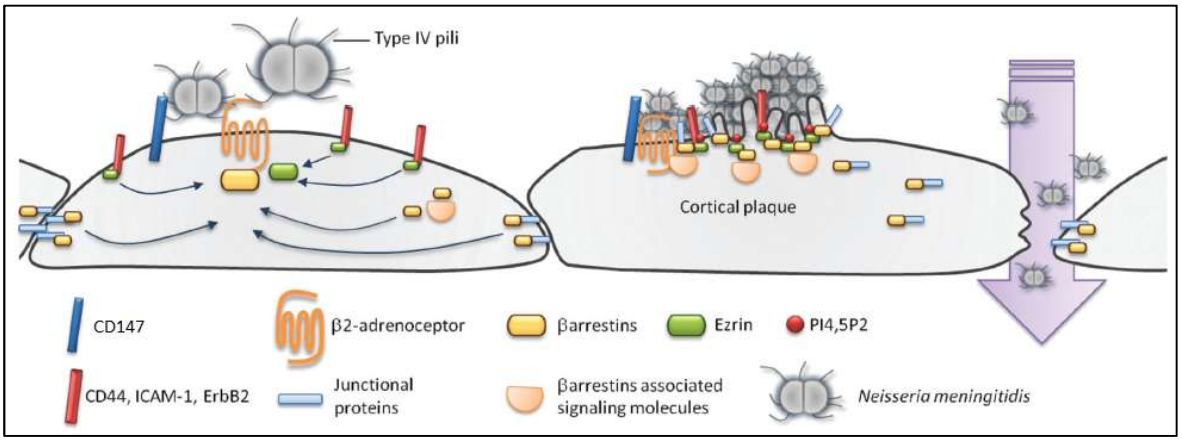

Figure 5. Attachment of Tfp to host receptors induces a cascade of signaling events leading to opening of cell-cell junctions.

Binding of Tfp to CD147 represents the first step required for vessel colonization by meningococci. Subsequent interaction of Tfp with receptor β2AR promotes downstream signaling events that include the activation of β-arrestin-mediated pathways and the recruitment of factors such as Ezrin, CD44, ICAM-1, ErbB2, phosphatidylinositol 4,5-bisphosphate (PI4,5P2, or PIP_2), and junctional proteins to the adhesion site. Membrane protrusions known as cortical plaques are induced by actin polymerization due to cortactin phosphorylation. Adapted and modified from (Coureuil et al., 2012).

Recruitment of the polarity complex together with adherens and tight junction proteins has been shown to cause the depletion of cell-cell junctions between adjacent cells opening a paracellular route that may facilitate bacterial passage (Coureuil et al., 2009). In accordance, modification of tight junction architecture in response to *Nm* includes proteolytic cleavage of Occludin by matrix-metalloproteinase MMP-8 (Schubert-Unkmeir et al., 2010). Upon prolonged infection time, Occludin vanishes from the cell periphery in infected cells, resulting in cell detachment and increased paracellular permeability (Schubert-Unkmeir et al., 2010). Although these studies point to paracellular migration as the main route for crossing of the b-CSF, *Nm* is also internalized by ECs in membrane-bound compartments referred to as *Neisseria*-containing vacuoles, presumed to offer a protective niche for intracellular multiplication and potentially serve as a vehicle for transcytosis (Nikulin et al., 2006). Crossing of the b-CSF is a subject currently under debate (Coureuil et al., 2012).

1.1.4.4. Additional Host Responses to Infection

Besides the recruitment of proteins of the polarity complex and formation of cortical plaques, host BECs show additional cellular responses to *Nm* infection. Promotion of invasion into host cells by manipulating intracellular calcium signaling has been reported (Asmat et al., 2014; Källström et al., 1998). Release of calcium from intracellular stores on host BECs can be induced by meningococci via PilC1 (Asmat et al., 2014). Another mechanism promoting meningococcal internalization relies on transient activation of acid sphingomyelinase, resulting in surface ceramide display in host BECs (Simonis et al., 2014). Previous studies also reported that *Nm* infection induces the release of proinflammatory cytokines such as IL-6, IL-8 and MCP-1, involved in neutrophil and monocyte recruitment by BECs (Dick et al., 2017; Schubert-Unkmeir et al., 2007). Transcriptomic analysis has revealed that besides immune activation, host responses to infection are associated with differential expression of genes related to signal transduction, MAPK signaling pathway, transcription factors/regulation of transcription, pro-apoptosis, ECM and adhesion, and cytoskeleton/motility proteins (reviewed in (Schubert-Unkmeir et al., 2009)). Some of these cell responses are presumed to be part of host hijacking mechanisms triggered by the bacteria in order to invade and cross the b-CSF barrier (Coureuil et al., 2010).

Known cell responses to infection have been studied mostly through the use of immortalized cell lines, primary cells, or animal models. However, as *Nm* is a human-exclusive pathogen, the establishment of suitable models for studying the mechanisms by which *Nm* is capable of crossing host barriers has proved challenging, and there is currently the need to develop more physiological models that more closely recapitulate *in vivo* infection (Schubert-Unkmeir, 2017).

1.2. Stem Cells

Stem cells are undifferentiated cells that are defined by their functional capacity to self-renew as well as generate differentiated progeny. One example of a truly totipotent cell, capable of generating all cell types of a complete organism (including the extraembryonic tissues) is the fertilized egg, and the cells that result from its first divisions (Fortier, 2005). As the fertilized egg starts to asymmetrically divide, giving rise to the blastocyst, the cells from the epyblast (the inner mass of the blastocyst) are no longer totipotent, as they can only differentiate into cells from the three germ layers: mesoderm, ectoderm and endoderm (**Figure 6**) (Fortier, 2005). These embryonic stem cells are classified as pluripotent, together with other cell types such as embryonic germ cells and embryonal carcinoma cells (isolated from teratocarcinomas) and, more recently, induced pluripotent stem cells (iPSCs) (Hui et al., 2011).

The following term in the cell potency hierarchy is "multipotent", attributed to cells capable of differentiating into a limited range of cell types, within the same germ layer (e.g. hematopoietic stem cells) (Fortier, 2005; Hui et al., 2011). These are also denominated as progenitor cells. Lastly, precursor cells such as angioblasts, hepatoblasts or neural progenitors, are regarded as unipotent, as they can only sustain one cell lineage or cell type (Hui et al., 2011). When referring to stem cells obtained from any postnatal organism, the term "adult stem cell" is commonly applied in order to distinguish them from embryonic stem cells (ESCs) (Fortier, 2005). Stem cells in adult animals are extremely important to maintain tissue and organ mass during normal cellular turnover, with each tissue having a resident population of stem cells (Fortier, 2005). It is still not clear if adult stem cells retain some plasticity and are able to go through a phenomenon called "transdifferentiation", which is described to occur when stem cells derived from one adult tissue change into cellular phenotypes not normally found in that tissue (Sanchez-Ramos, 2002). Although the legitimacy of this phenomenon has been highly debated, some authors claim that adult stem cells from mature tissues retain the potential to "transdifferentiate" (Sanchez-Ramos, 2002).

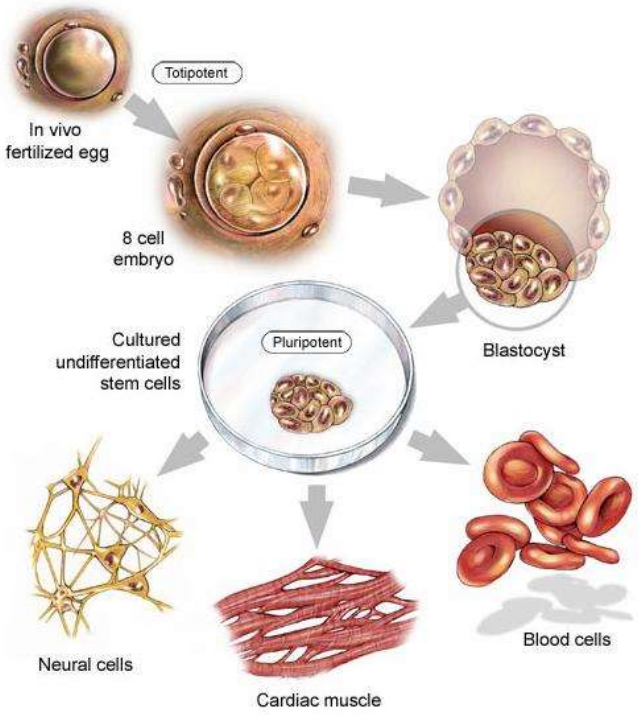

Figure 6. Stem cell differentiation potential hierarchy.

The fertilized egg and its immediate progeny (until the 8-cell embryo) are totipotent cells. The cells from the inner mass of the blastocyst are pluripotent, as they can only give rise to the 3 germ layers of the embryo. Once cultured *in vitro*, pluripotent stem cells are capable of differentiating into neural cells (ectoderm), cardiac muscle or blood cells (mesoderm), hepatoblasts (endoderm, not depicted), among others. Adapted from the website of Division of Biology and Medicine from Brown University (http://biomed.brown.edu).

1.2.1. Properties and Applications of induced Pluripotent Stem Cells

As their denomination suggests, iPSCs are obtained by artificially reprogramming adult cells into a pluripotent state. The original method, developed by Yamanaka and Takahashi, consisted in using retrovirus to deliver into mouse adult skin fibroblast cells a combination of four genes, the pluripotency keepers Oct 3/4 and Sox2, and the oncogenes c-Myc and Klf4 (Takahashi and Yamanaka, 2006). Cells that were successfully reprogrammed grew as colonies, expressed pluripotency markers and were capable of differentiating into cell types of the three germinal layers, either spontaneously (teratoma formation *in vivo*) or when induced with specific stimuli to generate a specific cell type. This ground-breaking discovery that mature cells can regain

pluripotency through reprogramming earned Yamanaka the Nobel Prize in Medicine in 2012. The use of iPSCs overcomes important hurdles of using ESCs for research and therapeutics, as ESCs are associated with ethical issues regarding usage of human embryos, potential immune rejection upon transplantation, and have limited availability (Omole and Fakoya, 2018). iPSCs represent a highly available alternative source of pluripotent stem cells with the same differentiation potential as ESCs that does not elicit ethical issues. However, iPSCs are subject to safety concerns linked to their generation procedure and their tumorigenic potential.

In 2007, Yamanaka and co-workers achieved the reprogramming of human adult cells into iPSCs, while other laboratories were able to independently generate iPSCs through different delivery systems (Hanna et al., 2007; Maherali et al., 2007; Okita et al., 2007; Yu et al., 2007). The group of J.A. Thomson reported the generation of iPSCs without the use of oncogenes, replacing c-Myc and Klf4 by Lin28 and Nanog (Yu et al., 2007). Further progress has been made towards developing strategies for iPSC generation without the usage of integrative viral delivery systems, hereby bypassing risks of insertion mutagenesis and tumor development. Non-integrative delivery methods include episomal vectors, small molecules, and direct protein and RNA delivery (Hou et al., 2013; Omole and Fakoya, 2018). These advancements have contributed to the application of iPSC technology in regenerative medicine, particularly in the development of patient-specific cell therapy, although hurdles in cell delivery and survival rate have yet to be overcome (Martin, 2017). Other applications of iPSC technology include the generation of cell-based models as platforms for drug screening and the study of human diseases (Suh, 2017). By reprogramming human cells derived from patients and differentiating them into specific cell types, it is possible to study phenotypes of genetic diseases and develop diagnosis tools and novel therapies. The same can be applied to the study of infectious diseases, by reprogramming and describing phenotypes of cells from patients suffering from a particular infectious disease. Alternatively, *in vitro* modelling of infection with iPSC-derived cells instead of immortalized cell lines should provide more physiologically relevant data describing pathogenic mechanisms and host-pathogen interactions. One study using iPSC-derived cardiomyocytes infected with coxsackievirus B3 strain (cause of viral myocarditis) reported that the cells could be used to model the pathogenic processes of viral disease (Sharma et al., 2014). Importantly, besides recapitulating human pathogenesis, the model could be used to screen antiviral therapeutics for efficacy (Sharma et al., 2014). As a human-

exclusive pathogen, it would be of great importance to develop novel cellular models for *Nm* that properly reflect *in vivo* host properties.

1.3. Aim of the Study

The present study sought to establish iPSC-derived BECs as a cellular model for meningococcal infection research. To this end, the following specific goals were pursued:

- Characterize the interaction of different *Nm* strains with iPSC-BECs in order to assess the suitability of the model, through gentamicin protection assays for quantification of invasion, as well as microscopy techniques;
- Confirm the expression of presumed pilus receptor CD147 by iPSC-BECs and observe its localization during infection through immunofluorescence;
- Describe host endothelial inflammatory responses to *Nm* infection by Luminex® bead-based multiplex assays and RT-PCR;
- Characterize changes in barrier properties and tight junction dynamics caused by *Nm* through implementation of techniques such as Western blot, Microscopy, RT-PCR, TEER measurements and paracellular transport studies during infection;
- Assess the relevance of the transcellular and paracellular pathways for bacterial crossing of endothelial surfaces by the establishment of bacterial transmigration assays;
- Characterize the impact of *Nm* infection on the host transcriptome of specifically infected cells, by implementing FACS prior to RNA-Seq of infected iPSC-BECs.

2. Materials

2.1. Cell Lines and Bacterial Strains

All cell lines used in this work are listed in **Table 1**. IMR90 are fetal lung fibroblasts obtained in 2007 at the University of Wisconsin in the working group of J.A. Thomson. These cells were reprogrammed to human iPSCs by lentiviral transduction, through introduction of human ESC genes *OCT4, SOX2, NANOG* and *LIN28* into their genome. Clone 4 had no integration of the *LIN28* gene and presented a population doubling time of 17.1 ± 2.4 hours (Yu et al., 2007). Cells derived from this clone were used for p18 + 34 (9) passages (Lot: iPS(IMR90)-4-DL-01). This means that the IMR90 line was cultured for 18 passages until reprogramming, followed by 33 cell culture passages after transformation, and 8 passages under feeder-free conditions in mTeSR™1 and Matrigel™. WiCell adds +1 passage so the number of passages on the purchased cryotube exactly corresponds to the passage of cells after thawing. All work done with iPS(IMR90)-4-DL-01 was performed in the iPSC lab of Chair Tissue Engineering and Regenerative Medicine, University Hospital Würzburg, Würzburg, Germany, under the supervision of A. Appelt-Menzel. Human brain microvascular ECs (HBMECs) were obtained by immortalization of human cerebral ECs using SV40 large T antigen, in the working group of K.S. Kim at the Johns Hopkins University School of Medicine (Stins et al., 1997). All bacterial strains used in this work, their serogroup (Sg), sequence type (ST), and clonal complex (cc) are listed in **Table 2**.

Table 1. Cell lines used, their manufacturer /supplier, order number (when applicable), and who provided them.

Cell Line	Manufacturer/Supplier, order no.	Comments
IMR90-4	WiCell (USA) iPS (IMR90 (Clone (4)) Lot: iPS(IMR90)-4-DL-01	Purchased from WiCell. Work supported by A. Appelt-Menzel, University Hospital Würzburg, Chair Tissue Engineering and Regenerative Medicine, Würzburg, Germany
	WiCell (USA) iPS (IMR90 (Clone (4)) Lot: WB33712	Provided by E.V. Shusta, University of Wisconsin, Madison, Wisconsin, USA
HBMECs	-	Provided by K.S. Kim, Johns Hopkins University, Baltimore, USA

Table 2. Bacterial strains used, their description, reference, and who provided them (when applicable).

Bacterial Strain	Description	Resistance Marker	Reference
WT strains			
MC58	Sg B strain of the ST-74 (ST-32 cc)	-	(McGuinness et al., 1991) Provided by E. R. Moxon, University of Oxford, UK
8013/12	Sg C strain of the ST-177 (ST-18cc)	-	(Nassif et al., 1993) Provided by M. Taha, Institut Pasteur, France
Modified strains			
MC58Δ*siaD*	Non-capsulated, isogenic mutant of MC58	Erythromycin	(Unkmeir et al., 2002)
8013/12Δ*pilT*	Highly piliated, isogenic mutant of 8013/12	Ampicillin, Streptomycin	(Martins Gomes et al., 2019)
8013/12Δ*pilE*	Non-piliated, isogenic mutant of 8013/12	Ampicillin, Streptomycin	(Peters et al., 2019) (Martins Gomes et al., 2019)
MC58-GFP	GFP-expressing, isogenic mutant of MC58	Erythromycin	(Simonis et al., 2014)
MC58Δ*siaD*-GFP	GFP-expressing, isogenic mutant of MC58Δ*siaD*	Erythromycin	(Simonis et al., 2014)
8013/12-GFP	GFP-expressing, isogenic mutant of 8013/12	Erythromycin	(Peters et al., 2019) (Martins Gomes et al., 2019)

2.2. Kits

Table 3. Overview of the commercial kits used.

Kit (use)	Reagents	Manufacturer, order no.
Pierce™ BCA Protein Kit Assay (Western blot)	- Reagent A (2x500 mL) - Reagent B (25 mL) - Albumin Standard Ampules	ThermoFisher Scientific GmbH (D), 23225
Clarity™ Western ECL kit (Western blot)	- Clarity Western Peroxide Reagent (100 mL) - Clarity Western Luminol/Enhancer Reagent (100 mL)	BioRad (D), 170-5060
NucleoSpin® (mRNA isolation)	- Lysis Buffer RA1 (125 mL) - Wash Buffer RAW2 (80 mL) - Wash Buffer RA3 (3x25 mL) - Membrane Desalting Buffer MDB (125 mL) - Reaction Buffer for rDNase (30 mL) - rDNase, RNase-free (lyophilized) - RNase-free H_2O (60 mL) - NucleoSpin® RNA Columns	Macherey-Nagel (D), 740955
SuperScript™ IV VILO™ kit (cDNA synthesis)	- 10X SuperScript® Enzyme Mix - 5X VILO™ Reaction Mix - Master Mix "No RT" Control, 200 µL - Nuclease-free water, 1.25 mL	Invitrogen (D), 11756050
PowerUp™ SYBR™ Green Master Mix (qRT-PCR)	2X Mix contains: - SYBR Green dye - Dual-Lock Taq DNA Polymerase - dNTPs with dUTP/dTTP blend - heat-labile UDG - ROX passive reference dye - Optimized buffer components	ThermoFisher Scientific GmbH (D), A25741
Taqman™ Master Mix (qRT-PCR)	2X Mix contains: - AmpliTaq Gold® DNA Polymerase (Ultra Pure) - Uracil-DNA glycosylase - dNTPs (with dUTP) - ROX™ Passive Reference - Optimized buffer components	ThermoFisher Scientific GmbH (D), 4369016

Table 3. Overview of the commercial kits used. (*continued*)

Magnetic Luminex® Assay	Human Premixed Multi-Analyte kit contains: - Premixed cocktail of antibody-coated Magnetic beads - Premixed cocktail of biotinylated detection antibody - Standard Cocktail(s) - Bead Diluent - Biotin Antibody Diluent - Standard/Sample Diluent - Wash Buffer - Streptavidin-PE	R&D Systems (USA), customized kit provided on request

2.3. Antibodies

Table 4. Overview of the antibodies used for immunofluorescence assays.

Antibody	**Host**	**Dilution**	**Manufacturer, order no.**
CD147 MEM 6/1	mouse	1:100	BioRad (D), MCA1876
CD147 MEM 6/6	mouse	1:100	BioRad (D), MCA2882Z
CD31	rabbit	1:200	Abcam (UK), Ab32457
Claudin-5	rabbit	1:100	Abcam (UK), Ab15106
GLUT1	mouse	1:200	Abcam (UK), Ab40084
Occludin	mouse	1:200	ThermoFisher Scientific GmbH (D), 33-1500
ZO-1	rabbit	1:100	Proteintech (UK), 21773-1-AP
Secondary Antibody			
Anti-mouse Alexa Fluor 488	goat	1:400	ThermoFisher Scientific GmbH (D), A11001
Anti-mouse Alexa Fluor 647	donkey	1:400	ThermoFisher Scientific GmbH (D), A31571
Anti-rabbit Alexa Fluor 555	donkey	1:400	ThermoFisher Scientific GmbH (D), A31572

Table 5. Overview of the antibodies used for flow cytometry assays.

Antibody	Host	Dilution	Isotype	Manufacturer / Supplier, order no.
CD147:RPE MEM-6/1	mouse	1:100	IgG1	BioRad (D), MCA1876PE
CD147 MEM 6/6	mouse	1:100	IgG1	BioRad (D), MCA2882Z
Secondary Antibody				
Anti-mouse Alexa 488	goat	1:400	IgG	ThermoFisher Scientific GmbH (D), A11001
Isotype Control				
RPE Negative Control	mouse	1:100	IgG1	BioRad (D), MCA928PE
Anti-mouse Control	goat	1:100	IgG1	Invitrogen (D), MA1-10405

Table 6. Overview of the antibodies used for Western blot assays.

Antibody	Host	Dilution	Manufacturer, order no.
β-Actin	rabbit	1:1000	Cell Signalling (D), 4967
Claudin-5	rabbit	1:250	Abcam (UK), Ab15106
COX IV	rabbit	1:1000	Cell Signalling (D), 4850S
Occludin	mouse	1:500	ThermoFisher Scientific GmbH (D), 33-1500
ZO-1	rabbit	1:1000	Proteintech (UK), 21773-1-AP
Secondary Antibody			
Peroxidase anti-mouse	goat	1:10000	Jackson ImmunoResearch (UK), 115-035-044
Peroxidase anti-rabbit	goat	1:5000	Jackson ImmunoResearch (UK), 115-035-006

2.4. Primers

The primers used herein for quantitative real-time polymerase chain reaction (qRT-PCR) assays are listed in **Table 7**. These primers were previously described in the literature, and were purchased from ThermoFisher Scientific GmbH.

Table 7. Overview of the primers used for qRT-PCR assays.

Primer	NCBI-Number	Primer Sequence	Reference
18S	NR_003286	F: GTA ACC CGT TGA ACC CCA TT R: CCA TCC AAT CGG TAG TAG CG	Rho *et al*. 2010
CCL20	NM_004591.3 NM_001130046.1	F: GCG CAA ATC CAA AAC AGA CT R: CAA GTC CAG TGA GGC ACA AA	van Sorge *et al*. 2008
CXCL1	NM_001511.3	F: CTC TTC CGC TCC TCT CAC AG R: GGG GAC TTC ACG TTC ACA CT	
CXCL2	NM_002089.4	F: CTC AAG AAT GGG CAG AAA GC R: AAA CAC ATT AGG CGC AAT CC	
CXCL8	NM_000584.4 NM_001354840.1	F: AGC TCT GTG TGA AGG TGC AG R: AAT TTC TGT GTT GGC GCA GT	
GAPDH	NM_002046.7	F: GAA GGT GAA GGT CGG AGT CAA CG R: TCC TGG AAG ATG GTG ATG GGA T	
IL6	NM_000600.5 NM_001318095.1	F: GGA GAC TTG CCT GGT GAA AA R: CAG GGG TGG TTA TTG CAT CT	
SNAI1	NM_005985.4	F: GGA CCC ACA CTG GCG AGA AG R: ATT CGG GAG AAG GTC CGA GC	Han *et al*. 2011

For Taqman qRT-PCR, a primer mix is provided for each selected target gene. Taqman probes were used for detection of *TJP1* (ZO-1) (Hs0155186_m1), *CLDN5* (Claudin-5) (Hs00533949_s1), *OCLN* (Occludin) (Hs00170162_m1), *CCL5* (RANTES) (Hs00982282_m1), *IFNG* (IFN-γ) (Hs00989291_m1), *VEGFA* (Hs00900055_m1), *TNFAIP2* (Hs00969305_m1) and *18S* (Hs99999901_s1).

2.5. Chemicals

Table 8. Overview of the chemicals used.

Chemicals	Manufacturer/Supplier, order no.
Accutase	Sigma-Aldrich (D), A6964
Agarose	Invitrogen (D), 16500-500
Ammonium-Peroxydisulfat (APS)	Carl Roth (D), 9592.3
β-Mercaptoethanol	Sigma-Aldrich (D), M3148-25ML
BSA	Carl Roth (D), 8076.3
Collagen IV	Sigma-Aldrich (D), C5533-5MG
DAPI	Sigma-Aldrich (D), D8417-5MG
Dispase	ThermoFisher Scientific GmbH (D), 17105-041
DMEM/F-12 + Glutamax	Gibco (D), 31331-028
DMEM/F-12 without L-Glutamin	Gibco (D), 11330-057
ECGS	CellSystems, CS-A0030
EDTA	Sigma-Aldrich (D), E5134-1kg
Endothelial Serum Free Medium, human (hESFM)	ThermoFisher Scientific GmbH (D), 11111-044
Erythromicin	Sigma-Aldrich (D), 53889-5G
Ethanol, 100 %	Carl Roth (D), 9065.2
Ethanol, 96 %	Carl Roth (D), P075.4
Fetal Calf Serum (FCS)	Life Technologies (D), 10270
Fibronectin	Sigma-Aldrich (D), F2006
GC Medium Base	BD Biosciences (D), 228950
Gelatin	SERVA Electrophoresis GmbH (D), 22151
Gentamicin	Merck Millipore (D), A2712
Glutamax	Invitrogen (D), 35050-061
Glycin	Carl Roth (D), 3908.3
GlycoBlue	Ambion GmbH (D), AM9516
Goat serum	Sigma-Aldrich (D), G9023
hbFGF	R&D Systems (USA), 233-FB
Heparin	Merck Millipore (D), L6510
Human Serum (HS)	TCS Biosciences (UK), CR100-500
Isopropanol	Carl Roth (D), 6752.4
KH_2PO_4	Merck Chemicals GmbH (D), 7778-77-0
K_2HPO_4	Merck Chemicals GmbH (D), 7758-11-4
KnockOut™ Serum Replacement (KO-Serum)	ThermoFisher Scientific GmbH (D), 10828-028
L-Glutamin	ThermoFisher Scientific GmbH (D), 25030024

Table 8. Overview of the chemicals used. (continued)

Matrigel, growth factor reduced	BD Biosciences (D), 354230
MEM NEAA	ThermoFisher Scientific GmbH (D), 11140-035
Methanol	Carl Roth (D), 4627.5
mTeSR™1 Medium	STEMCELL Technologies (D), 05850
NaCl	Carl Roth (D), P029.2
NaF	Sigma-Aldrich (D), S7920-100G
Na-Fluorescein	Sigma-Aldrich (D), F6377-100G
$NaHCO_3$	Merck Chemicals GmbH (D), 144-55-8
Na_3VO_4	Sigma-Aldrich (D), S6508-10G
Nu-Serum	Corning Inc. (USA), 355500
PBS	Gibco (D), 21600-069 1X10L
Pefabloc SC PLUS	Sigma-Aldrich(D), 11873601001
PFA	Carl Roth (D), 0335.2
Platelet-Poor Plasma Derived Serum, bovine (PDS)	Alfa Aesar (ThermoFisher (Kandel) GmbH (D)), J64483
Proteose-peptone (Bacto™)	BD Biosciences (D), 211684
Protease inhibitor	Sigma-Aldrich (D), 5892791001
Retinoic Acid	Sigma-Aldrich (D), R2625-500MG
RNAlater®	Qiagen (D), 76104
RPMI 1640 medium	Gibco (D), 61870-010
Rotiphorese® Gel 30	Carl Roth (D), 3029.1
Saponin	SERVA Electrophoresis GmbH (D), 34655.02
SDS	Carl Roth (D), CN30.3
Skim Milk	Heirler (D), -
Starch	Sigma-Aldrich (D), 85642-100G
STEMFlex™	Gibco (D), A3349401
Sodium deoxycholate	Sigma-Aldrich (D), D6750-25G
Sodium pyruvate	ThermoFisher Scientific GmbH (D), 11360-039
TEMED	Carl Roth (D), 2367.3
Tris base	Carl Roth (D), 5429.3
Tris-HCl	Carl Roth (D), 9090.1
Triton-X 100	Carl Roth (D), 3051.3
TRIzol	Invitrogen (D), 15596026
Trypanblue (0.5 %)	Seromed (D), L6323
Trypsin-EDTA 0.05 % 1X	Gibco (D), 25300-054
Tween 20	Carl Roth (D), 9127.1

Table 8. Overview of the chemicals used. (continued)

Versene	Gibco (D), 15040-033
Y27632 (ROCK-Inhibitor)	Tocris (UK), 1254

2.6. Media, buffers and solutions

2.6.1. Media for cell culture

Table 9. Overview of the different types of mammalian cell culture media used and their composition.

Medium	Components	Mixture		Comments
EC-Medium	- hESFM	99	%	Mix components and store at
	- PDS	1	%	4°C
	- hbFGF	20	ng/mL	Store stock solutions 1:5000
	- RA	10	µM	Store stock solutions 1:1000
HBMEC Medium	- RPMI 1640	80	mL	Mix components and store at
	- FCS	10	mL	4°C
	- Nu-Serum	10	mL	
	- L-Glutamin	1	mL	
	- Sodium Pyruvate	1	mL	
	- MEM NEAA	1	mL	
	- ECGS	300	µl	
	- Heparin	100	µl	
Infection Medium	- hESFM, or	90	%	Mix components before usage
	- RPMI 1640			
	- HS	10	%	
mTeSR™1	- mTeSR™1-Basal medium	80	%	Prepare suppl. stocks to store at
	- mTeSR™1-Supplement	20	%	-20°C. Mix components and
				store at 4°C
StemFlex™	- StemFlex™-Basal medium	90	%	Prepare suppl. stocks to store at
	- StemFlex™-Supplement	10	%	-20°C. Mix components and
				store at 4°C
Unconditioned	- DMEM/F12 w/o L-Glutamine	78.5	%	Mix components and store at
Medium	- KO-Serum	20	%	4°C
	- MEM NEAA	1	%	
	- β-Mercaptoethanol	0.1	mM	
	- L-Glutamin or Glutamax	1	mM	

2.6.2. Media for bacteria culture

Table 10. Overview of the different types of bacteria culture media used and their composition.

Medium / Supplements	Components	Mixture		Comments
Kellog's Supplement I	- Glucose	40	g	Fill up 100 mL with deionized water
	- Glutamine	1	g	
	- Thiamine pyrophosphate	2	mg	
Kellog's Supplement II	- $Fe(NO_3)_3$	50	mg	Fill up 100 mL with deionized water
Kellog's Supplement for PPM+	- Kellog's supplement I	100	mL	Sterilize with 0.2 µm filter
	- Kellog's supplement II	10	mL	
Buffer solution for PPM medium	- KH_2PO_4	200	g	Add 1 L of H_2O, adjust pH to 7.25-7.5 and autoclave
	- K_2HPO_4	50	g	
PPM medium	- Proteose-peptone	7.5	g	Fill up 500 mL with deionized water, adjust pH to 7.2 and autoclave
	- NaCl	2.5	g	
	- Starch	0.25	g	
	- Buffer solution	10	mL	
PPM+ for *Nm*	- PPM	10	mL	
	- Kellog's supplement	100	µL	
	- $MgCl_2$, 2 M	50	µL	
	- $NaHCO_3$, 8.4 %	50	µL	
PPM+ for *Nm*-GFP	- PPM+	10	mL	
	- Erythromicin, 50 mg/mL	1,4	µL	

2.6.3. Buffers and solutions

Table 11. Overview of the solutions used and their composition.

Solutions	Components	Mixture		Comments
FACS Buffer (Flow Cytometry)	- PBS	95	%	
	- FCS	5	%	
2X Stop Mix (Western blot)	- 0.5 M Tris-HCl pH = 6.8	14	mL	Add β-Mercaptoethanol last, under a fume hood.
	- Glycerin 100 %	11.2	mL	
	- 20 % SDS	11.2	mL	
	- H_2O	9.8	mL	
	- β-Mercaptoethanol	3.43	mL	

Table 11. Overview of the solutions used and their composition. (continued)

Lysis Buffer (Western blot)	- 0.5 M Tris-HCl pH = 6.8	10	mM	Store at 4°C. Use cold.
	- NaCl	100	mM	
	- EDTA	1	mM	
	- Glycerol	10	%	
	- Triton-X 100	1	%	
	- SDS	0.1	%	
	- Sodium deoxycholate	0.5	%	
	- Na_3VO_4	2	mM	
	- NaF	50	mM	
	- Pefabloc	50	µg/ml	
	- Proteaseinhibitor	1	Tabl/mL	
Lysis Buffer (PCR)	- RA1 Buffer	0.1	mL	Mix and use fresh
	- β-Mercaptoethanol	1	µL	
Stacking gel (Western blot)	- 0.5 M Tris-HCl pH = 6.8	1.25	mL	
	- 20 % SDS	25	µL	
	- 16 % APS	30	µL	
	- TEMED	5	µL	
	- Rotiphorese® Gel 30	0.7	mL	
	- H_2O	3	mL	
Separating gel (Western blot)	- 1.5 M Tris-HCl pH = 8.8	2.5	mL	Rotiphorese® Gel 30 and H_2O volumes depends on desired final gel %
	- 20 % SDS	50	µL	
	- 16 % APS	60	µL	
	- TEMED	10	µL	
	- Rotiphorese® Gel 30	x	mL	
	- H_2O	x	mL	
PBS/T (Western blot)	- PBS	500	mL	
	- Tween 20	0.5	mL	
Blocking solution (Western blot)	- Skim milk	5	%	
	- PBS/T	95	%	
10X SDS	- Glycin	144	g	Add distilled water to fill up 1 L.
	- Tris	30	g	
	- SDS	10	g	
1X SDS (Western blot)	- 10X SDS	10	%	
	- PBS	90	%	

Table 11. Overview of the solutions used and their composition. (continued)

Transfer Buffer (Western blot)	- Glycin - Tris - Methanol	14.4 3 20	g g %	Add distilled water to fill up 1 L. Re-use up to 3x
Blocking Buffer (Immunofluorescence)	- PBS - Serum	90 10	% %	Serum = FCS or goat serum
DAPI (Immunofluorescence)	- DAPI, 5 mg/mL - PBS	- -	µL mL	Directly dilute DAPI 1: 50,000 in PBS
Dispase (Cell Culture)	- Dispase - DMEM/F-12 w/o L-Glutamin	2	mg/mL	Prepare fresh, sterile filter

2.7. Laboratory equipment and materials

Table 12. Overview of the consumables used.

Consumables	Manufacturer / Supplier
5PRIME Phase Lock Gel Heavy tubes	Quantabio (USA)
Blotting Membrane (Nitrocellulose)	GE Healthcare Life Sciences (D)
Blue Protein Standard Broad Range	New England Biolabs GmbH (D)
Columbia Agar (with 5 % sheep blood)	bioMérieux Deutschland (D)
Cell culture flasks	Sarstedt AG & Co. KG (D)
Cell culture inserts, 12-well format	Corning Inc. (USA)
Cell culture inserts, 24-well format	Greiner Bio-One GmbH (D)
Cell culture multi-well plates, *Nunclon Delta Surface*	ThermoFisher Scientific (D)
Cell density meter cuvettes	Sarstedt AG & Co. KG (D)
Chambered coverslip slides	Ibidi GmbH (D)
Conical tubes	Greiner Bio-One GmbH (D)
Electrode STX3	Merck Millipore (D)
FACS tubes	Corning Inc. (USA)
Hemocytometer (Neubauer chamber)	Karl Hecht GmbH & Co KG (D)
Mini-PROTEAN Tetra Systems	BioRad (D)
Multiwellplate for Fluorescence (black, flat bottom)	ThermoFisher Scientific (D)
Multiwellplate for Fluorescence (standard)	Sarstedt AG & Co. KG (D)
qRT-PCR Adhesive Films	Applied Biosystems (D)
qRT-PCR Plates	Applied Biosystems (D)
Serological pipets 5 mL, 10 mL, 25 mL (plastic)	Sarstedt AG & Co. KG (D)

Table 12. Overview of the consumables used. (continued)

Sterile filters (0.2 µm pore size)	Sarstedt AG & Co. KG (D)
Serynges	Sarstedt AG & Co. KG (D)
Whatman paper	GE Healthcare Life Sciences (D)

Table 13. Overview of the equipment used.

Equipment	Manufacturer / Supplier
Analytical balance PT120	Sartorius AG (D)
BZ-9000 BIOREVO System Microscope	KEYENCE Deutschland GmbH (D)
ChemiDoc™ MP Imager	BioRad (D)
Centrifuge Megafuge 1.0R	Kendro Laboratory Products GmbH
Centrifuge CT15RE	VWR (USA)
CERTOMAT® Shaking incubator	B. Braun Biotech International GmbH (D)
CO8000 Cell Density Meter	Biochrom GmbH (D)
Eclipse Ti Inverted Microscope	Nikon GmbH (D)
FACSAria III	BD Biosciences (D)
FACSCalibur	BD Biosciences (D)
Infinite F200 Pro Reader	Tecan Deutschland GmbH (D)
LabGard NU-437S Class II Biosafety Cabinet	Nuaire Limited (UK)
LSM 780 microscope	Carl Zeiss AG (D)
MAGPIX® Luminex reader	BioRad (D)
Millicell ERS-2	Merck Millipore (D)
Multiskan EX Reader	ThermoFisher Scientific (D)
Nanodrop ND-1000	Peqlab Biotechnologie GmbH (D)
Pipetboy Accu-jet Pro	Brand GmbH + Co. KG (D)
Pipettes Research Plus	Eppendorf Vertrieb Deutschland GmbH (D)
ProtoCOL Colony Counter	Meintrup DWS Laborgeräte GmbH (D)
Safe 2020 Class II Biological Safety Cabinet	ThermoFisher Scientific (D)
Standard Power Pack P25 Power Supplier	Biometra GmbH (D)
StepOnePlus qRT-PCR Thermocycler	ThermoFisher Scientific (D)
Thermoshaker	Eppendorf Deutschland (D)
T3000 PCR Thermocycler	Biometra GmbH (D)

2.8. Software (Data Analysis)

Table 14. Overview of the software used for data analysis.

Software	Version	Use	Supplier
FlowJo	X 10.0.7r2	Flow Cytometry	FlowJo (USA)
GraphPad Prism 6	6.01	Data presentation	GraphPad Software, Inc. (D)
Fiji (ImageJ)	version 1.2h	Microscopy/WB	National Institutes of Health (USA)
ZEISS	2.3 blue edition	Confocal Microscopy	Carl Zeiss Microscopy GmbH (D)

3. Methods

3.1. Cell culture techniques

All sterile work presented in this dissertation was performed in class II safety workbenches. Prior to use, all sterile solutions were sterile filtered. Autoclaving or hot air sterilization was done for all reused materials. Culture of mammalian cells and *Nm* strains took place in incubators that provided a relative humidity of 95 %, constant temperature of 37 °C and 5 % CO_2.

3.1.1. Culture of HBMECs

The EC line HBMEC was used as a positive control in gentamicin protection assays and Luminex bead-based multiplex assays. These cells were cultured in flasks or well plates coated with 0.1 % gelatin in PBS, until the 25th passage. Medium change was performed every 2 to 3 days and cell passaging was done with Trypsin-EDTA once the cells reached about 80 % of confluence.

3.1.2. Culture of human iPSCs

The following section describes feeder-free, adherent culture of iPSC line IMR90-4. iPSCs were cultured using the mTeSR™1-Matrigel™ system according to WiCell's feeder-independent stem cell protocols or using the Stem™Flex-Matrigel™ system.

3.1.2.1. Matrigel™ coating

To ensure optimal adhesion and culture of iPSCs, multiwell plates (Nunclon™delta Surface, or Sarstedt) and T75 flasks (Sarstedt) were coated using Matrigel™. As Matrigel™ rapidly forms a gel at room temperature (RT), all work was performed quickly and on ice. Matrigel™ aliquots (2.5 mg) were thawed on ice and resuspended with 30 mL of DMEM/F-12 without L-glutamine in a 50 ml centrifuge tube. After total resuspension, 1 mL of mix was distributed per well of a 6-well plate while 12 mL of mix was distributed per T75 flask. An additional 1 mL of DMEM/F12 was added per well of a 6-well plate to prevent drying. Plates and flasks were stored at 37°C in an incubator overnight (O/N), or until ready for use for up to two weeks. Every week, 0.5-1 mL of fresh DMEM/F12 were added to wells of coated 6-well plates to avoid drying.

3.1.2.2. Media change of human iPSCs

iPSCs were checked daily to control for confluency and spontaneous differentiation. Daily medium changes with mTeSR™1 medium were performed by aspiring spent medium with Pasteur pipettes and adding 2 mL or 12 mL of fresh medium to cells seeded onto 6-well plates or T75 flasks, respectively. To minimize the risk of contamination, one pipette per 6-well plate and per flask was used. As an alternative to mTeSR™1, Stem™Flex medium was also used following exactly the same instructions. Cells supplied with fresh mTeSR™1 or Stem™Flex medium were placed in the incubator and media change was performed the next day in the same time window of ± 2 h.

3.1.2.3. Passaging of human iPSCs

Passaging of iPSCs was done through detachment with Dispase or Versene once undifferentiated iPSC colonies reached 80 % confluence (typically 3–5 days after passage). Dispase detachment was done by adding 2 mL/well of 2 mg/mL freshly prepared Dispase solution, resuspended with RT DMEM/F-12 w/o L-glutamine after aspiration of spent medium. Following approximately 7 min of incubation, cells were checked microscopically for assessment of detachment progression. Once the edges of the colonies began detaching, the enzyme incubation was stopped by aspirating the Dispase solution and gently rinsing with DMEM/F-12 without L-glutamine 3 times. Versene detachment was done by adding 1 mL/well of cold Versene solution, incubating the cells for exactly 7 min, and subsequently aspirating Versene from wells. By gently spraying 1 mL of mTeSR™1 over the cells with a 1000 µL pipette, and spraying the plate again for several times, cells were released from the well bottom, collected and pooled into a 50 mL conical tube. The cells were then seeded at a ratio of 1:6 or 1:12 onto new Matrigel™-coated 6-well plates in 2 mL/well of mTeSR™1 or Stem™Flex medium. Cells cultured with mTeSR™1 required the addition of ROCK inhibitor Y27632 (apoptosis inhibitor) for 24 h at a concentration of 10 µM for cell survival. Homogeneous distribution and adhesion of the cells in the wells was ensured by shaking back-to-forth, then left-to-right, and then pausing for 3 s, for a total of three cycles.

3.2. Differentiation of human iPSCs into BECs

IMR90-4 iPSC cells were differentiated according to previously published methods, as illustrated in **Figure 7** (Appelt-Menzel et al., 2017, 2018; Lippmann et al., 2012, 2014; Stebbins et al., 2016; Wilson et al., 2015).

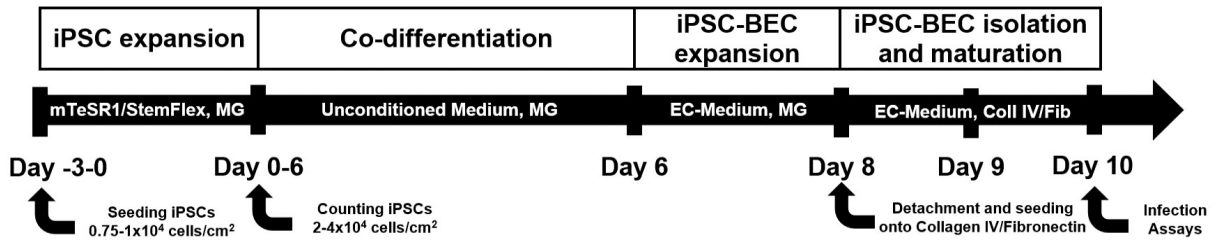

Figure 7. Schematic representation of the protocol for differentiation of human iPSCs into BECs.

Differentiation takes usually 10 days and starts with expansion of single iPSCs for 3 to 4 days in Matrigel™. Once iPSC colonies reach the appropriate density, medium is changed to Unconditioned Medium ('UM phase'). After six days in UM, medium is changed to EC medium supplemented with RA and hbFGF ('EC phase'), which targets the expansion and maturation of the BEC population amongst other cell types that are present (e.g. neural progenitors). By subculturing onto collagen IV and fibronectin-coated cell culture surfaces on day 8 of the differentiation, iPSC-BECs are selected and purified. Abbreviation: Matrigel™ (MG), Collagen (Coll), Fibronectin (Fib).

3.2.1. Seeding of singularized iPSCs and expansion for BEC differentiation

Prior to BEC differentiation, iPSCs require to be seeded as single cells at a defined cell density. For this purpose, Accutase® solution was used for enzymatic detachment of the cells from the culture surface and for cell singularization. Cells were incubated at 37 °C for approximately 7 min with 1 mL of cold Accutase per well. The cells were then collected and gently sprayed over the surface 2–3 times with a 1000 µL pipette. Cells were diluted 5x with mTeSR™1 or Stem™Flex medium, spun down for 5 min at 1000 rpm and resuspended in 1 mL of medium. Cells were counted using a hemacytometer and seeded at a density of 7,500–10,000 cells/cm^2 in 6-well plates or T75 flasks. Medium was supplemented with 10 mM of ROCK inhibitor Y27632 prior to seeding. Stem cells treated with ROCK inhibitor present a spread, mesenchymal-like morphology, however, approximately 24 h later (i.e., D-2) the medium is renewed and ROCK inhibitor is removed, causing the cells to grow as round-shaped colonies without cell processes.

3.2.2. UM phase/EC phase: Induction of BEC/neural co-differentiation

Differentiation is induced by changing the medium composition to Unconditioned Medium once the cells reach cell densities of 2-4x10^4 iPSCs/cm^2. For this, inspection of the cell density by light

microscopy and/or cell counting were done. Once UM is added, daily medium changes are carried out until day 6 of the differentiation process. UM induces co-differentiation of BECs and neural cells, therefore, isolation of BECs is further required. At day 6, medium is changed to EC medium supplemented with 20 mg/mL of hbFGF and 10 µM of RA, and left for 48 h.

3.2.3. BEC subculturing and maturation

BECs are isolated from neighboring cells by splitting and seeding onto collagen IV/fibronectin-coated surfaces at day 8 of the differentiation protocol. To this end, Accutase treatment for at least 30 min at 37°C is performed and cells are sprayed over the surface several times until complete detachment. Single cells are spun for 5-7 min, resuspended in EC medium with RA and hbFGF, and counted. For seeding into transwell systems, cells were seeded at a cell density of $1x10^6$ cells/cm^2, while for standard tissue culture plates and ibidi slides, cell density could be reduced to $0.5x10^6$ cells/cm^2. To distribute the cells evenly, plates were shaken back-to-forth, then left-to-right, and then pausing for 3 s, for a total of 3 cycles. After 24 h (i.e., D9), spent medium and floating cells were removed and hESFM + 1% PDS (without hbFGF or RA) was added.

3.3. Culture of *Neisseria meningitidis* strains

Nm strain MC58 was used as a representative strain of the *Nm* species (see **Table 2** for further information on all meningococcal strains used). Meningococci were cultured on Columbia Agar plates with 5 % sheep blood and incubated at 37 °C with 5 % CO_2 O/N. Subsequent liquid culturing was performed in PPM plus 1 % Kellogg's supplement I and II (i.e. PPM+ medium, see **Table 10**).

3.4. Infection of cells with *Neisseria meningitidis*

The medium of confluent iPSC-BECs at day 10 of differentiation was changed to hESFM medium supplemented with 10 % human serum (HS). Cells were infected with *Nm* strains with a Multiplicity of Infection (MOI) of 10 (unless specifically noted) and without any medium changes thereafter. MOI were calculated assuming 200,000 attached iPSC-BECs per well of a 48-well plate. Infection and bacterial growth were carried out as described in (Kim and Schubert-Unkmeir, 2019).

Bacteria grown O/N in solid culture were resuspended in 10 mL of PPM+ medium and incubated in a shaker at 37 °C, 200 rpm for 60 to 90 min. Bacteria concentration was estimated by OD_{600} measurements. Bacteria or PPM+ medium alone (i.e. mock-infected controls) were then inoculated into differentiated iPSC-BEC monolayers. Infection was carried out at 37 °C and 5 % CO_2 to a maximum of 32 h.

3.5. Gentamicin Protection Assays

Gentamicin protection assays were done to determine numbers of intracellular bacteria per cell monolayer in duplicate or triplicate wells per condition. Cells were grown in 48-well plates and infected with *Nm* at an MOI of 10 in the presence of RPMI (HBMECs) or hESFM (iPSC-BECs) medium, plus 10 % HS. After the selected infection time point, the supernatant was removed and transferred to a 1.5 mL cap. For adhesion assessment, the cells were washed once with RPMI/hESFM, and 100 µL of RPMI/hESFM plus 1 % saponin was added per well. Following 15 min of incubation at 37 °C and 5 % CO_2, cells were scrapped several times with a pipette tip and transferred to a 1.5 mL cap. For invasion assessment, the medium was removed and cells were washed once. Then, 0.5 mL of gentamicin solution (200 µg/mL in RPMI or hESFM) was added per well, and the cells were incubated for 2 h at 37 °C and 5 % CO_2. Following this incubation period, the cells were washed once, and 100 µL of 1 % saponin solution was added per well. The cells were then incubated and scrapped as described above. For determination of adherent bacteria, dilution series up to -5 were performed and 100 µL of dilutions -3/-4/-5 were plated into blood agar plates for O/N incubation at 37 °C and 5 % CO_2. The same applied for assessing bacteria numbers in the supernatant (optional). For determination of invasive bacteria, dilution series up to -3 were performed and 100 µL of dilutions -1/-2/-3 were plated into blood agar plates. For low invasive strains (e.g. 8013/12) direct plating into blood agar plates was tested and lead to optimal results. The number of adherent/invasive colony forming units (CFUs) per cell monolayer was then determined.

3.6. Immunofluorescence and Microscopy

iPSC-BEC monolayers seeded onto 8-well ibidi µ-Slides were washed 3 times with PBS and fixed with ice-cold methanol or 3.7 % PFA for 15 min. After washing, PFA-fixed cells were permeabilized with 0.1 % Triton-X 100 in PBS for 15 min. Washing was followed by blocking in 10 % FCS or 10 % goat serum (depending on the chosen secondary antibody) in PBS for 1 h at RT. Incubation with primary antibodies was performed O/N at 4 °C. After washing, incubation with secondary antibodies was done at RT for 1 h. A list of all the used antibodies is provided in **Table 4**. Confocal microscopy images were acquired with a Zeiss LSM 780 microscope. ZEN software (version 2.3) was used for image analysis.

3.7. Trans-endothelial Electrical Resistance Measurements

At day 10 of differentiation the electrical resistance of iPSC-BECs was measured using a Millicell ERS-2 instrument and a STX3 electrode at 12.5 Hz. Cells seeded onto 0.4 µm inserts were used for assessment of TEER as a measure of barrier strength and quality of the differentiation batch. Measurement was performed by sterilizing the electrode in 70 % ethanol solution for 30 s, followed by air-drying, and directly placing the electrode inside the inserts, without any previous medium change. After measuring, the electrode was placed in 70 % ethanol for 2-5 min, and air-dried. The medium was then changed to hESFM + 1 % PDS for assays where the TEER profile was followed during infection. For these experiments, TEER was measured in triplicate inserts for each experimental condition. To determine the TEER value ($Axcm^2$) of BECs, the measured raw resistance value was multiplied by the insert culture area (1.1 cm^2) to obtain the TEER value and the TEER of an empty, non-cell-populated but collagen IV/fibronectin-coated insert (i.e. blank insert) was subtracted.

3.8. Paracellular Permeability Studies

The transport coefficient (Pe) of sodium fluorescein (Na-Fluorescein) was determined as a measure of paracellular permeability of BEC monolayers. Inserts with pore size of 0.4 µm were used to

follow transport from the apical to the basolateral chamber at pre-determined time points, according to the method published by (Stebbins et al., 2016). Na-Fluorescein (10 µM) was diluted in hESFM + 1 % PDS. To determine clearance slopes and Pe values, blank, collagen/ fibronectin-coated inserts were included in the experiment. The experiment was done in triplicate for all conditions (mock controls, infected inserts and blank inserts). TEER was measured before medium renewal at day 10 of differentiation and infection was carried out until the selected time points. At 24 h and 32 h p.i., the medium from the apical compartment was removed and replace with 0.5 mL of Na-Fluorescein solution in all samples and blank inserts. At 15, 30, 45, and 60 min, 150 µL was collected from the bottom chamber and placed into a black, flat bottom 96-well plate. Before collecting the 150 µL of basolateral medium, homogenization by pipetting gently up and down 2-3 times with a p200 was done. The missing volume was replaced with 150 µL pre-warmed cell culture medium into the bottom chamber. At the 60 min time point, an additional 150 µL from the top chamber was collected and transferred to the 96-well plate. Additionally, 150 µL of EC medium without Na-Fluorescein was pipetted in one well of the 96-well plate for background subtraction. Finally, fluorescence was measured in a TECAN Infinite M200 reader (485 nm excitation/530 nm emission). Clearance slopes and Pe values were calculated as described in (Stebbins et al., 2016).

3.9. Bacterial Transmigration Assays

Inserts with pore size of 3 µm that allow bacterial passage were used for bacterial transmigration studies. At each mentioned time point, inserts were washed with PBS and moved to fresh pre-warmed EC medium for 30 minutes. Homogenization by pipetting gently up and down 2–3 times with a p100 was done, after which 100 µL of bottom basolateral medium were plated into 5 % sheep blood agar plates for counting of colonies, in duplicate for each insert. The missing volume was replaced with 200 µL pre-warmed cell culture medium into the bottom chamber. For the 24 h time point, 1:10; 1:100 and 1:1000 dilutions of the collected medium were plated for MC58, while direct plating without dilution was done for MC58Δ*siaD*. Blood agar plates were incubated O/N at 37 °C and 5 % CO_2, and colonies were counted the next day (method adapted from (Coureuil et al., 2009; Sutherland et al., 2010)). The limit of detection of the technique was determined by multiplying the minimum CFU possible to be measured on agar plates (15 CFU per 1.5 mL of

basolateral medium) by the minimum CFU number recommended for usage in spread plate protocols for CFU enumeration by the American Society for Microbiology (Wise, 2006).

3.10. Flow Cytometry

iPSC-BECs were grown in 48-well plates and 250 µL of Accutase was added to detach cells. Once cells were completely detached, 500 µL of medium was added and cells were transferred to a 1.5 mL cap. Cells were spun down for 3 min at 1300 rpm and the supernatant was discarded. All further steps were done on ice. The pellet was dissolved in 500 µl FACS buffer, and after spinning down the cells for 2 min at 2500 rpm and 4 °C, the supernatant was discarded and the pellet was dissolved in 100 µL of FACS buffer. Primary antibodies or isotype controls were added and incubated 1 h 30 min on ice. Samples were spun for 2 min at 2500 rpm and 4 °C and washed for 2-3 times with FACS buffer. The pellet was dissolved in 500 µL of FACS buffer and secondary antibodies were added (dilution 1:400-1:500). After incubating 30 min on ice in the dark, samples were spun, resuspended in FACS buffer and washed 2 more times. For measuring surface expression, the samples were resuspended in FACS buffer, transferred to FACS tubes, and analyzed in a FACSCalibur instrument from BD Biosciences.

3.11. Western Blot

iPSC-BEC monolayers were grown in 48-well plates and washed with ice-cold PBS 3 times at specific infection time points, then total protein lysates were collected with 50 µL/well lysis buffer (10 mM Tris-HCL pH 6.8, 100 mM NaCl, 1 mM EDTA, 10 % Glycerol, 1 % Triton-X100, 0.1 % SDS, 0.5 % sodium deoxycholate, 2 mM Na_3VO_4, 50 mM Sodium Fluoride, 50 µg/ml Pefabloc and protease inhibitors). Protein lysates were vortexed and incubated for 30 min on ice, then centrifuged for 20 min at 12 000 g and 4 °C. Supernatants were collected and stored at -20 °C. Total protein concentration in the supernatant of all samples was determined via DC protein assay (Bio-Rad). For the calibration curve, bovine serum albumin (BSA) standards with concentrations 50, 100, 200, 400, 600, 800, 1000 and 1200 µg/ml were used. Working solution was done by mixing Reagent A and B (provided in the kit, **Table 3**) in a ratio of 50:1, which was added to all samples

and standards (200 µL of working solution plus 10 µL of sample of unknown concentration or standard). The mixtures were pipetted into wells of a 96-well plate and incubated for 30 min at 37 °C. Absorption was measured at 562 nm in a Multiskan EX Reader. Samples were then diluted with 2X Stop Mix (**Table 11**) for a final concentration of 0.5 or 0.65 µg/µL of protein for all samples of the same replicate experiment, depending on the protein amount collected. The samples were heated for 10 min at 95 °C in a heating block and spun down after heating.

Proteins were separated electrophoretically in 1X SDS buffer (**Table 11**) using acrylamide SDS-gels (6 % for ZO-1, and 12 % for β-Actin, Occludin, Claudin-1, Claudin-5, and COX IV) for 1 h 30 min and current of 160 V with a Standard Power Pack P25 power supplier. Acrylamide SDS-gels were prepared using the reagents mentioned in **Table 11**, using the Mini-PROTEAN Tetra Systems from BioRad. Once the gels were ready, 5 µL of protein ladder and 10 to 25 µg of protein/well were pipetted, depending of the maximum loading volume per well of the system, and the protein of interest to be detected.

Following electrophoretic separation, proteins were transferred to a Whatman® nitrocellulose membrane using the Mini-PROTEAN Tetra System. To this end, wet transfer was carried out in a standard 'sandwich' system where the nitrocellulose membrane was placed beneath the gel and in between four sheets of Whatman paper. During this process, all components were soaked in Western blot buffer and the formation of bubbles was avoided. Protein transfer was then carried out using a current of 350 mA for 1 h to 1 h 30 min. The blot process was successful when the transfer of the markers to the membrane could be visualized. The membranes were then blocked with 5 % milk powder solution diluted in PBS/T, for 1 h, and washed with PBS/T 3 times for 10 min. Antibody staining was performed by incubating the membranes with primary antibodies against the desired proteins, diluted in 10 mL of 5 % milk powder in PBS/T, on a shaker O/N at 4 °C. The following day, the membranes were washed with PBS/T 3 times for 10 min and incubated with HRP-coupled secondary antibodies diluted in 10 mL of 5 % milk powder solution in PBS/T at RT for 1-2 hours. Following a final washing step, the Pierce™ ECL Western Blotting Substrate detection system was used to visualize the immunoreactive bands. The developer solution, consisting of 1 mL Peroxide Reagent and 1 mL Luminol/Enhancer Reagent, was mixed and added on top of the blot. The developed blot was acquired using the ChemiDoc™ MP Imager from BioRad and integrated software.

3.12. Quantitative RT-PCR

To investigate the gene expression of particular iPSC-BEC genes, isolation of RNA was performed, which was transcribed into cDNA by reverse transcriptase reaction, amplified by means of qRT-PCR, and analyzed. Contamination of samples, reagents, and materials with foreign RNA and DNA was prevented by wearing gloves during all steps, and cleaning all surfaces before working. All centrifugation steps were performed for 1 min at 11 000 g, unless otherwise specified.

3.12.1. RNA isolation

The isolation of RNA of iPSC-BEC monolayers was carried out using the NucleoSpin kit by Macherey-Nagel. Monolayers grown in 48-well plates were lysed with 350 µL Lysis Buffer RA1 supplemented with 3.5 µL ß-mercaptoethanol. The lysates were stored at -20 °C until isolation of the RNA. RNA isolation was initiated when 350 µL of 70 % ethanol was added to each sample, and mixed by vortexing. The lysate was pipetted up and down 2–3 times and loaded to a NucleoSpin® RNA Column placed in a collection tube. The column was spun down and the collection tube was discarded. Then, 350 µL of MDB (Membrane Desalting Buffer) was added to dry the membrane, placed in a new collection tube. The column was spun down and rDNase digestion was followed to remove contaminating DNA. DNase reaction mixture was prepared by adding 10 µL of reconstituted rDNase to 90 µL Reaction Buffer for rDNase, per sample. Then, 95 µL DNase reaction mixture was added directly onto the center of the silica membrane of the column and incubated at RT for 15 min. The silica membrane was then washed and dried by adding 200 µL of Buffer RAW2 and centrifuging, to inactivate the rDNase. A second wash step was performed by adding 600 µL of Buffer RA3 to the column, centrifuging and placing the column back into the collection tube. A final wash step was done by adding 250 µL of Buffer RA3 to the column and centrifuging for 2 min at 11 000 g to dry the membrane completely. To elute the RNA, the column was placed into a nuclease-free tube, 20 µL of RNase-free H_2O was added to the center of the column, and the column was centrifuged. The isolated RNA was then directly converted into cDNA.

3.12.2. cDNA synthesis

Prior to cDNA synthesis, it was necessary to measure the RNA concentration of the samples using a Nanodrop ND-1000 instrument. The pedestal was cleaned, and blanking was done using 2 µL of RNase-free water. The measurement of the RNA content at 260 nm and 280 nm allowed the estimation of the degree of possible contamination of the sample with proteins and DNA.

For cDNA synthesis, the SuperScript™ VILO kit was used, where 500 ng of RNA were added to 4 µL of 5X VILO™ Reaction Mix and 2 µL of 10X SuperScript™ Enzyme Mix plus RNase-free water to give a final volume of 20 µL. The cDNA synthesis was carried out in the thermocycler according to the protocol listed in **Table *15***. The cDNA samples were stored at – 20°C until qRT-PCR.

Table 15. Temperature protocol for cDNA synthesis on a thermocycler.

Temperature (°C)	Time (min)	Reaction
25	10	Annealing of the primer
42	60	Elongation of the cDNA
85	5	Enzyme deactivation
4	∞	Storage of the cDNA

3.12.3. qRT-PCR reaction

qRT-PCR was used to measure gene expression of specific target genes through cDNA amplification and quantification by measurement of fluorescence at the end of each amplification cycle. SYBRGreen Supermix (BioRad) and Taqman (ThermoFisher Scientific) were used for qRT-PCR, depending on the target gene. When using SYBRGreen, both the forward and reverse primers were stored at a concentration of 10 µM, while a working stock was used with dilute concentrations of 1:10 with ultrapure water. TaqMan probes were used for detection of *TJP1* (ZO-1), *CLDN5* (Claudin-5), *OCLN* (Occludin), *CCL5* (RANTES), *IFNG* (IFN-γ), *VEGFA*, *TNFAIP2* and *18S*. All samples were pipetted in duplicates in a PCR 96-well plate in a total volume of 20 µL (**Table 16**). Quantitative PCR data was collected with a StepOnePlus RT-PCR

thermocycler. Data are presented as fold change over *18S* using the cycle threshold (ΔΔCT) calculation.

Table 16. Reagents and volumes per well for SYBRGreen and Taqman qRT-PCR reactions done in 96-well plates.

SYBRGreen		**Taqman**	
Reagent	**Volume**	**Reagent**	**Volume**
Forward Primer	0.4 µL	20X Gene Expression Mix	1 µL
Reverse Primer	0.4 µL	2X Taqman Master Mix	10 µL
SYBRGreen Supermix	10 µL	cDNA	2 µL
cDNA	0.8 µL	H_2O	7 µL
H_2O	8.4 µL	-	

3.13. Cytokine/chemokine Multiplex Bead Assays.

Supernatants of iPSC-BEC monolayers of mock controls or cells infected with MC58, MC58Δ*siaD* and 8013/12 at 2, 4, 6, 8 and 24 h p.i were collected and frozen at -20°C until the day of the assay. Supernatants were tested for IL-1β, IL-6, IL-8, Gro-α, Gro-β, GM-CSF, TNF-α, IFN-γ, VCAM-1, ICAM-1, E-selectin, vWF-A2, MCP-1 and RANTES presence using a customized anti-human cytokine Luminex Multiplex Assay (R&D Systems). Briefly, reagents including standard cocktails and microparticle cocktail solutions were brought to RT and reconstituted with the respective diluent solution. For the standard cocktails, a dilution series was performed, according to manufacturer's instructions. For supernatant samples, a 1:2 dilution with wash buffer was performed. A volume of 25 µL of the diluted microparticle cocktail was added to each well of the microplate, followed by 25 µL of standard or sample per well and 50 µL of wash buffer to fulfill 100 µL of liquid. The mixture was incubated for 2 h at RT on a horizontal orbit microplate shaker set at 800 ± 50 rpm. Then, a magnetic device designed to accommodate the microplate was used for washing by applying the magnet to the bottom of the microplate and removing the liquid by pipetting. Washing was done by adding 100 µL of wash buffer and removing the liquid 3 consecutive times. Diluted biotin antibody cocktail was then added to each well (25 µL of cocktail plus 25 µL of wash buffer) and incubation for 1 h at RT on a shaker set at 800 ± 50 rpm was

followed. After washing, diluted Streptavidin-PE solution was added to each well and incubation for 30 min at RT on a shaker was done. After washing, the microparticles were resuspended by adding 100 µL of wash buffer to each well and incubating for 2 min on a shaker. The Luminex analyzer was then used for reading of the samples. Baseline levels of all targets present in infection medium alone (hESFM supplemented with 10 % HS) were subtracted from sample measurements for data analysis.

3.14. RNA-Sequencing.

3.14.1. FACS, RNA extraction and DNase treatment.

iPSC-BECs seeded onto 6-well plates were infected with GFP-expressing MC58 in hESFM + 10 % HS for 2, 4, 8 and/or 24 h p.i., for 3 independent experiments. Cells were dissociated using Accutase for at least 20 min at 37 °C and detached cells were centrifuged at 1200 rpm for 5 min. Cells were resuspended in RNAlater® solution (Qiagen) supplemented with 200 µg/mL gentamicin for safety purposes and stored at 4 °C until the sorting day. Cells were pelleted (250 g, 5 min at RT) and resuspended in 300 to 1500 µL of ice-cold PBS for sorting. Cells were analyzed and gated based on their size and complexity (FSC and SSC), and sorted into GFP-negative and GFP-positive sub-populations using a FACSAria III device (BD Biosciences) at 4 °C and using a 100 micron nozzle, as previously described (Westermann et al., 2016). Fractioned cells were lysed by resuspension in TRIzol and RNA was precipitated through the TRIzol method. Briefly, resuspended cells and chloroform (0.2 mL/mL) were added to 5PRIME Phase Lock Gel Heavy tubes (Quantabio). The tubes were spun at 12 000 g for 15 min at 4 °C. Isopropanol (1 volume) and GlycoBlue (1-2 µL) were added to the obtained aqueous phase and the mixture was incubated at -20 °C O/N. The mixture was then spun for 30 min at full speed and the pellet was rinsed with cold 70-75 % ethanol. After air-drying for 10 min, the pellet was dissolved in RNase-free water by 5 min of incubation at 65 °C and 850 rpm on a thermoshaker. DNase I digestion (Fermentas) was carried out as described in **Table 17** for an incubation period of 30-45 min at 37 °C. Total RNA was precipitated by phenol-chloroform extraction followed by ethanol precipitation. Dnase I was removed by phenol-chloroform extraction. The reaction volume was adjusted to 100 µL by addition of 50 µL of dH_2O to each tube. A volume of 100 µL of Roti-P/C/I was added to 2 mL Phase-Lock tubes, followed by the Dnase I-digested RNA samples. The tubes were shaken for 15 s for proper

homogenization, followed by centrifugation for 12 min at 4 °C and 16 000 g. The upper phase was transferred to a fresh 2 mL Eppendorf tube and RNA was precipitated. Briefly, 2.5 volumes of 30:1 RNA precipitation mix (EtOH: 3 M NaOAC, pH 6.5) and Glycoblue were added to the aqueous fraction containing DNA-depleted RNA and precipitation was performed as described above. Nanodrop was used to measure RNA concentration prior to DNase I treatment and at the end of the isolation protocol.

Table 17. Reagents and volumes per samples of total RNA used for DNase I digestion reaction.

Reagent	Volume (µL)
10X Dnase I buffer (containing $MgCl_2$)	5
Rnase Inhibitor (20 U/µL)	0.5
Dnase I (1 U/µL)	5
Sample (RNA)	Up to 39.5

3.14.2. mRNA enrichment, cDNA library generation and RNA-Sequencing.

After total RNA isolation, mRNA enrichment and cDNA library generation was outsourced to the company Vertis Biotechnologie AG. RNA-Sequencing was then performed at the CoreUnit SysMed (Institute for Molecular Infection Biology, University of Würzburg, Würzburg, Germany). From the total RNA preparations, first-strand cDNA was synthesized using an oligo$(dT)_{25}$ primer. After fragmentation, the Illumina TruSeq sequencing adapters were ligated in a strand-specific manner to the 5' and 3' ends of the cDNA fragments. The cDNA was amplified by PCR using a proof reading enzyme and the primers used for PCR amplification were designed for TruSeq sequencing according to the instructions of Illumina (the combined length of the flanking sequences was 136 bases). The final cDNA samples were analyzed on a Shimadzu MultiNA microchip electrophoresis system. For Illumina sequencing, cDNA libraries samples were pooled in equimolar amounts. The cDNA pools were size fractionated in the size range of 200–600 bp using a differential clean-up with the Agencourt AMPure kit. An aliquot of the size-fractionated cDNA pool was analyzed by capillary electrophoresis. Sequencing was performed on a NextSeq500 platform (Illumina) in single-end mode, for 75 cycles.

3.14.3. Computational analysis of RNA-Seq data.

Illumina reads were initially quality trimmed with a Phred quality score cut-off of 20 and afterwards the adapter sequences were removed. Both trimming steps were done by Cutadapt version 1.17 (Martin, 2011). For the poly(A) trimming, size filtering and mapping, the RNA-Seq analysis tool READemption version 0.4.3 (Förstner et al., 2014), which integrates the short read mapper segemehl (Hoffmann et al., 2009), was used. Before mapping, poly(A) sequences were clipped from the reads. Afterwards, all reads that had a length shorter than 20 nucleotides were discarded. The remaining reads were mapped, using segemehl's split align feature, to the genomes of *Nm* MC58 (NCBI RefSeq accession number: NC_003112.2; as an additional quality control) and human (GENCODE release 28: GRCh38.p12). Reads with an accuracy equal or greater than 95 % were kept for further analysis. Segemehl's realigner lack (Otto et al., 2014) was used for remapping reads that previously could not be mapped due to multiple splice events. For the human-mapped reads, gene quantification was carried out by READemption (Förstner et al., 2014) and differential gene expression analysis was performed using DESeq2 version 1.20.0 (Love et al., 2014). Coverage files in wiggle (WIG) format were produced by READemption in a strand-specific manner and normalized by the total number of aligned reads per organism multiplied by 1 million.

3.15. Statistics.

GraphPad Prism was used for statistical significance, for which a *P*-value of less than 0.05 was accepted. Student´s t test was used for two-group comparisons. ANOVA was used for three-group comparisons.

4. Results

4.1. Differentiation and Characterization of iPSC-BECs

BECs are essential components of the meningeal b-CSF barrier and BBB, and are thought to be the first barrier that *Nm* faces before infecting the meninges. Here, BECs were differentiated from iPSCs according to previously described methods (**Figure 7**) (Appelt-Menzel et al., 2017; Lippmann et al., 2012, 2014; Stebbins et al., 2016; Wilson et al., 2015). Single iPSCs were seeded at a density of 0.75–1x10^6 iPSCs/cm^2 to ensure maximal efficiency of the differentiation process (Wilson et al., 2015). iPSCs grew as round colonies in feeder-free conditions, and were induced to differentiate once the right cell density was achieved (2–4x10^6 iPSCs/cm^2), typically 3 to 4 days after seeding single iPSCs. Once medium change to UM medium was performed (i.e. day 0, **Figure 8A**), iPSCs elongated and independent colonies merged, as shown in **Figure 8B**. At day 6 of differentiation, cells are usually confluent and significantly larger than at day 0, and medium composition is changed to hESFM medium supplemented with PDS (i.e. EC medium), RA and hbFGF, for two days. BECs growing in pocket-like structures (**Figure 8C**) are purified into collagen IV/fibronectin-coated surfaces in the presence of supplemented EC medium at high densities (1x10^6 cells/cm^2). This step allowed for neighboring cells to be removed through adhesion-based cell separation, as ECs display high affinity for collagen/fibronectin matrixes (Lippmann et al., 2012). Contaminating cells are removed 24 h later by medium change, and at day 10 of differentiation a pure iPSC-BEC monolayer is obtained (**Figure 8D**).

iPSC-BECs were characterized at day 10 of differentiation, when barrier properties reach their maximum. Expression of tight junction markers ZO-1, Occludin and Claudin-5, as well as endothelial-specific marker CD31 and Glut-1 could be detected (**Figure 9**), as previously described (Lippmann et al., 2012, 2014; Stebbins et al., 2016).

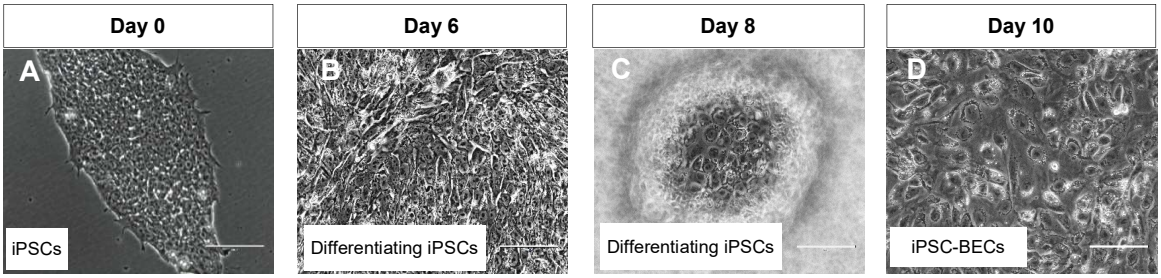

Figure 8. Generation of BECs from iPSCs.

iPSCs seeded onto Matrigel™-coated plates (A) are induced to differentiate into BECs once the appropriate cell density is reached. From day 0 to day 6 (i.e. 'UM phase'), co-differentiation takes places and cells become significantly larger, resulting in merging of colonies (B). From day 6 to day 8 (i.e. 'EC phase'), BECs grow in pocket-like structures (C), and are isolated from neighboring cells by purifying onto collagen IV and fibronectin at day 8 of the protocol. Cell morphologies during the differentiation process were similar to that observed in (Lippmann et al., 2012). The cells reach the highest TEER values at day 10, when they are used for experiments (D). Scale bars = 100 µm.

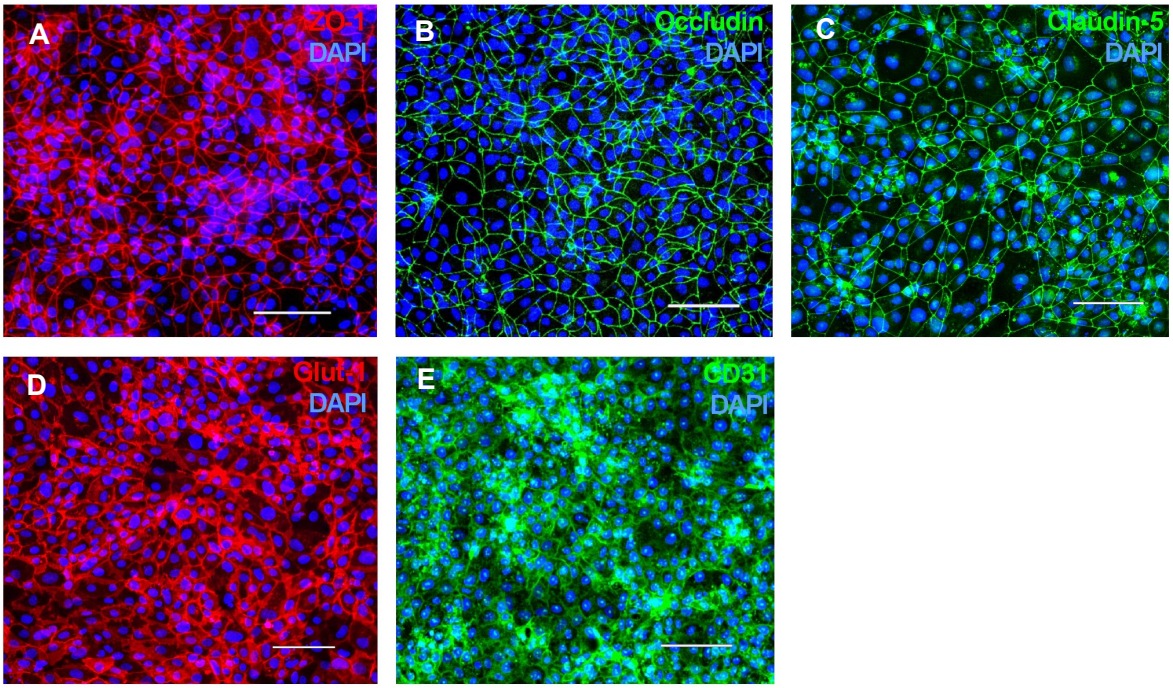

Figure 9. Marker expression by terminally differentiated iPSC-BECs.

Immunofluorescence staining of iPSC-BECs at day 10 of differentiation. Differentiated BECs express tight junction markers (A) ZO-1, (B) Occludin and (C) Claudin-5, as well as (D) Glut-1 and (E) endothelial-specific CD31. Nuclei were stained with DAPI. Scale bars = 100 µm.

4.2. Characterization of *Neisseria meningitidis* infection in iPSC-BECs

Nm was previously demonstrated to interact with a variety of immortalized lines of BECs, namely HBMECs, which have been useful to determine many known host-*Nm* interactions. To investigate whether *Nm* interacts with iPSC-BECs, monolayers were infected with 2 WT and 3 mutant *Nm* strains, all expressing a variety of characterized virulence factors (**Figure 10A**). These include reference Sg B disease strain MC58, its non-capsulated isogenic mutant (MC58Δ*siaD*) and Sg C disease isolate 8013/12. Expression of capsule in Sg B meningococcus is a phase-variable phenotype caused by slip-strand mispairing within the reading frame of the gene *siaD* (polysialyltransferase), leading to premature translational arrest (Hammerschmidt et al., 1996). Mutation of this gene was previously shown to not affect the growth of the mutant strain compared to the parent WT strain (Johswich et al., 2013). While MC58 and MC58Δ*siaD* express adhesion molecules Opa and OpcA, 8013/12 lacks Opa and OpcA proteins (**Figure 10A**). Interaction of the mentioned *Nm* strains with iPSC-BECs was determined through gentamicin protection assays. It was previously described that the absence of capsule leads to enhanced invasion of *Nm* into HBMECs, as shown in **Figure 10B** (Unkmeir et al., 2002). In accordance to data collected with HBMECs, MC58Δ*siaD* was more invasive than its parent WT strain in iPSC-BECs (**Figure 10C**). However, while invasion of the WT strain was similar between HBMECs and iPSC-BECs, invasion of the non-capsulated strain was around 1 to 2 orders of magnitude lower throughout infection for iPSC-BECs when compared to HBMECs. Lastly, 8013/12 was overall less invasive than MC58 in iPSC-BECs (**Figure 10C**). Similar patterns of adhesion and invasion could be observed by confocal microscopy, where MC58Δ*siaD* colonies were more abundant, followed by MC58, and 8013/12 (**Figure 10D**).

Sg C strain 8013/12 is widely used in the literature to assess the influence of pili during infection (Nassif et al., 1993). As PilE is the major component of meningococcal pili, the corresponding PilE deletion mutant is described as non-piliated and non-invasive (Hoffmann et al., 2001). Conversely, deletion of PilT leads to hyperpiliation. PilT deletion mutants are not able to retract the pilus machinery, leading to pilus over-expression and enhanced invasion when compared to the parent WT strain. (Hoffmann et al., 2001; Yasukawa et al., 2006). To determine if the *ΔpilE* and *ΔpilT* phenotypes impact invasion onto iPSC-BECs, relative invasion rates were compared with the WT 8013/12 strain (**Figure 10E**). Surprisingly, the Δ*pilE* mutant was invasive and showed

invasion rates similar to the parent WT strain. However, hyperpiliation resulted in significantly increased invasion ability of the Δ*pilT* mutant compared to WT (1435-fold increase, **Figure 10D**), suggesting a role for the pilus during infection.

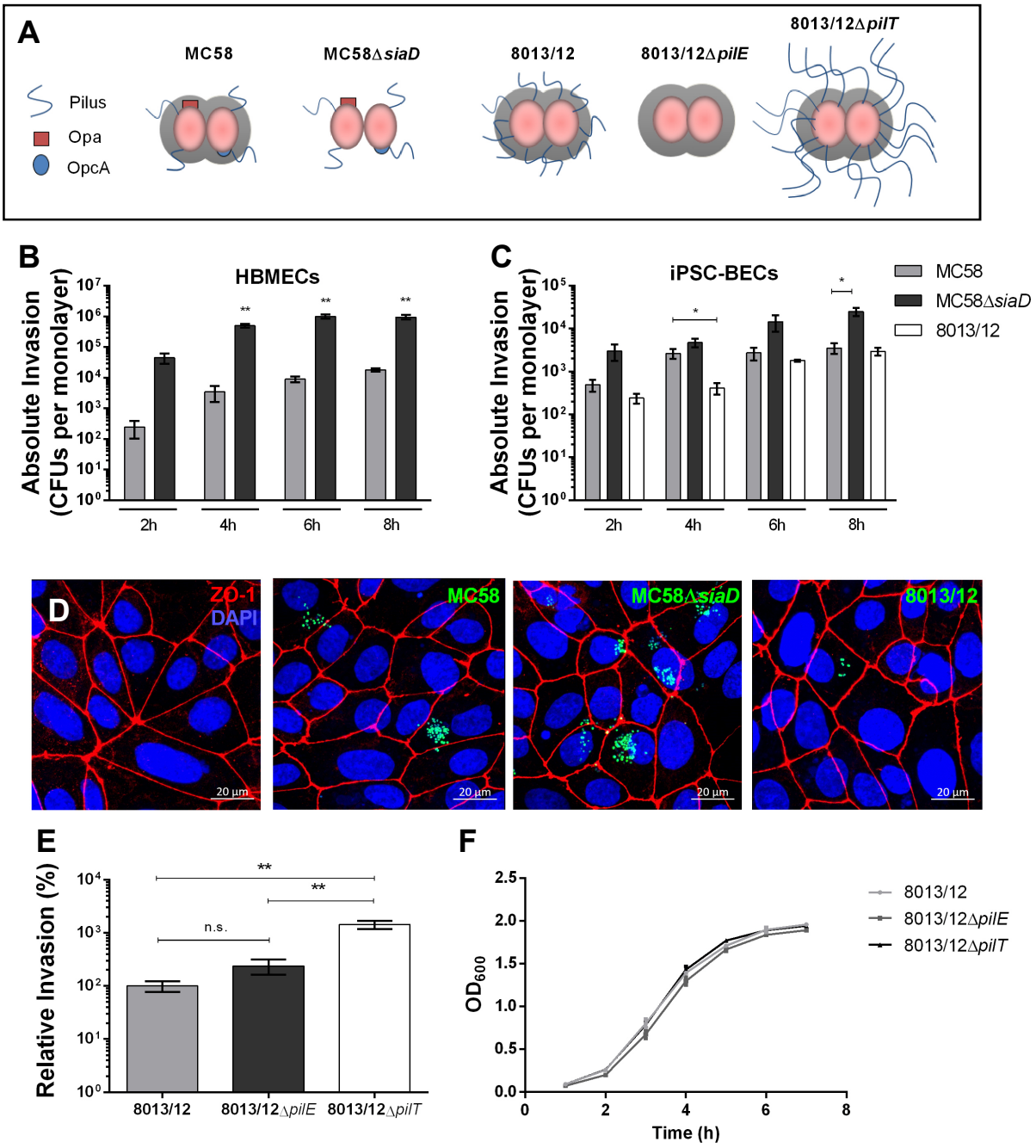

Figure 10. Characterization of Nm interaction with iPSC-BECs.

Figure 10. Characterization of Nm interaction with iPSC-BECs. (continued)

(A) Schematic cartoon of *Nm* strains used. MC58 is a Sg B strain and MC58Δ*siaD* is its isogenic non-capsulated mutant. 8013/12 is a Sg C strain, 8013/12Δ*pilE* is a non-piliated mutant and 8013/12Δ*pilT* is a pilus-overexpressing mutant. (B and C) Gentamicin protection assay of *Nm* showing absolute invasion at the indicated time points and MOI of 10, of (B) HBMECs seeded onto 48-well Nunc™ tissue culture plates infected with MC58 and MC58Δ*siaD*, and (C) iPSC-BECs seeded onto 48-well Nunc™ tissue culture plates infected with MC58, MC58Δ*siaD*, and 8013/12. (D) Confocal microscopy images of iPSC-BECs seeded onto ibidi slides infected with the *Nm* strains mentioned in (C), at 4 h p.i. and MOI 100. Image is a maximum image projection. Scale bar = 20 μm. (E) Gentamicin protection assay showing invasion of Δ*pilE* and Δ*pilT* mutants relative to WT 8013/12 *Nm* strain into iPSC-BECs at 4 h p.i. and MOI 10. (D) Growth curves of WT strain 8013/12 and the corresponding Δ*pilE* and Δ*pilT* mutants, obtained in PPM+ medium. No obvious differences were found between mutants and the corresponding parental strain. For B, C and E data is presented as mean ± S.E.M of 3 independent experiments. Student's *t* test was used to determine significance in B and C. Two-way ANOVA was used to determine significance in E. *, $p < 0.05$; **, $p < 0.01$.

Binding of Tfp to BECs is an essential step for progression of meningitis (Mairey et al., 2006). CD147 was recently found to be the BEC host receptor for Tfp, in a study conducted with immortalized EC lines (Bernard et al., 2014). In order to confirm previously published results, flow cytometry and immunofluorescence for CD147 were performed. Two antibodies targeting CD147 were used: MEM-6/6 and MEM-6/1, which bind to the C-terminal Ig and the extracellular N-terminal domains of CD147, respectively. CD147 was confirmed to be expressed on the surface of undifferentiated iPSCs, iPSC-BECs, and HBMECs by flow cytometry (**Figure 11A**). Moreover, CD147 expression was observed through immunofluorescence in iPSC-BECs, with distinct types of cellular staining between the two antibodies (**Figure 11B**). Upon infection of iPSC-BECs, co-localization of CD147 around bacterial microcolonies was observed, in accordance to the previous study (**Figure 11B**) (Bernard et al., 2014). This co-localization could only be observed when using the MEM-6/6 antibody. Together, these results indicate that similar patterns of invasion and phenotypes displayed by various *Nm* strains and mutants could be observed in iPSC-BECs, in accordance to previously described models. These results also demonstrate that the iPSC-BEC model expresses an important receptor for virulence and that it should be suitable for the study of *Nm* virulence factors.

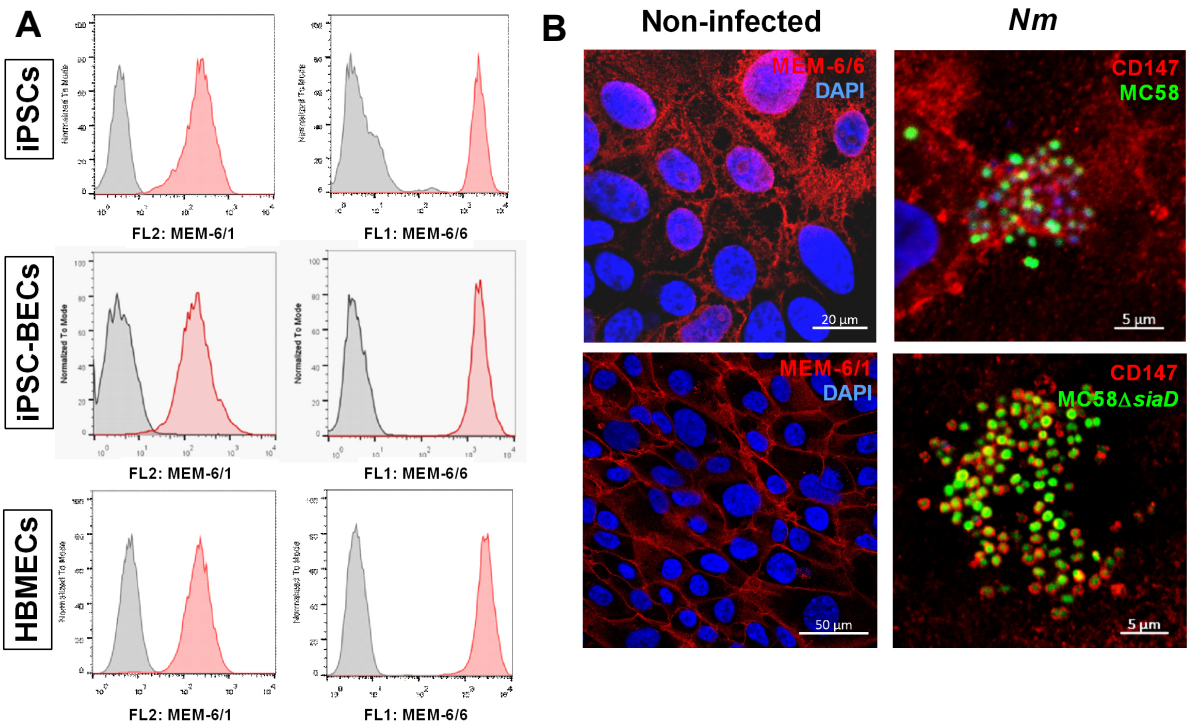

Figure 11. Expression and co-localization of CD147 by iPSC-BECs around Nm microcolonies.

(A) Flow cytometry data showing expression of CD147 by undifferentiated iPSCs, differentiated iPSC-BECs, and HBMECs. Gray = Isotype control. Red = CD147 MEM-6/6 or MEM-6/1. (B) Confocal microscopy images showing expression of CD147 by iPSC-BECs without *Nm* challenge (left), and with *Nm* challenge (right, GFP-expressing MC58 and MC58Δ*siaD* strains, at 4 h p.i. and MOI 100), leading to the recruitment of CD147 beneath *Nm* microcolonies.

4.3. Loss of Barrier Properties during *Neisseria meningitidis* infection

One of the main strengths of the iPSC-BEC model is the presence of continuous tight junction complexes and high barrier potential. Conversely, previous models precluded the study of changes in barrier properties in BECs upon *Nm* infection due to low barrier potential. To investigate the impact of *Nm* challenge on barrier integrity of BECs, iPSC-BECs were seeded onto collagen IV/fibronectin-coated 0.4 µm pore size inserts, and the TEER profile of mock and infected monolayers was measured over time. Initially, the TEER profile was measured in 24-well size Greiner inserts in the presence of hESFM + 10 % HS (i.e. infection medium). However, preliminary results indicated that the presence of HS sharply decreased the barrier potential of control, non-infected inserts, as well as infected inserts, as soon as 2 h after medium change (**Table 18** and **Figure**

12). This did not allow distinguishing changes in TEER caused by *Nm* infection. For this reason, the experimental procedure was optimized and carried out exactly as described in (Stebbins et al., 2016), i.e. in 12-well Corning inserts and in the presence of EC medium alone (hESFM + 1 % PDS). In these conditions, TEER values before infection surpassed 3000 Ωxcm^2, and were maintained until 8 h of infection (**Table 19** and **Figure 13A**). At 24 h, a trend for TEER decrease could be observed in infected transwells, which became significant at 28 h (*P*-value < 0.05). At 32 h, TEERs of infected monolayers dropped 90 % when compared to controls, suggesting that *Nm* causes barrier disruption at late infection time points.

To further establish that *Nm* infection impairs barrier function, paracellular permeability to sodium fluorescein (Na-Fluorescein) was quantified. iPSC-BECs were seeded onto collagen IV/fibronectin-coated 0.4 µm size 12-well Corning inserts and infection was carried out for 24 and 32 h in the presence of EC medium alone (**Table 19** and **Figure 13B**). Na-Fluorescein permeability was tested as described in (Stebbins et al., 2016). In support of the TEER dynamics, an increase in Na-Fluorescein permeability was observed at 24 h. At 32 h, the Na-Fluorescein permeability coefficient (Pe) was 4.9-fold higher for infected cells when compared to controls. Taken together, these data suggest that *Nm* infection impairs barrier function of iPSC-BEC monolayers by increasing its barrier permeability.

Table 18. Human serum impacts TEER measurements of polarized monolayers of iPSC-BECs.

Time	**TEER ± S.E.M. (Ωxcm^2)**				
p.i.	**Control (n=3)**		**MC58 (n=3)**		**ESFM + 1 % PDS (n=1)**
0 h	2771	± 412	2657	± 266	2585
2 h	1133	± 404	1299	± 488	2150
4 h	762	± 328	742	± 342	2364
6 h	495	± 208	457	± 210	2368
8 h	356	± 142	298	± 122	2384
24 h	108	± 60	89	± 21	1572

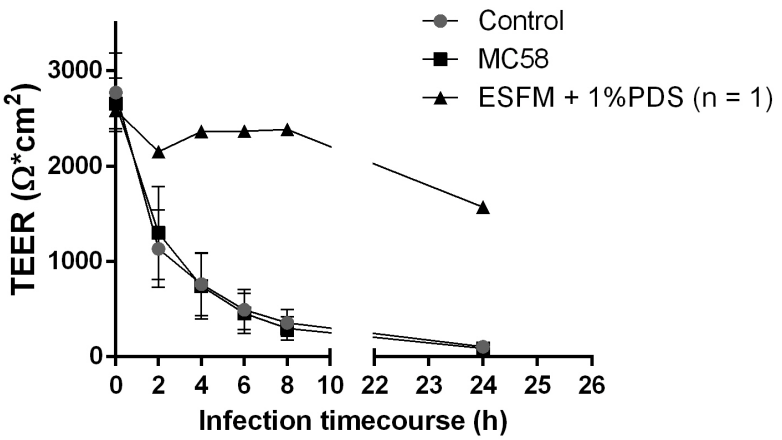

Figure 12. Human serum impacts TEER measurements of polarized monolayers of iPSC-BECs.

Polarized iPSC-BEC monolayers seeded onto 0.4 µm pore size 24-well size Greiner transwells in the presence of hESFM medium supplemented with 10 % HS, with or without MC58 challenge at MOI 10 were used for monitoring of TEER values (Ωxcm^2) for 3 independent experiments. To assess the impact of HS compared with PDS serum on TEER, 1 control transwell in the presence of hESFM + 1 % PDS was added and TEER was followed without infection.

Table 19. Nm infection alters barrier properties of polarized monolayers of iPSC-BECs.

Time p.i.	TEER ± S.E.M. (Ωxcm^2)				*P*-value	Na-Fluorescein coefficient (Pe) ± S.E.M. (cm/min)		*P*-value
	Control		MC58			Control	MC58	
0 h	3479	± 36	3701	± 194	n.s.	-	-	-
2 h	3194	± 342	3488	± 473	n.s.	-	-	-
4 h	3324	± 349	3110	± 504	n.s.	-	-	-
6 h	3028	± 342	3277	± 328	n.s.	-	-	-
8 h	3361	± 242	3820	± 208	n.s.	-	-	-
24 h	2563	± 260	1650	± 525	n.s.	$2.7 \times 10^{-4} \pm 5.3 \times 10^{-5}$	$1.8 \times 10^{-3} \pm 5.8 \times 10^{-4}$	0.06
26 h	2621	± 165	1396	± 491	n.s.	-	-	-
28 h	2581	± 205	916	± 351	0.015	-	-	-
30 h	2303	± 190	393	± 93	0.0008	-	-	-
32 h	2376	± 210	251	± 58	0.0006	$6.3 \times 10^{-4} \pm 9.8 \times 10^{-5}$	$3.1 \times 10^{-3} \pm 7.5 \times 10^{-4}$	0.03

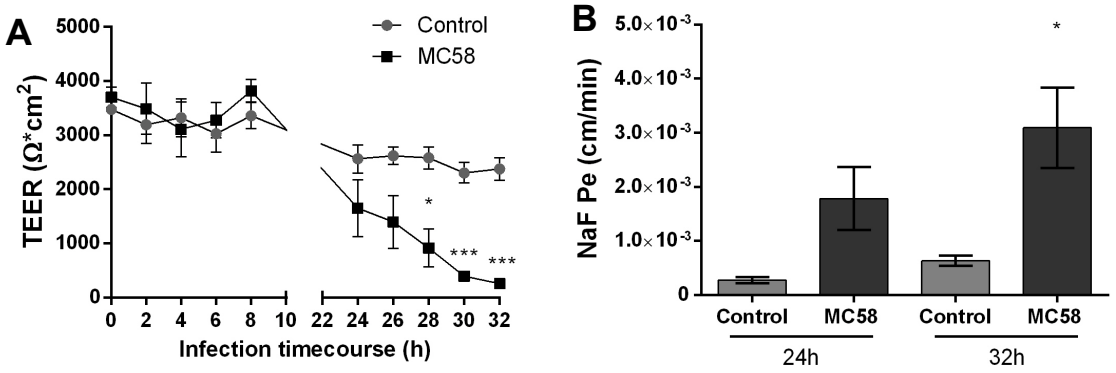

Figure 13. Nm infection alters barrier properties of polarized monolayers of iPSC-BECs.

Polarized iPSC-BEC monolayers seeded onto 0.4 µm pore size 12-well size Corning transwells in the presence of hESFM + 1 % PDS, with or without MC58 challenge at MOI 10 were used for (A) monitoring of TEER values (Ωxcm^2) over a timecourse of 32 h, and (B) determination of Na-Fluorescein permeability coefficient (cm/min) at 24 h and 32 h p.i. The data show mean ± S.E.M. of 3 independent experiments done in triplicate. Student's *t* test was used to determine significance.

4.4. Tight junction disruption at late *Neisseria meningitidis* infection time points

Taking into consideration the observed increase in barrier permeability during *Nm* infection, the impact of infection on tight junction dynamics was assessed. To determine if changes in protein content take place during *Nm* infection, protein lysates were collected at various time points and quantification by Western blot was done. Interestingly, on standard 48-well Nunc™ tissue culture plates, the monolayers tended to detach as a sheet from the border of the wells at around 24 h p.i., and by 32 h p.i. these would be completely detached; however, this did not preclude the collection of protein samples. By contrast, initial infection kinetic studies showed that samples collected at 48 h p.i. did not generate usable protein lysates, therefore, 32 h p.i. was selected as the latest possible time point of infection for further experiments.

Protein samples were collected from iPSC-BECs at 4, 8, 24 and 32 h p.i. and analyzed by Western blot with antibodies against tight junction proteins ZO-1, Occludin, Claudin-1 and Claudin-5 (**Figure 14**). While no changes in protein content occurred at early infection stages, a trend for decrease in content of ZO-1, Occludin, and particularly Claudin-5, could be observed at 32 h of

infection. Of note, an additional band at lower molecular weight was observed for Occludin (**Figure 14**, black arrow), which might correspond to a cleavage product generated upon *Nm* infection, as previously described in immortalized HBMECs (Schubert-Unkmeir et al., 2010). A higher molecular weight band for Occludin could be observed at 24 h and 32 h p.i. (**Figure 14**, grey arrows), possibly corresponding to post-translational modifications (Cummins, 2012; Ni et al., 2017). Of note, although protein quantification was performed for all samples after protein isolation and the same protein amount per well was loaded for electrophoretic separation, samples derived from monolayers infected at 32 h p.i. consistently showed lower protein levels of β-Actin, which may have negatively impacted the statistical significance of the results. COX IV was tested as an alternative reference protein, however, the same phenomenon was observed (**Figure 15A**). Conversely, Ponceau staining after transfer to the nitrocellulose membranes showed that protein content was overall homogeneous among samples from the same replicate (**Figure 15B**).

To further observe if changes in tight junction proteins occur during infection, immunostaining for tight junction components ZO-1, Occludin, and Claudin-5 was carried out. iPSC-BECs were seeded onto collagen IV/fibronectin-coated 8-well ibidi slides and challenged with *Nm* for up to 24 h. In accordance, no changes in tight junction proteins could be observed by immunostaining at 8 h p.i. (**Figure 16A**). On the contrary, immunostaining at 24 h p.i. revealed tight junction re-arrangements, namely gaps with various sizes between cells and junctions with highly frayed edges. Junction discontinuity could be observed for Occludin and Claudin-5, but not ZO-1. At 16 h p.i., no change in tight junction proteins between non-infected and infected cells was detected by immunostaining (**Figure 16B**), suggesting that the observed re-arrangements occur between 16 h and 24 h of infection. Gaps between cells were likely caused by cell detachment due to *Nm* infection, as previously reported in immortalized HBMECs (Schubert-Unkmeir et al., 2010).

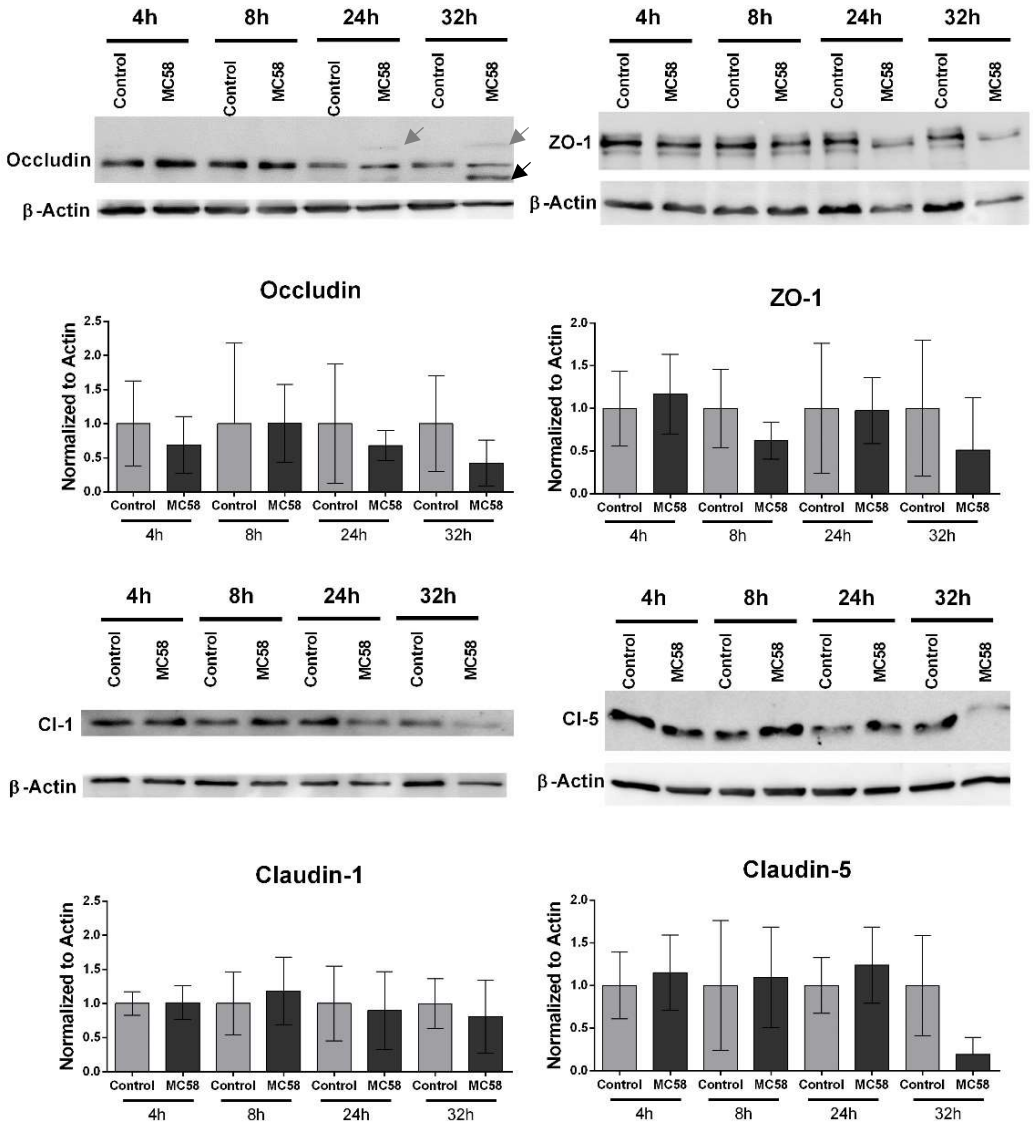

Figure 14. Tight junction protein dynamics during Nm infection.

Immunoblots showing changes in tight junction proteins during infection with *Nm* (MOI 10). Protein samples were collected from iPSC-BECs plated on 48-well Nunc^{TM} tissue culture plates at 4, 8, 24 and 32 h p.i. with or without *Nm* challenge. Arrows point to potential modifications of Occludin generated upon MC58 infection: black arrow - potential cleavage product; grey arrows - potential post-translational modification. Densitometry normalized to β-Actin is shown for comparison. Data shows mean ± S.D. of three independent experiments.

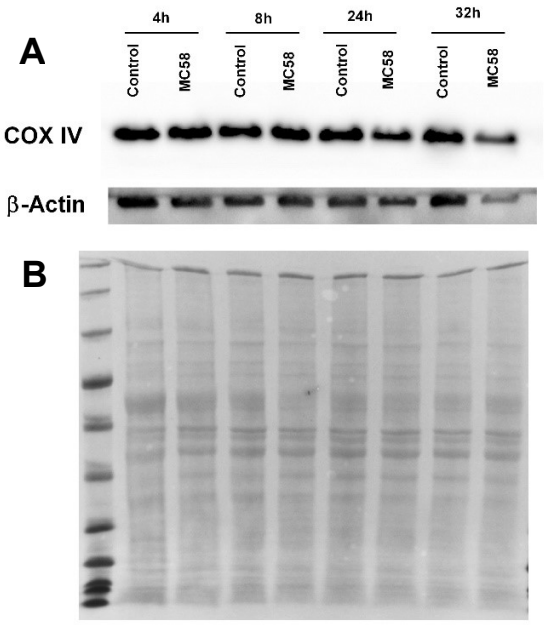

Figure 15. Comparison between sample loading for two reference proteins, and Ponceau staining.

(A) Immunoblots showing changes in band intensity and thickness for reference proteins COX IV and β-Actin at late time points of infection between control and infected lysates. (B) Ponceau staining showing even protein distribution between all loaded samples of a single replicate.

To assess if possible tight junction protein modifications occur due to changes in transcriptional regulation during infection, qRT-PCR for *TJP1* (ZO-1), *OCLN* (Occludin) and *CLDN5* (Claudin-5) using Taqman probes was performed. Consistent with the protein data, regulation of tight junction expression at the mRNA level in response to infection was not observed at 8 h p.i., whereas at 24 h *TJP1* and *CLDN5* expression decreased to 0.53- and 0.16- fold, respectively (**Figure 17A, B and C**).

Previous reports show that tight junctional downregulation in response to invasive bacterial pathogens *Streptococcus pneumoniae*, *Haemophilus influenzae* and Group B *Streptococcus* is preceded by the upregulation of host Snail-1 (*SNAI1*), a transcriptional repressor of tight junction components (Clarke et al., 2015; Kim et al., 2017, 2015). To assess if this transcription factor plays a role in tight junction disruption during *Nm* infection, qRT-PCR for *SNAI1* was done. The results obtained indicate that upregulation of *SNAI1* occurs as early as 4 h p.i. in infected cells, peaking at 16 h p.i. (4.0-fold) and maintaining elevated levels of expression at 24 h p.i. (**Figure 17D**). Together, these results indicate that *Nm* exposure causes tight junction disruption of iPSC-BECs possibly through activation of host *SNAI1*.

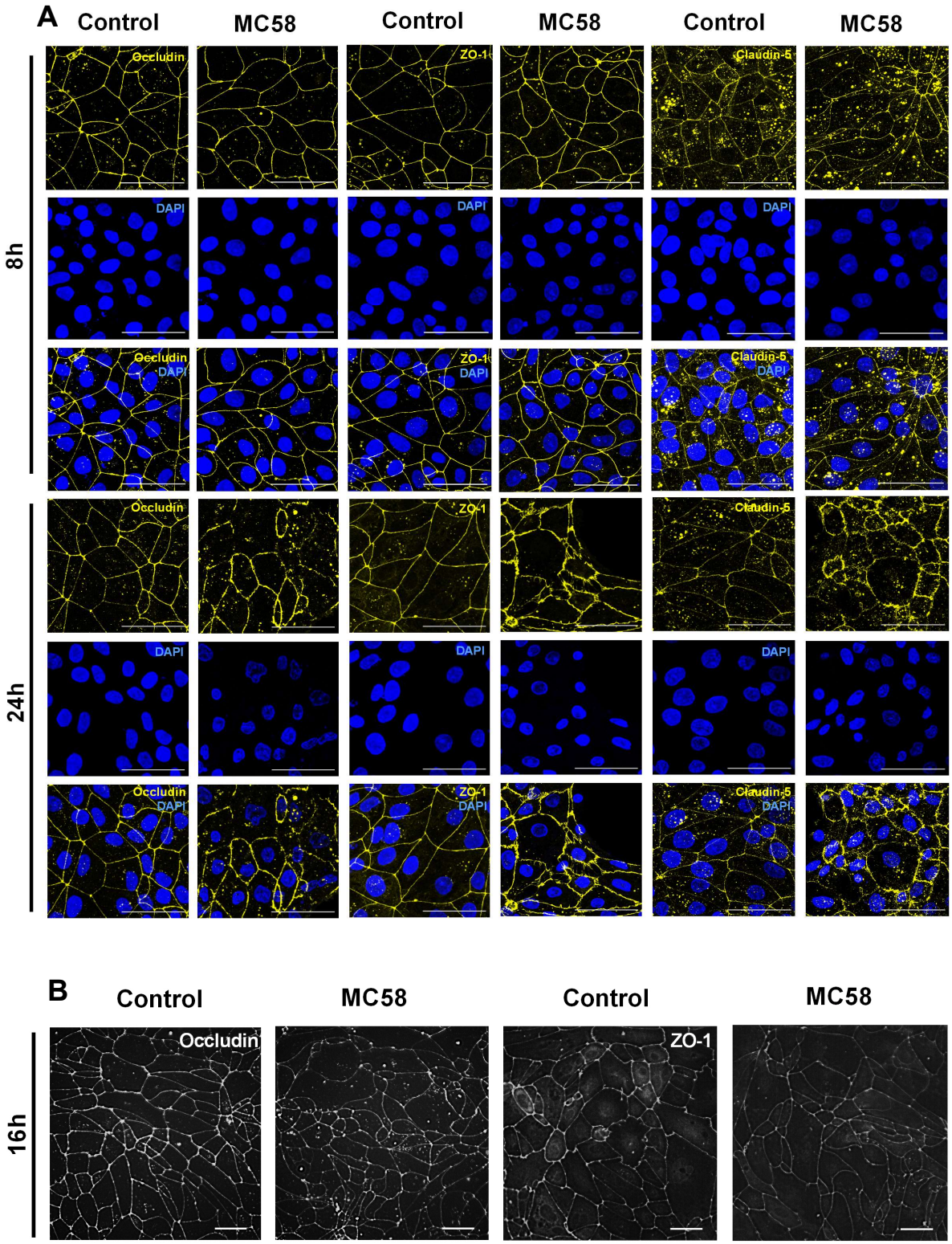

Figure 16. Nm induces time-dependent junctional disruption in iPSC-BECs.

Figure 16. Nm induces time-dependent junctional disruption in iPSC-BECs. (continued)

(A) Confocal microscopy images showing tight junction staining for Occludin, ZO-1 and Claudin-5 in iPSC-BECs seeded onto ibidi microscopy slides with and without *Nm* challenge at MOI 10 at 8 and 24 h of infection. Areas lacking DAPI and tight junction staining correspond to gaps between cells. Image is a maximum image projection. Yellow = tight junctions, Blue = DAPI. Scale bar = 50 µm. (B) Immunofluorescence staining of tight junctions Occludin and ZO-1 at 16 h p.i. with and without *Nm* challenge at MOI 10 on iPSC-BECs seeded onto 48-well Nunc™ tissue culture plates. Single channel images were converted to grayscale. Scale bar = 50 µm.

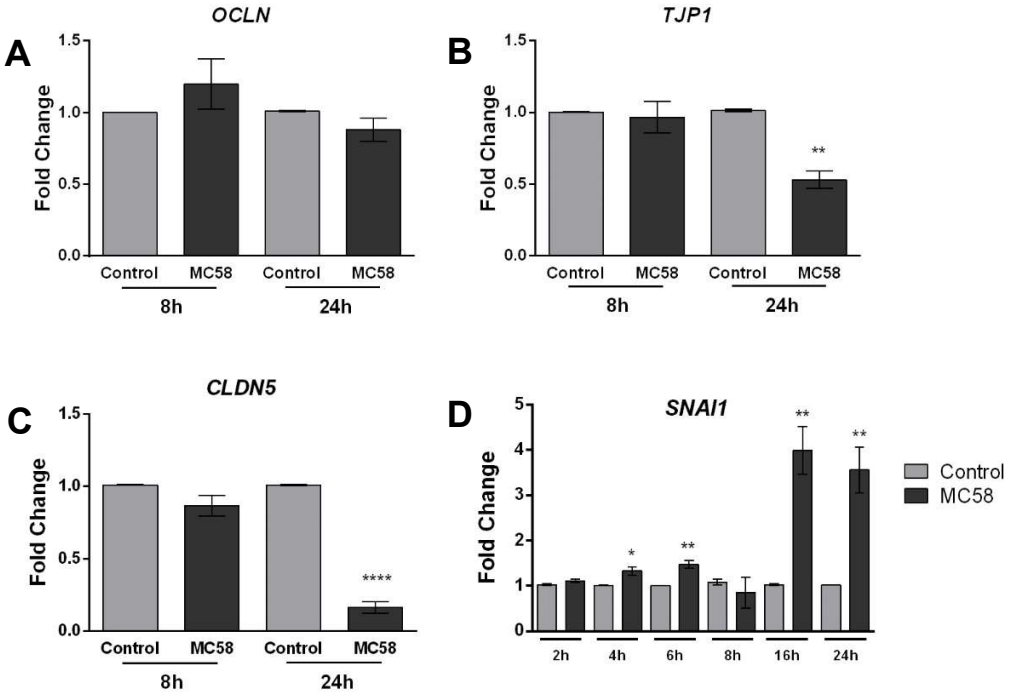

Figure 17. Nm infection dysregulates expression of tight junction-related genes.

qRT-PCR results showing relative expression compared to reference gene *18S* of tight junction-coding genes (A) *OCLN*, (B) *TJP1* and (C) *CLDN5* at 8 h and 24 h p.i., and (D) tight junction repressor gene *SNAI1* over a time course of 24 h, performed on iPSC-BECs seeded on 48-well Nunc™ tissue culture plates with (dark grey bars) or without (light grey bars) *Nm* challenge at MOI 10.

4.5. Tight junction disruption correlates with *Neisseria meningitidis* transmigration

The primary route for *Nm*-BEC transit is a question still under debate. To determine if the observed opening of cell-cell junctions causes *Nm* to cross iPSC-BECs, transmigration studies were carried

out. Bacteria were added to the apical compartment of seeded transwells with a pore size of 3 μm to allow *Nm* diffusion. Electrical resistance before infection surpassed 1200 Ωxcm^2, indicating that the larger pore size of the selected transwells still allowed seeded monolayers to maintain high barrier properties. In order to assess changes in bacterial traversal across iPSC-BEC monolayers over time, transwells were washed and moved into fresh medium for 30 min at 2, 4, 6, 8 and 24 h of infection, and CFUs on the basolateral chamber were counted. During transmigration assays for MC58, bacterial colonies could not be detected on the basolateral chamber of infected transwells before 6 h of infection (**Table 20** and **Figure 18B**). At 6 and 8 h of infection, the number of MC58 CFUs was below the reliable detection limit of the assay (see Methods section), although some colonies could be observed. At 24 h, results suggest that the number of CFUs crossing the monolayer significantly increases when compared to 8 h of infection (19,531-fold) (**Table 20** and **Figure 18B**). This increase in bacterial transmigration correlates with tight junctional disruption as assessed by immunofluorescence (**Figure 16**), suggesting that the paracellular pathway has a major contribution to the crossing of *Nm* through BECs. Surprisingly, transmigration of non-capsulated mutant MC58Δ*siaD* could not be detected before 24 h, and remained significantly lower at this time point when compared to the WT parent strain, despite its enhanced invasion ability (**Table 20** and **Figure 18A**). Moreover, TEER values for transwells infected with this strain increased when compared to control transwells, until a sharp decrease in TEER was detected at 48 h.

Table 20. Nm crosses polarized monolayers of iPSC-BECs.

Time p.i.	TEER ± S.E.M. (Ωxcm^2)						Bacterial Transmigration (CFUs)			
	Control		MC58		MC58Δ*siaD*		MC58		MC58Δ*siaD*	
0 h	1304	± 202	1267	± 171	1254	± 148	-		-	
2 h	1344	± 219	1287	± 416	1387	± 131	0	± 0	0	± 0
4 h	1287	± 256	1208	± 357	1302	± 169	0	± 0	0	± 0
6 h	948	± 413	1027	± 382	1212	± 212	95	± 31	0	± 0
8 h	950	± 311	1058	± 339	1148	± 186	256	± 107	0	± 0
24 h	1102	± 119	917	± 151	1612	± 433	5x10^6	± 7x10^5	46	± 28
26 h	1233	± 109	772	± 194	1732	± 495	-		-	
28 h	1148	± 92	516	± 139	1535	± 383	-		-	
30 h	939	± 107	322	± 121	1344	± 328	-		-	
32 h	887	± 128	241	± 98	1293	± 316	-		-	
48 h	696	± 148	29	± 15.5	126	± 24	-		-	

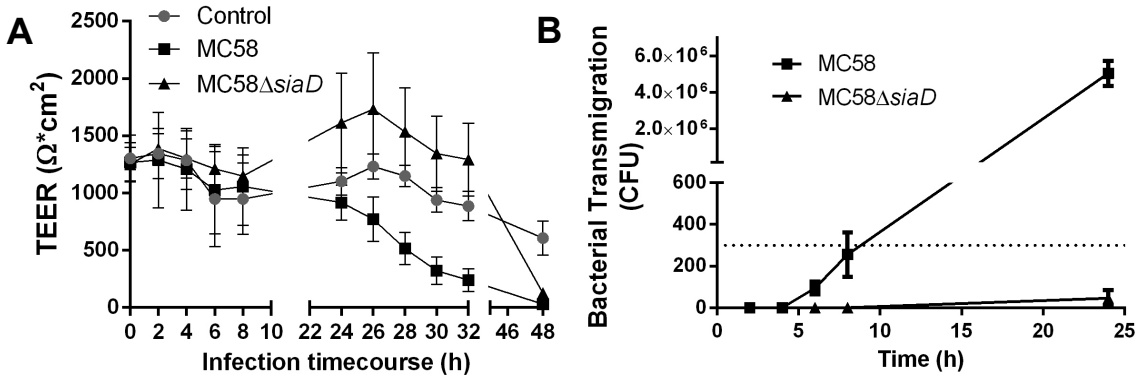

Figure 18. Nm crosses polarized monolayers of iPSC-BECs.

Polarized iPSC-BEC monolayers seeded onto 3 µm pore size 12-well size Corning transwells in the presence of hESFM + 1% PDS were used for monitoring of (A) TEER values (Ωxcm^2) over a time course of 48 h, without infection or in the presence of MC58 or MC58Δ*siaD* challenge at MOI 10 (n=2 for all conditions), or (B) transmigration of *Nm* (MC58 or MC58Δ*siaD*) across monolayers at 2, 4, 6, 8 and 24 h. Bacterial transmigration was determined by assessing the number of CFUs in the basolateral chamber for MC58 (n=3) and MC58Δ*siaD* (n=2). Data show mean ± S.E.M. of 2 or 3 independent experiments done in triplicate.

4.6. *Neisseria meningitidis* infection triggers proinflammatory activation of iPSC-BECs

Upon bacterial transmigration through the b-CSF, meningitis progression is characterized by the inflammation of the meninges (Hoffman and Weber, 2009; Tunkel and Scheld, 1993). BECs are known to produce chemokines once stimulated by bacterial or viral infection, LPS or proinflammatory cytokines such as TNF-α (Chaudhuri et al., 2008; Vadeboncoeur et al., 2003; van Sorge et al., 2011; Verma et al., 2006). To investigate whether iPSC-BECs are activated upon *Nm* infection, a panel of 14 cytokines/chemokines was selected for Luminex bead-based multiplex assays based on literature studies. This panel consisted of IL-1β (Kofler et al., 2005; Sprong et al., 2001), IL-6 and *CXCL8*/IL-8 (Christodoulides et al., 2002; Fowler et al., 2004, 2006; Vadeboncoeur et al., 2003), *CXCL1*/Gro-α and *CXCL2*/Gro-β (Krishnaswamy et al., 1999; Robinson et al., 2004), GM-CSF (Christodoulides et al., 2002; Fowler et al., 2004, 2006), TNF-α (Taha, 2000), IFN-γ (Sprong et al., 2001; Wei et al., 2002), *CCL2*/MCP-1 (Christodoulides et al., 2002; Fowler et al., 2004, 2006; Vadeboncoeur et al., 2003), *CCL5*/RANTES (Christodoulides et

al., 2002; Fowler et al., 2004, 2006; Shukaliak and Dorovini-Zis, 2000), adhesion molecules VCAM-1 (Dixon et al., 1999) and ICAM-1 (Dixon et al., 1999; Ivarsson et al., 2013) and endothelial-specific molecules E-Selectin (Baines et al., 1999) and vWF-A2 (Lüttge et al., 2012). Infection was carried out with MC58, MC58Δ*siaD* and 8013/12 for a timecourse kinetics of 2, 4, 6, 8 and 24 h p.i. and supernatants of mock- and bacteria-infected monolayers were collected and tested for presence of the mentioned molecules.

The results obtained show that RANTES and IFN-γ are significantly secreted at 8 h and 24 h of MC58 infection (**Figure 19A**). Although a statistically significant increase in IL-8 presence in supernatants derived from MC58-infected monolayers at 24 h p.i. was observed, it should be noted that the magnitude of secretion (8 pg/mL) is not biologically relevant (Dick et al., 2017). Surprisingly, IL-6 was not detected in any experimental condition. No detection or detection below the standard limit was observed for IL-1β, Gro-α, GM-CSF, TNF-α, ICAM-1 and v-WFA2, while no statistical difference between control versus infection conditions was observed for VCAM-1, E-Selectin, and Gro-β (**Figure 19B**). Similar trends were observed for supernatants collected from MC58Δ*siaD*- and 8013/12- infected monolayers. By contrast, for immortalized HBMECs, time-dependent increase of IL-6 and IL-8 could be detected, reaching 1235 and 1701 pg/mL, respectively, at 8 h p.i. for supernatants of MC58-infected cells. These results are in accordance with previous literature (Dick et al., 2017) and therefore validate the reliability of the Luminex experimental approach (**Figure 19C**).

It was hypothesized that RA used for the differentiation of iPSCs into BECs from day 6 to day 9 of the protocol might have influenced the cells' cytokine secretion ability, since RA has been reported to possess anti-inflammatory properties (Choi et al., 2005; van Neerven et al., 2010). For this reason, RA was withdrawn from the differentiation protocol, after cell detachment and seeding onto collagen IV and fibronectin (i.e. day 8 of differentiation), to avoid potential anti-inflammatory effects after purifying BECs. Of note, RA was not completely removed from the differentiation protocol to avoid decreases in TEER. Moreover, HS was removed from the infection medium and infections were carried out with hESFM basal medium alone to eliminate any impacts of serum components on the inflammatory potential of the cells. The collection of supernatants of mock- and bacteria-infected monolayers was then repeated and the same panel of chemokines/cytokines and method were used. Under these experimental conditions, no candidate of the panel could be detected at 24 h p.i. for mock- and MC58-infected supernatants.

To assess if iPSC-BECs respond transcriptionally to *Nm* infection, we returned to the original differentiation and infection protocols and performed qRT-PCR on samples collected from mock- and MC58-infected iPSC-BEC monolayers, to test for *IL6, CXCL8*/IL-8, *CXCL1*/Gro-α, *CXCL2*/Gro-β and *CCL20*/MIP3A gene expression. Lysates were extracted at 2, 4, 6, 8 and 24 h p.i., then RNA was isolated and reverse transcription to cDNA was performed. Both *GAPDH* and *18S* rRNA were tested as reference genes for this experiment. Ct values for *GAPDH* tended to not be constant between non-infected and infected samples (in general, lower Cts in infected samples), while *18S* yielded more consistent results. The results show that all the tested inflammatory genes are significantly upregulated at some point during infection (**Figure 20A**). *CXCL8* was upregulated 3.45- and 5.33-fold at 8 and 24 h p.i., respectively, while *IL6* was upregulated by 2.7-fold at 24 h p.i. *CXCL1* showed 9.27-fold upregulation at 8 h p.i., while *CXCL2* was upregulated at earlier infection time points (14.8-fold at 2 h p.i. and 7.92-fold at 6 h p.i.). Lastly, *CCL20* showed significant upregulation at 6 h p.i. (3.39-fold) and 24 h p.i. (12.3-fold). Using Taqman probes, a tendency for upregulation of *CCL5* (RANTES) and *IFNG* (INF-γ) at 24 h p.i. could be detected (**Figure 20B**). Taken together, these results indicate that iPSC-BECs are transcriptionally activated upon *Nm* challenge to respond in a proinflammatory manner, and this response includes secretion of biologically relevant amounts of RANTES (Pashenkov et al., 2002) and IFN-γ (Kornelisse et al., 1997) at late infection time points.

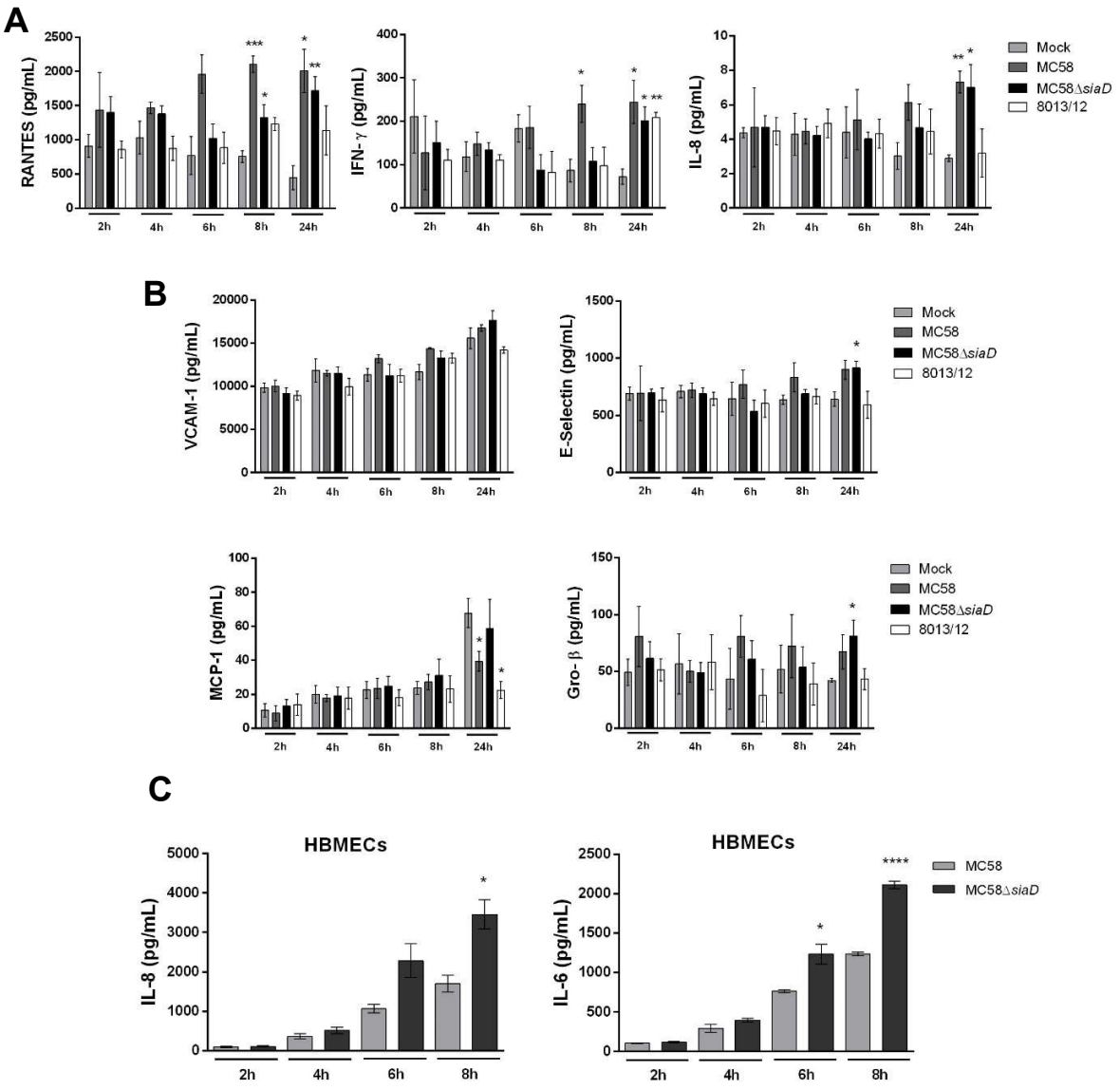

Figure 19. Nm infection leads to restricted cytokine secretion in iPSC-BECs.

(A and B) Detection of RANTES, IFN-γ, and IL-8 (A), and VCAM-1, E-Selectin, MCP-1, and GRO-β (B) on supernatants of mock-, MC58-, MC58Δ*siaD*- and 8013/12-infected iPSC-BECs by Luminex bead-based multiplex assays during a time course of 2, 4, 6, 8 and 24 h of infection. (C) Time-dependent secretion of IL-8 and IL-6 by HBMECs in response to *Nm* infection detected by Luminex bead-based multiplex assays. Data show mean ± S.E.M of 3 independent experiments done in duplicate. For A, B and C Student's *t* test was used to determine significance compared to non-infected controls. *, $p < 0.05$; **, $p < 0.01$; ****, $p < 0.0001$.

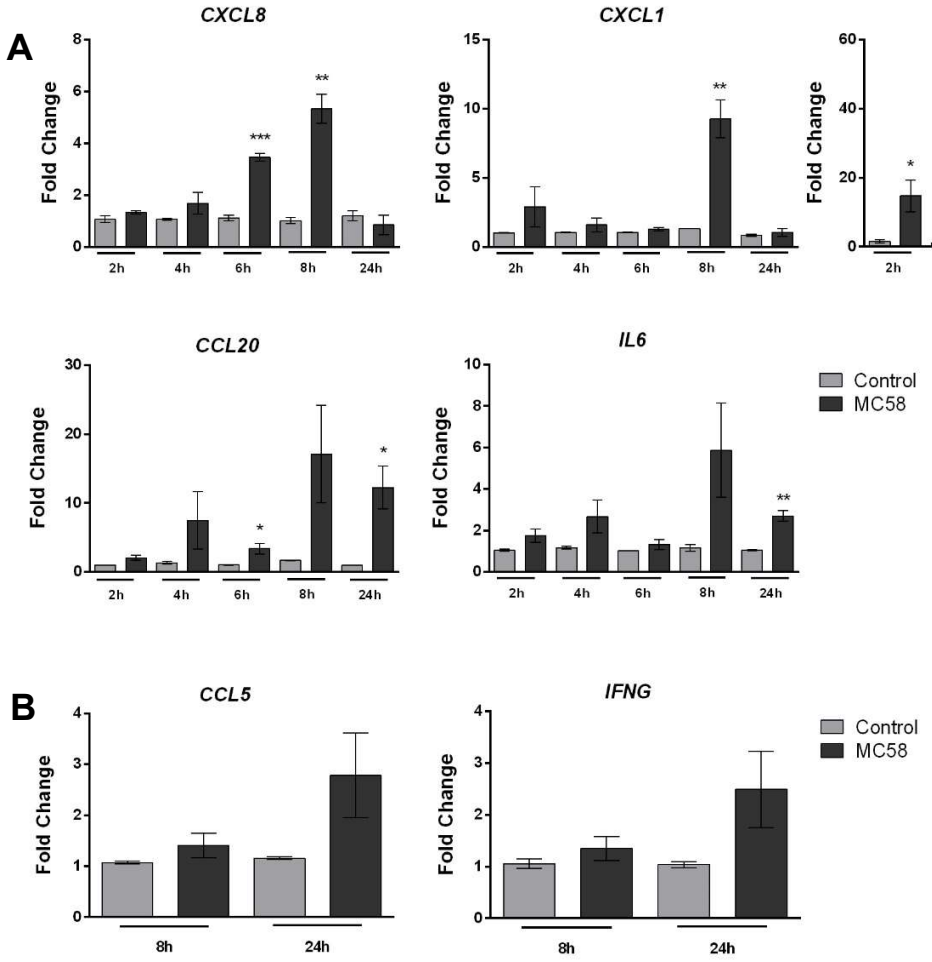

Figure 20. Nm infection leads to transcriptional inflammatory activation of iPSC-BECs.

Quantitative PCR showing relative expression of (A) *CXCL8*, *CXCL1*, *CXCL2*, *CCL20* and *IL6* transcripts during a time course of 2, 4, 6, 8 and 24 h of infection, and (B) *CCL5* (RANTES) and *IFNG* (IFN-γ) transcripts at 8 and 24 h of infection, for mock- (light grey bars) and *Nm*-infected (dark grey bars) monolayers. Data are presented as mean ± S.E.M of 3 independent experiments done in triplicate. Student's t test was used to determine significance. *, $p < 0.05$; **, $p < 0.01$; ***, $p < 0.001$.

4.7. RNA-Seq of *Neisseria meningitidis*-infected iPSC-BECs

To track host transcriptomic changes during the progression of *Nm* infection, a previously described method for isolating infected from non-infected cells was established to the setting of *Nm* infection on iPSC-BECs (Westermann et al., 2016). GFP-expressing MC58 and FACS were

used to select infected cells carrying intracellular *Nm* (**Figure 21A**). Sorting was performed at several time points of infection to test if sufficient numbers of infected cells could be obtained (**Figure 21B** and **Table 21**). Simultaneously, sorting of GFP-negative events for mock control samples was performed, to ensure that all samples sent to sequencing were submitted to exactly the same experimental procedures. Previous studies suggested that the minimum cell number per sample required for successful RNA-Seq is around 10,000 cells (Westermann et al., 2016), meaning that at least 10,000 GFP-positive events (i.e. infected cells) should be collected during sorting. For this reason, the seeding format of iPSC-BECs at 10 day of differentiation was scaled up, and iPSC-BECs were seeded onto 6-well Nunc^{TM} tissue culture plates for this assay. Initially, the time points of infection 2, 8 and 24 h were selected for carrying out infection and FACS. However, even after scaling up cell culture, infection at 2 h p.i. did not yield sufficient infected cell numbers due to very low infection rates (0.1–1 %) (**Table 21**). Infection and sorting were then repeated at 4, 8 and 24 h p.i., where infection rates increased for the earliest infection time point (**Table 21**). On average, infection rates varied from 1.7 % at 4 h p.i. to 13.3 % at 24 h p.i., while the infected cell number obtained ranged from 3,400 to 48,700, respectively. Upon RNA extraction from each sample, polyadenylated transcripts were converted into cDNA libraries and sequenced to ~25-30 million reads/library through Ilumina technology.

The sequencing results suggested that the total number of sequenced reads that could be uniquely mapped directly correlated with the number of sorted cells (**Table 22**). Infected GFP-positive samples showed lower mapping rates when compared to mock control samples (without MC58 challenge), presumably due to the lower number of cells that could be sorted, resulting in lower RNA amounts. Nonetheless, there was a clear enrichment of *Neisseria* reads in the GFP-positive samples as compared to the mock control, indicating that the sort-enrichment was efficient (**Figure 22**).

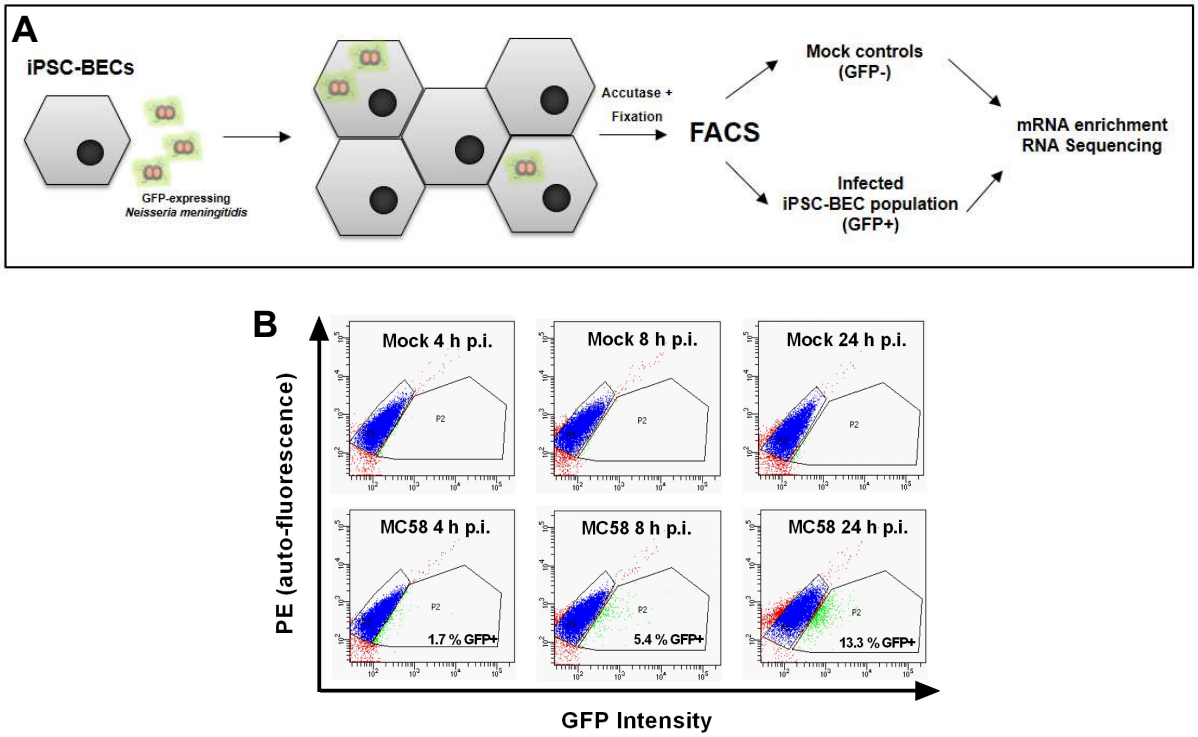

Figure 21. RNA-Seq of sort-enriched, infected iPSC-BECs.

(A) Experimental workflow. iPSC-BECs were infected with MC58-GFP at MOI 10, detached through Accutase treatment, and fixed in RNAlater©. Mock controls without *Nm* challenge were collected in parallel (gated GFP-negative population). An outline of the gating strategy is illustrated in (B). As infection progressed, GFP-positive events could be detected and separated from GFP-negative events. Total RNA was extracted from each sample and polyadenylated transcripts were converted into cDNA libraries and sequenced to ~25-30 million reads/library.

Table 21. Establishment of sorting protocol for iPSC-BECs infected with GFP-MC58.

Sample	Exp. No	Infection rate (%)	GFP+ events	Sample	Exp. No	Infection rate (%)	GFP+ events
	1.1	0.5	~ 6,000		2.1	0.7	~ 5,700
2 h p.i.	1.2	0-1	~ 200	**4 h p.i.**	2.2	4.2	~ 28,881
	1.3	0.1	~ 2,800		2.3	0.2	~ 3,400
	1.1	11.3	~ 40,000		2.1	1.7	~ 31,600
8 h p.i.	1.2	1	~ 2,300	**8 h p.i.**	2.2	12.3	~ 48,000
	1.3	4.9	~ 8,800		2.3	2.3	~ 15,833
	1.1	19.1	> 50,000		2.1	8.8	~ 10,800
24 h p.i.	1.2	5.6	~ 5,300	**24 h p.i.**	2.2	25.2	~ 4,375
	1.3	30.5	~ 86,000		2.3	5.9	~ 49,678

Table 22. Overview of the mapping statistics of all sequenced samples. Samples analyzed for differential expression with DESeq2 are highlighted in bold.

		no. of sorted cells	total no. of input reads	total no. of all aligned reads	total no. of aligned human reads	total no. of aligned bacterial reads	percentage of aligned reads	percentage of unaligned reads	percentage of aligned human reads	percentage of aligned bacterial reads
R1	4 h Mock	100,000	32,377,868	25,460,558	25,457,084	3,463	79	21	99.99	0.01
	4 h MC58 GFP +	5,700	35,034,748	12,476,969	12,357,398	119,567	36	64	99.04	0.96
	8 h Mock	74,000	29,440,187	22,571,247	22,564,757	6,494	77	23	99.97	0.03
	8 h MC58 GFP +	31,600	21,159,745	7,663,760	7,631,288	32,481	36	64	99.58	0.42
	24 h Mock	100,000	26,681,304	25,201,762	25,201,145	619	**94**	6	100.00	0.00
	24 h MC58 GFP +	10,800	28,512,529	23,427,581	23,248,625	178,944	**82**	18	99.24	0.76
R2	4 h Mock	33,000	25,324,044	20,628,218	20,624,254	3,962	81	19	99.98	0.02
	4 h MC58 GFP +	28,900	23,620,402	18,328,311	18,085,324	242,990	78	22	98.67	1.33
	8 h Mock	34,000	24,125,280	18,850,641	18,845,417	5,222	78	22	99.97	0.03
	8 h MC58 GFP +	48,000	25,745,425	18,265,312	17,940,209	325,103	71	29	98.22	1.78
	24 h Mock	25,800	26,721,265	18,671,866	18,630,881	40,977	70	30	99.78	0.22
	24 h MC58 GFP +	4,400	17,194,388	7,700,518	7,598,122	102,387	45	55	98.67	1.33
R3	4 h Mock	68,800	23,882,642	20,513,722	20,512,387	1,335	86	14	99.99	0.01
	4 h MC58 GFP +	3,400	24,742,596	9,586,767	9,502,831	83,931	39	61	99.12	0.88
	8 h Mock	106,700	25,596,319	22,183,646	22,183,241	390	87	13	100.00	0.00
	8 h MC58 GFP +	15,800	17,039,837	9,397,361	9,342,353	54,990	55	45	99.41	0.59
	24 h Mock	201,200	31,279,733	28,951,474	28,951,187	287	**93**	7	100.00	0.00
	24 h MC58 GFP +	49,700	28,816,903	25,319,943	25,270,253	49,682	**88**	12	99.80	0.20

The human-mapped reads made up >98 % of the total mapped reads and the dataset consisted mostly of reads that mapped to mRNAs and long noncoding RNAs (i.e. the polyadenylated RNA species), while the otherwise abundant rRNAs and tRNAs were successfully depleted during the library preparation (**Figure 23**). In stark contrast, the *Neisseria* reads mostly consisted of rRNA-derived sequences and likely reflect the total RNA composition of the bacteria (**Figure 24**). Manual inspection of the sequencing quality (in particular, the inspection of read coverage files in the IGB) indicated that samples with <70 % mapping rates corresponded to low-quality libraries, which were discarded. Since at least two replicates are necessary for assessment of statistical significance, only samples R1 and R3 of the 24 h time point were selected for further analysis (**Table 22**).

Samples R1 and R3 of the 24 h time point were analyzed for differential expression using DESeq2 software (Love et al., 2014). A total of 100 genes (61 mRNAs and 39 non-coding RNAs (ncRNAs),) were differentially expressed when comparing GFP-positive infected and mock control cells at 24 h of infection (listed on **Table 23** and **Table 24**). Of those 61 mRNAs, 22 were downregulated while 39 were upregulated (**Figure 25**). Interestingly, while several of the upregulated mRNAs (e.g. *TNFAIP2*, *BCL3*) were previously reported as *Nm*-induced host transcripts in a human blood-cerebrospinal fluid barrier model by microarray analysis (Borkowski et al., 2014), others had not been identified in previous screens. Gene Ontology (GO) analysis of these mRNAs using DAVID software (Huang et al, 2009) yielded few significant GO Terms with *P*-value < 0.05 (**Figure 25**), which include “response to hypoxia”, “cellular ion homeostasis”, “epithelial cell differentiation”, and “positive regulation of apoptotic process”. In order to validate some of these results, independent qRT-PCR was performed on RNA samples from bulk, unsorted cell cultures. Specifically, the *VEGFA* mRNA, encoding vascular endothelial growth factor A, was upregulated by invaded iPSC-BECs, according to the RNA-Seq data (23-fold vs. mock). This strong induction could be confirmed by qRT-PCR (**Figure 25**). Likewise, induced expression of *TNFAIP2* mRNA, encoding the proinflammatory TNFα-induced protein 2 and known to be involved in the response to *Nm* infection (Borkowski et al., 2014), was observed by both RNA-Seq and qRT-PCR.

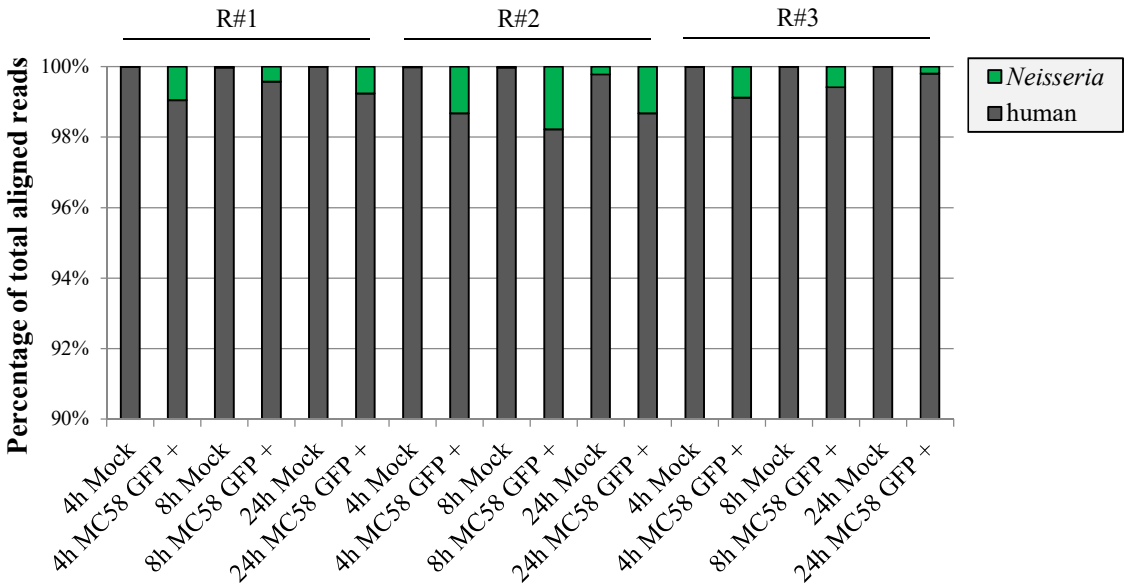

Figure 22. Relative fraction of reads mapped to the Neisseria and Human species in each experimental replicate.

Samples that were GFP-enriched presented significantly more *Neisseria* reads than mock controls samples. *Neisseria* reads varied from 0.2 to 1.78 % in infected GFP-enriched cells. Small percentages of *Neisseria* reads (less than 0.25 %) in mock control samples are due to mapping of reads to genomic sequences similar between the two species.

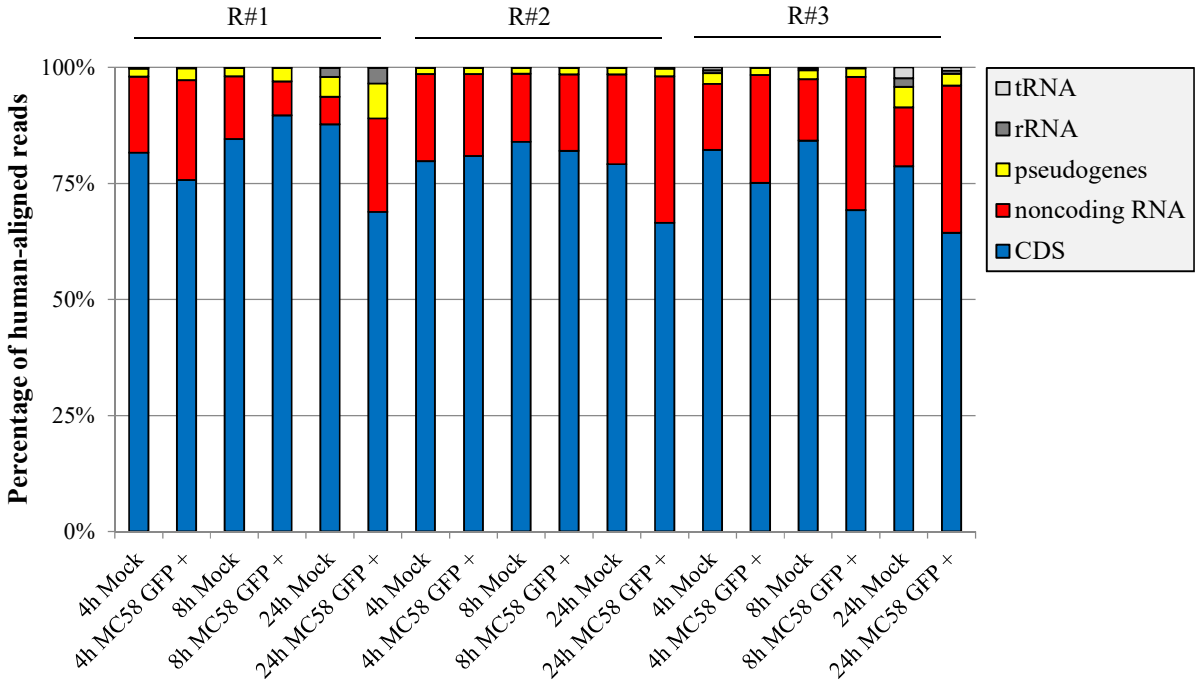

Figure 23. RNA class distribution of the human data subset in each experimental replicate.

Figure 23. RNA class distribution of the human data subset in each experimental replicate. (continued)

RNAs detected in samples include transfer RNAs (tRNAs), ribosomal RNAs (rRNAs), noncoding RNAs (ncRNAs), pseudogenes, and coding sequences (CDS).

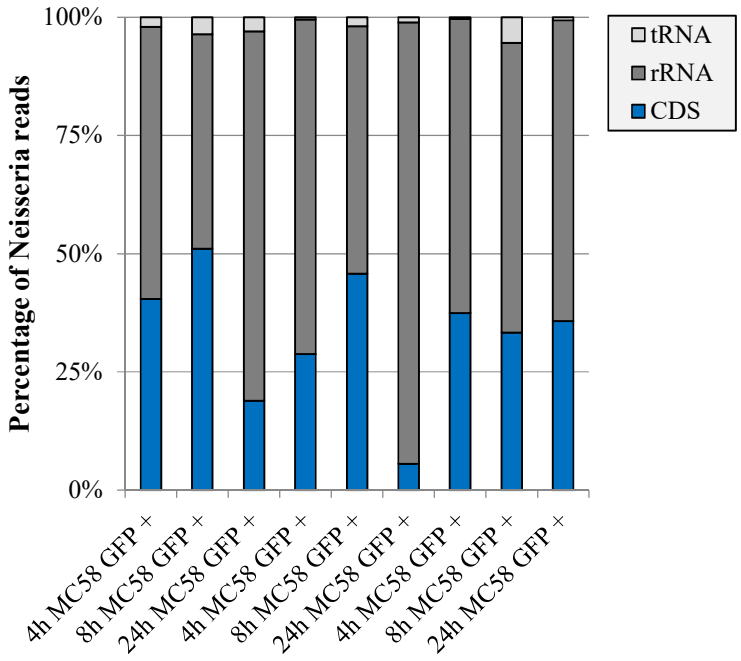

Figure 24. RNA class distribution of the bacterial data subset in the GFP-positive replicates.

Neisseria reads in GFP-enriched samples consisted of transfer RNAs (tRNAs), ribosomal RNAs (rRNAs) and coding sequences (CDS). *Neisseria* reads mostly consisted of rRNA-derived sequences.

Surprisingly, none of the mRNAs involved in tight junction regulation and cytokine secretion mentioned in the assays above could be detected in the RNA-Seq screen of differentially expressed genes at 24 h p.i. When analyzing the number of reads mapped to genes important for this study, it could be observed that no reads were mapped to *CLDN5*, and cytokine-related genes *CXCL8*, *CXCL2* and *CCL20*. Importantly, the number of reads mapped to these genes did not increase when decreasing the read-mapping accuracy cutoff from 95 % to 90 %. However, high numbers of reads could be mapped to endothelial-related genes such as *TJP1* (ZO-1), *OCLN* (Occludin), *vWF* (von Willebrand factor), *CDH5* (VE-Cadherin), *GLUT1* (Glut-1), and *ABCB1* (P-gp) (see **Table 25**), although these genes were not differentially expressed as assessed by DESeq2. In general, when comparing these results to previously shown qRT-PCR data, genes that generated Ct values lower

than 30 by qRT-PCR in bulk, unsorted RNA samples of iPSC-BECs, did not yield mapped reads on the RNA-Seq screen. Although RNA-Seq is considered a highly sensitive technique, this might indicate that the low RNA amounts obtained herein for sequencing only allowed capturing transcripts present in a high enough copy number (highly abundant transcripts).

Table 23. Overview of differentially expressed mRNAs between GFP-positive, infected cells and mock controls at 24 h of infection.

Gene	Gene ID	Log(2)F.C.	Chromossome	Start	End	Strand
C1QTNF126	ENSG00000184163	7.7	chr1	1242446	1246722	-
NRN1	ENSG00000124785	6.8	chr6	5997999	6007605	-
UBE2QL1	ENSG00000215218	5.8	chr5	6448623	6494909	+
ENO2	ENSG00000111674	5.1	chr12	6913745	6923698	+
ADM	ENSG00000148926	5.5	chr11	10304680	10307397	+
PTPRO	ENSG00000151490	-7.7	chr12	15322397	15597399	+
LDHA	ENSG00000134333	5.4	chr11	18394388	18408425	+
CLEC19A	ENSG00000261210	7.0	chr16	19285739	19322145	+
HR	ENSG00000168453	-8.1	chr8	22114415	22133384	-
HIST1H4B	ENSG00000278705	9.3	chr6	26026815	26027252	-
HIST1H3B	ENSG00000274267	8.4	chr6	26031650	26032060	-
PNMA2	ENSG00000240694	8.0	chr8	26504686	26514092	-
GABRG3	ENSG00000182256	-6.5	chr15	26971282	27541991	+
HIST1H2AJ	ENSG00000276368	8.8	chr6	27814354	27814740	-
TBX6	ENSG00000149922	6.9	chr16	30085793	30091887	-
GDPD3	ENSG00000102886	-7.7	chr16	30104810	30113856	-
ITGAX	ENSG00000140678	8.7	chr16	31355134	31382997	+
FAM83C	ENSG00000125998	8.9	chr20	35285731	35292401	-
DISP2	ENSG00000140323	-7.7	chr15	40358235	40378639	+
KRT15	ENSG00000171346	-7.7	chr17	41513743	41522529	-
VEGFA	ENSG00000112715	4.8	chr6	43770184	43786487	+
BCL3	ENSG00000069399	6.3	chr19	44747705	44760044	+
SLC12A5	ENSG00000124140	5.5	chr20	46021690	46060152	+
CCDC114	ENSG00000105479	6.1	chr19	48296457	48321894	-
PFKFB4	ENSG00000114268	6.1	chr3	48517684	48562015	-
A1CF	ENSG00000148584	8.0	chr10	50799409	50885675	-
GRM2	ENSG00000164082	-7.7	chr3	51707070	51718613	+

Table 23. Overview of differentially expressed mRNAs between GFP-positive, infected cells and mock controls at 24 h of infection. (continued)

GSTA1	ENSG00000243955	9.0	chr6	52791664	52803910	-
FAM151A	ENSG00000162391	7.8	chr1	54609182	54623556	-
FAM209B	ENSG00000213714	9.1	chr20	56533246	56536520	+
MT4	ENSG00000102891	9.0	chr16	56565049	56568957	+
DRC7	ENSG00000159625	6.8	chr16	57694793	57731805	+
CD226	ENSG00000150637	-5.1	chr18	69831158	69961803	-
ITGB1BP2	ENSG00000147166	-7.7	chrX	71301734	71305371	+
DDIT4	ENSG00000168209	7.7	chr10	72273920	72276036	+
PLCG2	ENSG00000197943	6.4	chr16	81739097	81962693	+
SLC16A3	ENSG00000141526	5.0	chr17	82228397	82261129	+
RHCG	ENSG00000140519	8.5	chr15	89471398	89496613	-
AZGP1	ENSG00000160862	9.0	chr7	99966720	99976157	-
TNFAIP2	ENSG00000185215	5.7	chr14	103123442	103137439	+
CALHM3	ENSG00000183128	8.5	chr10	103472804	103479240	-
TMEM31	ENSG00000179363	9.2	chrX	103710909	103714028	+
FICD	ENSG00000198855	-6.4	chr12	108515185	108525837	+
BTG4	ENSG00000137707	8.2	chr11	111467526	111512354	-
IL36B	ENSG00000136696	9.2	chr2	113022091	113052867	-
SDS	ENSG00000135094	6.6	chr12	113392445	113426301	-
VGLL2	ENSG00000170162	-8.9	chr6	117265558	117273565	+
C4orf3	ENSG00000164096	4.4	chr4	119296419	119304445	-
POPDC2	ENSG00000121577	-5.0	chr3	119636457	119665324	-
GPR156	ENSG00000175697	-5.8	chr3	120164645	120285094	-
FAM162A	ENSG00000114023	5.8	chr3	122384176	122412334	+
KIAA1024L	ENSG00000186367	-8.5	chr5	129748079	129766732	+
ADAMTS15	ENSG00000166106	-5.8	chr11	130448974	130476641	+
SLC2A6	ENSG00000160326	5.8	chr9	133471095	133479137	-
AKR1B15	ENSG00000227471	-8.0	chr7	134549136	134579875	+
CHRM2	ENSG00000181072	-6.2	chr7	136868669	137020255	+
MAGEA8	ENSG00000156009	9.3	chrX	149881141	149885835	+
ULBP3	ENSG00000131019	7.0	chr6	150063150	150069095	-
CCDC170	ENSG00000120262	-7.8	chr6	151494030	151621193	+
DUSP27	ENSG00000198842	-8.5	chr1	167094045	167129165	+
ENPP6	ENSG00000164303	-6.8	chr4	184088706	184221230	-
CFH	ENSG00000000971	-6.8	chr1	196651878	196747504	+

Table 23. Overview of differentially expressed mRNAs between GFP-positive, infected cells and mock controls at 24 h of infection. (continued)

STUM	ENSG00000203685	8.9	chr1	226548800	226609214	+
CATSPERE	ENSG00000179397	-4.9	chr1	244454377	244641177	+

Table 24. Overview of differentially expressed non-coding RNAs between GFP-positive, infected cells and mock controls at 24 h of infection.

Gene	Gene ID	Log(2)F.C.	Chromossome	Start	End	Strand
MIR210HG	ENSG00000247095	6.9	chr11	565660	568457	-
AL645608.8	ENSG00000272512	-8.2	chr1	995966	998051	-
AP005136.1	ENSG00000264150	8.9	chr18	2568392	2569122	+
RPL23AP86	ENSG00000262959	9.6	chr16	2922662	2923202	-
RN7SKP79	ENSG00000200243	5.8	chr5	6848127	6848462	-
RNU1-3	ENSG00000207513	5.2	chr1	16666785	16666948	-
RN7SKP90	ENSG00000199883	6.2	chr11	16842253	16842587	+
SNORD3C	ENSG00000264940	6.0	chr17	19189665	19190245	-
AC005083.1	ENSG00000233834	8.3	chr7	20217577	20221700	+
AL163195.2	ENSG00000258573	9.2	chr14	20587644	20607137	+
DEFB122	ENSG00000204547	7.9	chr20	31421436	31429180	-
RNU1-27P	ENSG00000206596	5.3	chr14	34546714	34546877	+
RNU1-28P	ENSG00000206588	5.3	chr14	34556226	34556389	-
SPG20-AS1	ENSG00000120664	-8.4	chr13	36346431	36369601	+
AC008392.1	ENSG00000268186	7.6	chr19	48262900	48271283	-
7SK	ENSG00000202198	6.5	chr6	52995620	52995950	+
RN7SK	ENSG00000283293	6.5	chr6	52995621	52995948	+
OR6C5P	ENSG00000230307	9.4	chr12	55311835	55312757	+
AC092868.2	ENSG00000259735	-5.7	chr15	59348648	59359889	-
GOLGA2P11	ENSG00000260062	9.2	chr15	62253730	62270680	-
SLC22A20	ENSG00000197847	-6.6	chr11	65213840	65242757	+
mascRNA	ENSG00000274072	-7.4	chr11	65506117	65506173	+
RN7SKP47	ENSG00000202217	6.5	chr9	74799895	74800222	+
RN7SKP176	ENSG00000260682	6.7	chr16	81961926	81962243	+
RN7SKP255	ENSG00000200312	7.2	chr14	89712511	89712823	+
AL158071.3	ENSG00000237422	-7.3	chr9	91119138	91163087	-
RN7SKP9	ENSG00000201793	5.8	chr13	99205708	99206006	+
RN7SKP230	ENSG00000202512	6.1	chr5	109699500	109699834	-

Table 24. Overview of differentially expressed non-coding RNAs between GFP-positive, infected cells and mock controls at 24 h of infection. (continued)

RN7SKP71	ENSG00000201428	6.3	chr12	112267077	112267394	+
AC244021.1	ENSG00000227082	-6.6	chr1	121396754	121463129	+
U6	ENSG00000283489	8.9	chr11	132525809	132525887	+
AL357060.1	ENSG00000230533	-8.0	chr6	137673378	137763984	+
RNVU1-18	ENSG00000206737	5.3	chr1	143729407	143729570	-
U1	ENSG00000270722	8.0	chr1	145465617	145465780	-
U1	ENSG00000273768	5.3	chr1	146376807	146376970	+
RNVU1-7	ENSG00000206585	5.3	chr1	148038753	148038916	-
FLJ42393	ENSG00000279891	-7.8	chr3	188178543	188180812	+
PCAT6	ENSG00000228288	6.3	chr1	202810954	202812156	+
AL451007.1	ENSG00000232059	11.1	chr1	244694432	244694720	-

Table 25. Read numbers assigned to important genes for the mock control and GFP+ samples analyzed for differential expression with DESeq2.

	R1, 24 h Mock	**R1, 24 h GFP+**	**R3, 24 h Mock**	**R3, 24 h GFP+**
CXCL8	0	0	0	0
CXCL2	7	6	0	0
IL6	9	17	11	0
CCL20	0	0	0	0
CLDN5	0	0	0	0
TJP1	10,544	1,332	2,719	1,121
OCLN	358	207	202	6
PECAM1	11	7	280	1
VWF	43	26	362	155
CDH5	212	142	436	0
GLUT1	428	177	25	56
ICAM1	2	42	1	7
ABCB1	315	148	161	174

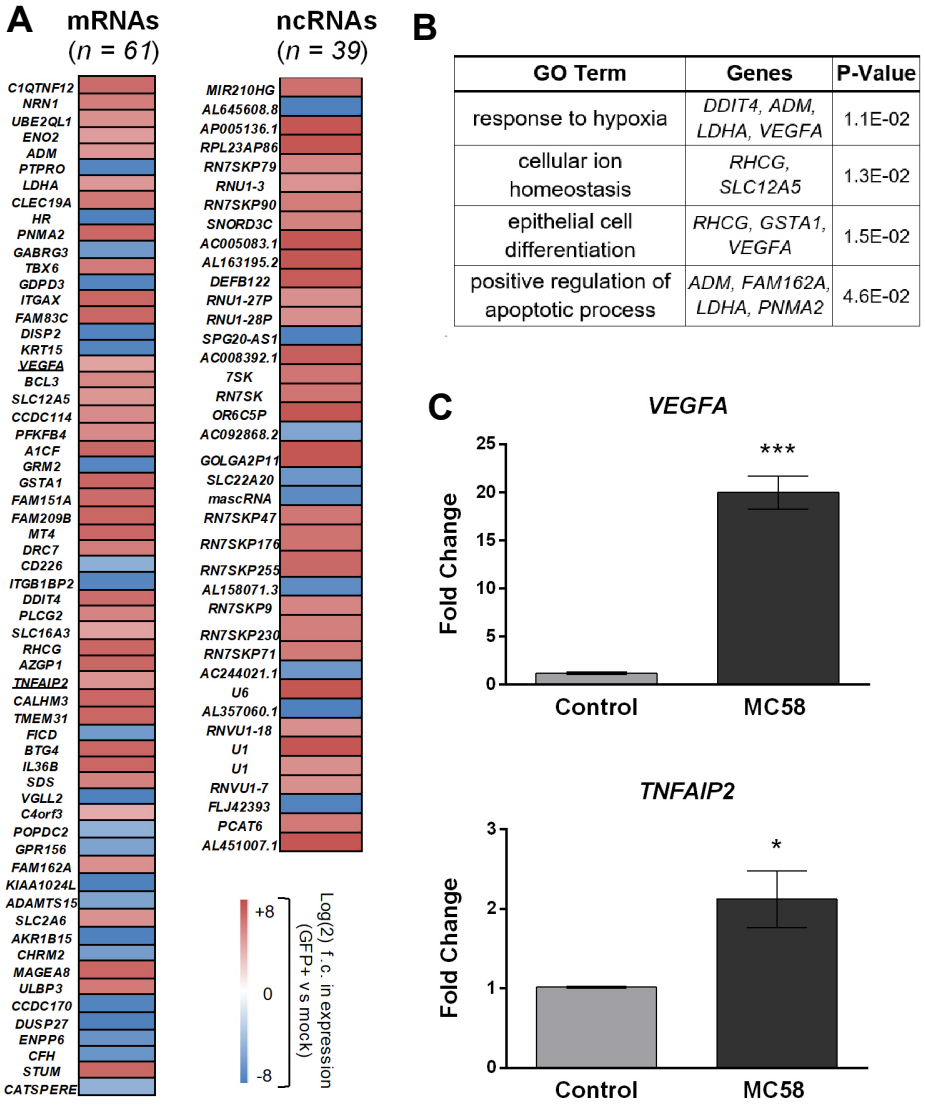

GO Term	Genes	P-Value
response to hypoxia	*DDIT4, ADM, LDHA, VEGFA*	1.1E-02
cellular ion homeostasis	*RHCG, SLC12A5*	1.3E-02
epithelial cell differentiation	*RHCG, GSTA1, VEGFA*	1.5E-02
positive regulation of apoptotic process	*ADM, FAM162A, LDHA, PNMA2*	4.6E-02

Figure 25. RNA-Seq results of sort-enriched, infected iPSC-BECs.

(A) Heat map showing differentially expressed mRNAs and ncRNAs at 24 h of infection. Plotted are all genes that were significantly differentially expressed (adjusted *P*-value < 0.1; DESeq2). Sequencing data is derived from 2 biological replicates. (B) Gene Ontology analysis of differentially expressed mRNAs shown in (B), acquired with DAVID bioinformatics resources. Enriched GO terms with *P*-value < 0.05 are shown as well as the differentially expressed mRNAs corresponding to the respective pathway. (C) Validation of RNA-Seq data by qRT-PCR. *VEGFA* and *TNFAIP2* mRNA levels were increased at 24 h after MC58 infection (MOI 10) as compared to mock-treated cultures. RNA was isolated from monolayers of iPSC-BECs without sorting. The data are presented as mean ± S.E.M of 3 independent experiments done in triplicate. Student's *t* test was used to determine significance. *, $p < 0.05$; ***, $p < 0.001$.

5. Discussion

The BECs that line brain microvessels of the b-CSF and BBB are highly specialized cells that help maintain brain homeostasis by protecting the CNS from pathogens and toxic compounds. The development of novel therapeutic intervention for meningococcal disease largely depends on the understanding of the host-pathogen interactions that allow bacterial crossing at the b-CSF level. However, the human-exclusive tropism of *Nm* and the specific properties of BECs have made it difficult to properly model this interaction. *In vitro* studies of *Nm* interaction with host ECs have largely relied on human bone marrow-derived ECs (Bernard et al., 2014; Hoffmann et al., 2001) and immortalized cell lines such as the brain microvascular EC line hCMEC/D3 (Bernard et al., 2014; Coureuil et al., 2009, 2010; Weksler et al., 2005) and HBMECs (Unkmeir et al., 2002; Nikulin et al., 2006; Simonis et al., 2014; Slanina et al., 2012). All 3 cell lines were generated upon transformation with SV40 large T antigen, allowing long-term culture and expansion. Human bone marrow ECs were isolated from adult human bone marrow and characterized for expression of endothelial markers during *in vitro* cell culture (Schweitzer et al., 1997). hCMEC/D3 cells were isolated from the temporal lobe of human brain tissue and represent a stable, fully characterized, well differentiated human BEC line (Weksler et al., 2005). Lastly, HBMECs were isolated from human brain capillaries and upon immortalization were observed to support bacterial invasion and transcytosis (Stins et al., 2001). However, none of these cell lines properly model the complex properties of BECs. While HBMECs lack Claudin-5 expression, hCMEC/D3 cells express Claudin-5 but lack continuous Occludin (Eigenmann et al., 2013; Weksler et al., 2005). Both immortalized cell lines present low barrier properties and respond poorly to co-culture with cells of the NVU (Eigenmann et al., 2013; Helms et al., 2015). By contrast, in animal experiments, TEER values of more than 1500 Ωxcm² were measured at the BBB (Butt et al., 1990; Crone and Olesen, 1982). Therefore, although these cell lines maintain BEC characteristics such as expression of important endothelial-specific factors, they do not mimic BEC function *in vivo* as they do not retain true barrier functionality.

Studies with primary BECs are highly restrictive as these can only be analyzed post-mortem or isolated during operative treatment of conditions such as brain tumors or epilepsy. Human BECs present extremely limited availability and low isolation yield, as microvessels represent only 0.1% of the total brain volume (Pardridge, 2001). Protocols for isolating primary BECs from whole brain

material have been published, however, these cells show only moderate barrier properties in *in vitro* culture and important markers such as ZO-1 and P-gp localize poorly at membrane extremities (Bernas et al., 2010). Moreover, BEC monocultures have been described to de-differentiate and rapidly lose their properties *in vitro* (Calabria and Shusta, 2008; Lacorre et al., 2004). Alternatively, humanized mice have been developed exclusively for the purpose of studying meningococcal disease. The first mouse model to be developed for *Nm* infection consisted of transgenic mice expressing human CD46 (Johansson et al., 2003). Notably, this model allowed the transversal of meningococci through the b-CSF barrier and modeling of meningitis, while non-transgenic mice developed high bacteremia but not lethal disease. Transgenic mice models expressing CEACAMs, that can bind the neisserial Opa protein adhesins, allowed the understanding of *Nm* interactions within the nasopharyngeal mucosa (Johswich et al., 2013, 2015). Humanized mice engrafted with human dermal microvessels, conversely, have been developed to study the impact of bacterial adhesion to the microvasculature on meningitis progression (Melican et al., 2013, 2014). Still, these models must rely on known interactions and/or have limited translatability.

The prospect of stem-cell based models have become an interesting part of disease modeling. Recently, an iPSC-derived model of BECs was developed, which possesses superior BEC phenotypes and closely mimics the *in vivo* BBB (Lippmann et al., 2012, 2014). In particular, this model is from human origin, highly scalable, and maintains high barrier properties, overcoming drawbacks of current models of immortalized cell lines, primary cells, and humanized rodents. As *Nm* is a human-specific pathogen, this model also represents the only way to readily interrogate barrier properties during infection. The aim of this dissertation work was to establish iPSC-derived BECs as a novel cellular model to study *Nm* infection, and to explore the impact of *Nm* on host barrier properties, tight junction complexes, inflammatory responses, and transcriptome.

5.1. Differentiation and Characterization of iPSC-BECs

The differentiation of iPSCs into BECs was performed according to previously published methods by the group of E.V. Shusta (Helms et al., 2015; Lippmann et al., 2012, 2014; Wilson et al., 2015). During embryonic development, cells of the developing brain provide factors, such as Wnt7a and Wnt7b, which promote the specific BBB evolution of BECs via the canonical Wnt signaling

pathway (Daneman et al., 2009; Stenman et al., 2008). Thus, the differentiation strategy developed by Lippmann et al., 2012 simultaneously targets the formation of neural cells and ECs. The presence of neural cells and other cell types of the NVU mimics the microenvironment of the embryonic brain and promotes BBB phenotypes of terminally differentiated BECs (Lippmann et al., 2012). Although several iPSC lines were tested in this study, IMR90 cells presented the highest differentiation potential and cell yield when compared to the iPSC lines DF6-9-9T and DF19-9-11T, and the ESC line H9. For this reason, IMR90 cells were used in this dissertation work. It is worth mentioning that in one other study using iPSC-BECs for infection studies, the iPSC line DF19-9-11T was used, as it was not generated through the use of viral integration vectors, eliminating the potential for inherent antiviral or anti-inflammatory responses (Kim et al., 2017).

The protocols of Lippmann et al. 2012, 2014 and Wilson et al. 2015, previously implemented at the Chair Tissue Engineering and Regenerative Medicine, University Hospital Würzburg, were implemented in our laboratory at the Institute of Hygiene and Microbiology, and the results could be reproduced. IMR90-4 cells were maintained in 2-dimensional feeder-free conditions in Matrigel™ substrate and mTeSR™1 or Stem™Flex culture medium. Seeding of single cells at optimal seeding densities (Wilson et al., 2015) precedes the induction of differentiation, followed by exposure of iPSC to UM for 6 days. This so-called 'UM phase' is described by co-differentiation of ECs and neural-like cells. At day 6 of differentiation several populations of cells can be discerned: potential immature neurons (29 %), neurons (26 %), BECs (around 30 %), and few cells positive for an astrocyte marker, and a pericyte-smooth muscle marker (Lippmann et al., 2012). The next step of the protocol involves changing the medium composition to EC medium supplemented with RA and hbFGF. RA has concentration-dependent effects on the cells, and by administering 10 μM of RA the expression of VE-cadherin is promoted, and Occludin expression as well as tight junctional continuity are increased (Lippmann et al., 2014). RA is also essential for high barrier properties at the end of the differentiation and increases the activity of MRPs (Lippmann et al., 2014). Finally, RA stimulation increases BEC yield, but has no influence on the differentiation efficiency (i.e. increases total cell proliferation without changing their relative abundance) (Lippmann et al., 2014). Notably, the positive effects of RA on BBB development have been previously reported in a study conducted with human brain tissue, hCMEC/D3 cells and a rodent model (Mizee et al., 2013). The final step in the differentiation protocol is the isolation of BECs from the heterogeneous cell population obtained at day 8 by ECM–based selective passaging,

through seeding onto collagen IV/fibronectin-coated surfaces. This step also allows EC maturation, as the cells form continuous junctions leading to the generation of a tight monolayer, and begin expressing vWF (Lippmann et al., 2012). The differentiation protocol has been further optimized to induce mesoderm commitment and remove serum usage, allowing the implementation of a completely chemically-defined method that can be more easily translated into therapeutic settings (Qian et al., 2017).

Further studies have confirmed the suitability of iPSC-BECs in modelling BBB functionality and pathogenesis. Apart from exhibiting key BBB phenotypes, iPSC-BECs were found to have gene expression profiles very similar to those of primary BECs (Qian et al., 2017). iPSC-BECs have also proved to be useful for the modeling of genetic disorders over the past few years (Lim et al., 2017; Vatine et al., 2017). By using patient-derived iPSCs and differentiating them to BECs, the authors were able to model Huntington's Disease (Lim et al., 2017) and severe psychomotor retardation (Vatine et al., 2017), and study phenotypes of iPSC-BECs that were not present in other *in vitro* models. Lastly, iPSC-BECs have been utilized for the study of Zika virus and Group B *Streptococcus* (Alimonti et al., 2018; Kim et al., 2017), opening the door for infection studies with other CNS pathogens. In general, these previous studies used iPSC-BEC to model the BBB, given the ability of these cells to respond to cues from other CNS cells, namely astrocytes, pericytes or neuronal stem cells (Appelt-Menzel et al., 2017; Lippmann et al., 2012). However, here it was proposed the modeling of the BECs that may resemble those of the meningeal b-CSF barrier. As mentioned before, BECs that constitute the vessels located within the SAS possess high barrier properties and maintain BEC phenotypes, without the support of NVU cell types such as pericytes and astrocytes (Cassella et al., 1997; Nabeshima et al., 1975; Rua and McGavern, 2018; Saunders et al., 2016; Weller et al., 2018).

5.2. Characterization of *Neisseria meningitidis* infection in iPSC-BECs

To date, iPSC-BECs have yet to be established for *Nm* infection modelling. iPSC-BECs were firstly used to confirm that multiple *Nm* strains and mutants follow similar phenotypes to previously described models. Non-capsulated mutant MC58Δ*siaD* was more invasive in iPSC-BECs than its parental strain MC58, in accordance to previously published data (Unkmeir et al., 2002). The lack

of polysaccharide capsule exposes important components of the meningococcal outer membrane, such as Opa and OpcA proteins, involved in internalization into host cells (Unkmeir et al., 2002). Although the presence of capsule blocks the interaction of meningococci with epithelial and endothelial cells, capsulated meningococci are protected against the host's immune system and exhibit serum resistance (Vogel and Frosch, 1999). Therefore, capsule expression is crucial during dissemination in the blood as it confers protection from attack by the immune system (Unkmeir et al., 2002). Conversely, the capsulated WT strain 8013/12 was overall less invasive than WT MC58. This can be explained by the lack of expression of the aforementioned components of the meningococcal outer membrane, Opa and OpcA (Nassif et al., 1993). When using 8013/12-derived strains to confirm pilus function, the hyperpiliated PilT-deficient mutant was significantly more invasive than the WT strain, in accordance to the literature (Hoffmann et al., 2001). PilT is an ATPase that drives pilus retraction. In the absence of PilT, pilus fibers are assembled and extruded to the bacterial surface but are not subjected to retraction, resulting in the accumulation of Tfp on the bacterial surface (Morand et al., 2004). Unexpectedly, the non-piliated PilE-deficient mutant showed invasion rates similar to the WT strain. Still, overall, the modeling of *Nm* attachment and invasion could be successfully modelled when utilizing iPSC-BECs.

Importantly, iPSC-BECs express the recently identified pilus receptor CD147 which seemed to be recruited underneath meningococcal colonies (commonly referred to in the literature as "honeycomb"-like structures) (Bernard et al., 2014; Coureuil et al., 2009, 2010). This contributes to the validation of previously published data showing the role of CD147 in Tfp-dependent adhesion to ECs, considering that here, for the first time, this interaction was observed using a clinical isolate of *Nm* (MC58). CD147-mediated meningococcal adhesion was shown to be a prerequisite for activating the β2AR–β-arrestin signaling pathway, triggering the signaling events that lead to meningococcal invasion and disruption of the BEC barrier (Bernard et al., 2014). CD147 is expressed in many cell types and its *in vivo* role may span along various biological processes. As demonstrated by flow cytometry analysis (**Figure 11A)**, CD147 is expressed in undifferentiated IMR90-4 iPSCs as well as in differentiated iPSC-BECs and immortalized HBMECs. CD147 expression by Western blot was previously shown in 9 distinct iPSC lines, including IMR90-1, while primary fibroblasts did not show CD147 expression (Pripuzova et al., 2015). Notably, it was previously shown that CD147 is also a target of HIV-1 (Pushkarsky et al., 2002), severe acute respiratory syndrome coronavirus (Chen et al., 2005), measles virus (Watanabe

et al., 2010), as well as the bacterial pathogen *Listeria monocytogenes* (Till et al., 2008), to adhere to and/or invade epithelial cells. For this reason, Bernard *et al*. hypothesized that CD147 constitutes an evolutionarily conserved efficient target for pathogens to infect tissues and spread within organisms. More recently, CD147 was found to be a human cytomegalovirus entry mediator, promoting virus entry into epithelial and endothelial cells (Vanarsdall et al., 2018). CD147 is a highly glycosylated cell surface transmembrane protein that is greatly expressed in malignant tumors to stimulate production of MMP-1 (interstitial collagenase), MMP-2 (gelatinaseA) and MMP-3 (stromelysin 1) in neighboring fibroblasts (Gabison et al., 2005). It is therefore possible that the role of CD147 in host-pathogen interactions also includes the induction of epithelial and endothelial barrier integrity disruption by promoting local production of MMPs (Bernard et al., 2014).

5.3. Loss of Barrier Properties during *Neisseria meningitidis* infection

Previously published work describing Zika virus and Group B *Streptococcus* infection on iPSC-BECs was crucial to shed light over the mechanisms of BEC crossing by these pathogens (Alimonti et al., 2018; Kim et al., 2017). Interestingly, while crossing of Zika virus does not compromise the viability and permeability of the BEC monolayer, GBS infection results in decreased junctional continuity and barrier properties. Similarly, the iPSC-BEC model was used herein to answer important questions regarding mechanisms of brain microvessel disruption and penetration by *Nm* that could not be approached with formerly available models. In particular, the low baseline TEER (< 100 $\Omega x cm^2$) displayed by these models did not allow the detection of subtle perturbations in paracellular tightness caused by infection with this pathogen. Using the RA-enhanced iPSC-BEC model (Lippmann et al., 2014), TEERs far greater than the previous papers using infectious agents were achieved here. Unexpectedly, HS had a negative impact on the TEER of polarized iPSC-BECs. For this reason, all studies involving polarized cells seeded onto transwell cell culture systems were performed in EC medium alone. HS is used during meningococcal infection studies as a supplement in the infection medium due to the presence of fibronectin. HS fibronectin was identified as the serum component that supports the invasion of strain MC58 via the α5β1 integrin receptor into HBMECs in OpcA-expressing meningococci (Unkmeir et al., 2002). For future studies, HS supplementation should be avoided when using iPSC-BECs and the

use of soluble commercially available fibronectin in the infection medium should be tested as an alternative.

Using the high TEER of this cellular model, it was possible to demonstrate that *Nm* infection causes loss of barrier properties in iPSC-BECs using two distinct transwell systems. TEER values were maintained up to 8 h p.i.; however, a tendency for TEER decrease could be observed at 24 h p.i., and at 32 h TEER values dropped 90 % for infection conditions when compared to controls (**Table 19**). Increases in Na-Fluorescein transport through the monolayer, a tracer molecule commonly used to follow BBB disruption, could also be detected at 24 h p.i., becoming statistically significant at 32 h. At the tight junction level, these modifications of barrier functionality were associated with the formation of highly frayed junctions, junctional discontinuity and opening of gaps between cells. Through immunofluorescence, it was possible to directly observe that *Nm* disrupts the tight junction proteins ZO-1, Occludin, and Claudin-5 (**Figure 16**). Importantly, this was unable to be observed in a single model prior to this iPSC-BEC model due to lack of expression of some or all tight junction components in immortalized cell lines. Moreover, these results are in accordance with an *in vivo* study using mice engrafted with human dermal microvessels reporting mild vessel damage at 6 h p.i. (despite large numbers of attached bacteria), whereas at 24 h extensive vascular and tissue damage could be observed (Melican et al., 2013).

Previous work has demonstrated that *Nm* is internalized by ECs in membrane-bound compartments referred to as *Neisseria*-containing vacuoles, presumed to offer a protective niche for intracellular multiplication and potentially serve as a vehicle for transcytosis (Nikulin et al., 2006). However, the primary transit route of BECs by *Nm* has yet to be determined. The generation of gaps between *Nm*-infected cells and subsequent opening of the paracellular route has been reported before (Coureuil et al., 2009). However, the data collected here suggests that bacterial transmigration preceding barrier disruption (i.e. before 24 h) is negligible compared to transmigration following cell-cell opening (i.e. at 24 h) (**Table 20**). Therefore, additional data is shown here that support the hypothesis that the paracellular route contributes for *Nm* crossing at the BEC level. By contrast, one *in vitro* study using polarized monolayers of Calu-3 human respiratory epithelial cells has shown that *Nm* crosses these cells via a transcellular pathway without causing barrier disruption (Sutherland et al., 2010). Together, these findings are consistent with current ideology that *Nm* acts as a commensal in the nasopharynx, crossing the nasopharynx epithelium potentially via

phagocytic vacuoles as a result of endocytosis (Stephens et al., 1983; Van Deuren et al., 2000), but provokes vascular and tissue damage during and/or after the blood phase.

Interestingly, significant differences were observed between results obtained with the WT strain MC58 and the non-capsulated mutant MC58Δ*siaD*. MC58Δ*siaD* mutant was shown to be highly invasive, therefore, it was hypothesized that if transcellular passage (i.e. invasion followed by passage to the basolateral chamber) occurs before 24 h p.i., then MC58Δ*siaD* would show increased transmigration levels when compared to the parent WT strain. Strikingly, no crossing CFUs could be detected for this mutant before 24 h, and at this time point CFU counts were significant lower than for the WT strain (around 10^6-fold lower). Due to the lack of capsule, this mutant autoaggregates and tends to form clusters of attached and floating bacterial colonies that can be seen by the naked eye at late time points of infection. It is therefore possible that this mutant shows lower levels of transmigration because these aggregates might be too large to cross the BEC monolayer. This further supports the hypothesis that *Nm* does not tend to cross the BEC monolayer transcellularly, given that a highly adhesive and invasive strain was not capable of enhanced transmigration. Finally, the MC58Δ*siaD* mutant also showed surprising results when measuring TEER during infection, as TEER tended to be higher for MC58Δ*siaD* infection when compared to control conditions, although it sharply decreases from 32 h to 48 h for infected cells (presumably due to cell death from infection). It was previously shown that under static and dynamic conditions, non-capsulated meningococci are highly effective in forming biofilms, whereas capsulated strains tend to lack this trait (Lappann et al., 2006). It could be possible that the formation of biofilms and bacterial clusters contributes to increases in TEER by further blocking the passage of ions and charged molecules from the apical to the basolateral chamber of the transwell system.

The impact of *Nm* infection on endothelial tight junctions also involves the activation of host MMPs (Ricci et al., 2014; Schubert-Unkmeir et al., 2010). It was previously shown that *Nm* induces cleavage of Occludin in the first extracellular loop through MMP-8, leading to the generation of a 50-kDa fragment detected by Western blot (Schubert-Unkmeir et al., 2010). MMP activation also resulted in cell detachment from the substrate. The results shown here are in accordance with both observations. However, protein quantification studies during long infection periods were challenging, as reference proteins were not consistent between control and infected samples despite prior protein quantification via a commercially available kit. In particular, β-Actin was consistently less abundant in samples collected from infected cells at 32 h p.i., although overall the protein

content was similar between samples collected from the same replicate, as observed with Ponceau staining. It could be possible that *Neisseria* proteins present in the infected samples at late infection time points overestimate host proteins when using protein quantification assays. It is worth mentioning that actin may not be the ideal reference "housekeeping protein" for Western blot studies during infection, as *Nm* was shown to regulate cytoskeleton alterations, namely actin polymerization, as a mechanism of inducing membrane protrusions that facilitate bacterial-host contact and promote internalization (Coureuil et al., 2012). However, the same phenomenon could be observed when using COX IV as reference protein (subunit IV of cytochrome c oxidase, the terminal enzyme complex in the respiratory chain), a commonly used mitochondrial loading control. Finding proper reference proteins for future Western blot studies is necessary, as the ideal reference protein should be consistent between samples and not be impacted by infection. Unfortunately, no studies exploring the potential impact of *Nm* on host metabolism (in particular, expression of β-Actin and COX IV) could be found in the literature. In the future, the establishment of techniques such as Live-cell Metabolic Assay Seahorse to cells infected with *Nm* would allow testing this hypothesis.

Finally, further mechanistic detail is provided here by showing that the decreased levels of tight junction proteins inversely correlated with *SNAI1* expression. A significant increase in *SNAI1* transcripts during *Nm* infection when compared to controls could be observed at 4, 6, 16 and 24 h, preceding the disruption of Occludin, Claudin-5 and ZO-1 at 24 h. Snail-1 is a zinc finger transcription factor that was shown to act as a repressor of genes involved in tight junction formation, and to facilitate bacterial-induced disruption of endothelial and epithelial barriers. (Clarke et al., 2015; Kim et al., 2015; Yang et al., 2016). Snail1-1 induction at the BBB and the nasopharynx is initiated by TLR2 and involves the ERK pathway of the MAPK signaling cascade (Clarke et al., 2015; Kim et al., 2015). Snail-1 binds directly to the E-boxes of the promoters of Claudin/Occludin genes, resulting in complete repression of their promoter activity and directly suppressing their gene expression (Ikenouchi et al., 2003). Interestingly, Snail-1 induction also leads to reduced protein levels of ZO-1 and Claudin-1 without affecting their transcription (Ohkubo and Ozawa, 2004).

5.4. *Nm* infection triggers proinflammatory activation of iPSC-BECs

Bacterial meningitis progression is characterized by the recruitment of highly activated leukocytes into the CSF, which is presumed to be triggered by the inflammatory activation of ECs (Dixon et al., 1999; Korthuis et al., 1994; Tang et al., 1996; Tunkel & Scheld, 1993). As such, the presence of elevated levels of proinflammatory cytokine IL-6 and chemokines IL-8, MCP-1, Gro-α, IFN-γ and RANTES in the CSF of patients suffering from bacterial meningitis was previously reported (Glimåker et al., 1994; Kornelisse et al., 1997; López-Cortés et al., 1995; Matsuzono et al., 1995; Pashenkov et al., 2002; Sprenger et al., 1996). Accordingly, using iPSC-BECs it was possible to detect RANTES and IFN-γ secretion upon meningococcal infection. RANTES was observed to be secreted by primary meningioma cells in response to 24 h of MC58 infection (Christodoulides et al., 2002; Fowler et al., 2004, 2006). RANTES is a proinflammatory cytokine that induces leukocyte migration, mediates the trafficking and homing of classical lymphoid cells but also acts on a range of other immune cells (Appay and Rowland-Jones, 2001). IFN-γ expression was linked to aging in primary BECs from mice (Wei et al., 2002), however its release in response to meningococcal infection has not been previously reported in *in vitro* studies. In addition, our data indicate that iPSC-BECs upregulate *IL6* (IL-6)*, CXCL8* (IL-8), *CXCL1* (Gro-α), *CXCL2* (Gro-β) and *CCL20* (MIP3A) in response to *Nm* infection. Interestingly, however, the observed transcriptional upregulation did not accompany secretion of IL-6, and of IL-8 at physiological levels. Overall, our data are in line with published findings regarding the modeling of Group B *Streptococcus* infection using a similar model of iPSC-BECs, in which transcriptional activation of the same panel of genes (with the exception of IL-6) was observed (Kim et al., 2017). The same group performed ELISA assays on iPSC-BEC lysates collected during infection with this pathogen, and concluded that intracellular accumulation of IL-6 and IL-8 did not occur (*personal communication*). This finding suggests that post-translational events should be responsible for negatively regulating protein synthesis of these cytokines. Further investigation is needed to clarify the regulation of cytokine secretion in this model. It could be possible that further stimuli such as co-culture with other b-CSF cell types might be required to trigger cytokine secretion by iPSC-BECs. Alternatively, it may be possible that those other cell types play a more pivotal role in the innate immune response to meningococcal meningitis. In fact, human meningioma cells secrete a great variety of cytokines in response to infection with meningeal pathogens (Christodoulides et

al., 2002; Fowler et al., 2006; Fowler et al., 2004). In accordance, it was previously hypothesized that the leptomeninges are likely to be a major producer of IL-6 during meningococcal infection (Christodoulides et al., 2002).

5.5. RNA-Seq of *Neisseria meningitidis*-infected iPSC-BECs

Finally, a strategy for sequencing specifically sorted iPSC-BECs that have been invaded by *Nm* was applied herein. Previous studies analyzing the host transcriptome in response to *Nm* infection have been based on cDNA microarrays (reviewed in (Schubert-Unkmeir et al., 2009)). Notably, RNA-Seq has not been applied to the setting of *Nm*-host interactions as of yet. The rationale for applying cell sorting to this RNA-Seq approach was to enrich bacteria-infected cells, potentially allowing full coverage of the host and bacterial transcriptome (i.e. 'dual RNA-Seq') (Westermann et al., 2017). Additionally, given the low infection rates displayed by *Nm*, this method would maximize the likelihood of identifying host gene expression changes upon infection by exclusively analyzing invaded host cells, and excluding bystander, non-invaded host cells. This technique has been previously applied to sorting of cells invaded with *Salmonella enterica* (Avraham et al., 2015; Westermann et al., 2016) and revealed that potent immune responses are only induced in invaded but not bystander host cells.

The methodology carried out in the Westermann et al. study was established here using GFP-expressing MC58 and iPSC-BECs. In the mentioned study, fixation with reagent RNAlater® was found to preserve both host and bacterial transcriptomes, as well as the GFP signal during the extended FACS procedure (Westermann et al., 2016). For this reason, fixation with RNAlater® was used here to stabilize and preserve RNA integrity between collection of samples and sorting. RNAlater® was supplemented with gentamicin to kill extracellular meningococci, while intracellular bacteria are protected due to the impermeability of the host membrane for the antibiotic. Sorting of samples revealed that the infection rate varied significantly between replicates, making it challenging to collect enough infected cells for early time points of infection. After sending the samples for synthesis of cDNA libraries it was clear that the low RNA amounts present in the samples precluded the pursuit of a "dual RNA-Seq" approach. For this reason, in

order to optimize the sequencing of the host transcriptome, poly(A) enrichment was selected to remove rRNAs and select for host mRNAs.

Bioinformatic analysis of the sequenced samples showed that samples with read mapping rates lower than 70 % corresponded to low quality samples. This observation implies that around 40,000 sorted iPSC-BEC cells were minimally required for sequencing to be successful. Achieving this cell number per samples was particularly challenging at early time points of infection when using FACS to select specifically infected iPSC-BECs. It is likely that this limitation was due to the low internalization rates observed for *Nm* at early stages of infection (around 1.7% at 4 h p.i. and MOI 10), resulting in low numbers of sorted, infected iPSC-BECs. By contrast, *Salmonella enterica*'s infectivity is around 10-fold higher for Hela-S3 cells in identical infection conditions (Westermann et al., 2016). Additionally, the RNA starting material limitation may have hindered the sensitivity of the RNA-Seq method and the collection of the host transcriptome in all its complexity. This RNA-Seq approach mostly detected abundant cellular transcripts, whereas several low abundant genes (Ct-value >30 in the qRT-PCR) were not covered by RNA-Seq reads. Therefore, RNA-Seq-based expression data for some of these low abundant genes (e.g. *CXCL8*, CCL20) could not be reported herein. Additionally, the cutoffs applied for the samples analyzed with DESeq2 (24 h p.i., 2 replicates; p-adj < 0.1) needed to be more relaxed than usual. Lastly, as only a low number of differentially expressed genes (in total, 100 genes) was obtained, this precluded a complex and complete GO analysis, with only a few enriched terms that do not include cytokine/chemokine activity or tight junction regulation. Still, RNA-Seq on GFP-positive cells revealed stronger fold-changes in gene expression as compared to qRT-PCR validation, which (due to material constraints) had to be done on unsorted, bulk infected cultures. This supports our initial hypothesis that analyzing bulk gene expression in unsorted cell cultures dilutes *Neisseria*-induced changes in host gene expression.

GO analysis of the differentially expressed genes obtained at 24 h p.i. suggests that *Nm* infection elicits hypoxia, cellular ion homeostasis and apoptotic responses in iPSC-BECs. Although the impact of hypoxia and oxidative stress during *Nm* infection has been poorly described, evidence of *Nm*-induced oxidative DNA damage in infected cells has been previously observed (Oosthuysen et al., 2016). Activation of hypoxia-inducible factor 1 (HIF1) is a well-known cell response to hypoxic conditions induced by sepsis and LPS stimulation (Peyssonnaux et al., 2007; Textoris et al., 2012; Werth et al., 2010) and HIF1 signaling was proposed to mediate VEGFA induction

during *Clostridium difficile* infection (Huang et al., 2019). *VEGFA* and *BCL3*, both upregulated on our RNA-Seq dataset (28- and 73-fold, respectively), lead to enhanced proliferative potential and neovasculogenesis in response to hypoxia conditions when under the control of STAT3 in endothelial colony-forming cells (Lee et al., 2015). Quantitative PCR confirmed that *VEGFA* is highly upregulated upon 24 h of MC58 infection. During infection, mechanisms of hijacking host cellular ion homeostasis as a way of promoting invasion include release of intracellular calcium (Källström et al., 1998). Our GO term analysis results suggest that *RHCG* and *SLC12A5* may play a role in regulating cellular ion homeostasis during infection. Of note, although the GO term "epithelial cell differentiation" is enriched in our gene set, it is likely that the genes *RHCG* and *VEGFA* are contributing to the already mentioned processes, and not to the biological process "epithelial cell differentiation". Finally, positive regulation of apoptosis is a well-known transcriptomic host response to *Nm* infection (Constantin et al., 2002; Schubert-Unkmeir et al., 2007).

Our RNA-Seq results revealed interesting differentially expressed genes that have been associated to *Nm* infection. *CFH*, a key immune regulator of the host immune response that is hijacked by *Nm* through binding to fBHP (see Introduction), is downregulated in host iPSC-BECs upon meningococcal infection, according to the RNA-Seq data. Since *Nm* directly binds to CFH as a strategy of evading the host's immune system, downregulation of host CFH must have implications during the course of infection. Additionally, *Integrin Subunit Alpha X* (*ITGAX*) encoding for CD18/CD11c, is upregulated by 76-fold. CD18/CD11c has been described to be expressed in human umbilical vein endothelial cells (Langeggen et al., 2002) and to function as a phagocytic receptor for *Nm* when transfected into CHO cells (Jones et al., 2008). *Tumor necrosis factor, alpha-induced protein 2* (*TNFAIP2*), upregulated 33-fold, is phosphorylated upon LPS stimulation (Chevrier et al., 2011) and its expression is linked to increased mortality in patients experiencing septic shock (Thair et al., 2016). Importantly, independent microarray analysis of human malignant choroid plexus papilloma cells and human umbilical vein ECs identified *TNFAIP2* as a gene regulated by *Nm* infection (Borkowski et al., 2014; Linhartova et al., 2006). Through qRT-PCR the upregulation of this gene was confirmed after 24 h of MC58 infection in iPSC-BECs. Other interesting upregulated genes include *ADM* (30-fold), encoding for Adrenomedullin. ADM is a vasoactive peptide that is highly expressed by cerebral microvessels of rat models and that improves BBB function in a dose-dependent matter when added exogenously (Honda et al., 2006).

Moreover, ADM might preserve endothelial function during sepsis and its autocrine expression has been linked to host defense against bacterial pathogens (Allaker and Kapas, 2003; Müller-Redetzky et al., 2014), although its association to *Nm* infection has yet to be confirmed.

The role of host A Disintegrin And Metalloproteinase (ADAM) proteases during meningococcal infection has been poorly explored. It has been shown that the plasma level of ADAMTS13 is correlated with outcome and severity of the disease in paediatric patients (Bongers et al., 2010). A strong decrease of ADAMTS13 and increase of vWF were seen in the first 24 h of meningococcal sepsis and both correlated with disease severity (Bongers et al., 2010). Recently, it was shown that meningococcal adherence to BECs induces the activation of the membranous protease ADAM-10, resulting in impaired activation of anti-coagulant protein C (Lécuyer et al., 2018). Interestingly, our RNA-Seq data showed no significant change in host regulation of *ADAM10* or *ADAMTS13*, however, significant downregulation of *ADAMTS15* after prolonged *Nm* infection could be detected.

Overall, here is reported for the first time the establishment of an RNA-Seq technique to the setting of host-pathogen interactions involving *Nm*. These results provide the field with an added important informational transcriptomic database, as analysis of the data set has identified potential key genes that have not been described thus far to play a role in *Nm* infection. Still, host transcriptomic responses to *Nm* infection are likely to be time-dependent and to vary considerably from early to late infection stages. The low infection rate at early time points and current sensitivity of bulk RNA-Seq technologies impeded similar transcriptomics at the 4 and 8 h time point. However, ongoing progress in (single-cell) RNA-Seq techniques (Saliba et al., 2014) should allow for transcriptome profiling during earlier stages of *Nm* infection in future efforts.

6. Conclusions and Future Perspectives

Here, the successful establishment of iPSC-derived BECs as a cellular model for meningococcal infection is reported. Similar patterns of BEC-*Nm* interactions could be shown with iPSC-BECs as previously published data with immortalized cell lines, namely the recruitment of pilus receptor CD147 beneath meningococcal colonies. iPSC-BECs were shown to be activated, and to respond in a proinflammatory manner upon infection. Prolonged infection with *Nm* resulted in barrier and tight junction disruption, the latter correlating with bacterial transmigration across monolayers of iPSC-BECs. Transcriptomic sequencing of specifically infected cells could be established to this infection setting at a late infection time points, providing data of host *Nm*-responsive genes.

The application of iPSC-derived cells as cellular models for infectious disease modeling is a relatively new field of research. One of the first examples of an iPSC-derived model adapted to bacterial infection involved the differentiation of iPSCs into macrophages for the study of *Chlamydia* pathogenesis (Yeung et al., 2017). Human iPSCs present advantages when compared with primary cells as they can be readily genetically manipulated, using CRISPR/Cas9 technology, or isolated from individuals with disease-associated genotypes. In this sense, isolation of cells from patients suffering from meningococcal disease could potentially give novel insights on unknown phenotypes and/or genetic predispositions for the disease or could be used as a valuable tool for screening of therapeutic options.

Currently, the field lacks on physiological cell culture systems that mimic the *in vivo* environment of the b-CSF, which would potentially allow capturing 3-dimensional (3-D) aspects of tissue biology that are important when studying meningococcal pathogenesis (Schubert-Unkmeir, 2017). For this, the establishment of a human *in vitro* 3-D model of the b-CSF to study colonization and penetration of brain microvessels by *Nm* would be the next step. Appropriate scaffolds for seeding of iPSC-BECs include small porcine intestine submucosa (serosa part), scaffolds derived from electrospinning techniques, or alternatively from a commercial source (e.g. collagen matrices). Co-culture with leptomeningeal cells would further improve mimicking of the b-CSF barrier. These could be derived from tumor biopsies (i.e. meningioma cells) (Christodoulides et al., 2002) or eventually from iPSCs.

Finally, the development of an *in vitro* circulatory *Nm*-iPSC-BEC interaction model mimicking physiological blood pressure would be important to assess the effects of dynamic conditions on meningococcal infection. Notably, seeding of iPSC-BECs on glass rods allows mimicking of capillary organization and the generation of 3-D vessels of distinct diameters *in vitro* (Katt et al., 2016). Lastly, combining dynamic conditions and 3-D cellular systems could be achieved by the implementation of organ-on-a-chip technologies (Sosa-Hernández et al., 2018), where the complete infection from nasal tract, to bloodstream, and finally the meninges, could potentially be modelled and studied.

7. References

Absinta, M., Ha, S.-K., Nair, G., Sati, P., Luciano, N. J., Palisoc, M., et al. (2017). Human and nonhuman primate meninges harbor lymphatic vessels that can be visualized noninvasively by MRI. *Elife* 6. doi:10.7554/elife.29738.

Alimonti, J. B., Ribecco-Lutkiewicz, M., Sodja, C., Jezierski, A., Stanimirovic, D. B., Liu, Q., et al. (2018). Zika virus crosses an in vitro human blood brain barrier model. *Fluids Barriers CNS* 15. doi:10.1186/s12987-018-0100-y.

Allaker, R. P., and Kapas, S. (2003). Adrenomedullin Expression by Gastric Epithelial Cells in Response to Infection. *Clin. Vaccine Immunol.* 10, 546–551. doi:10.1128/CDLI.10.4.546-551.2003.

Allt, G., and Lawrenson, J. G. (1997). Is the pial microvessel a good model for blood-brain barrier studies? *Brain Res. Rev.* 24, 67–76. doi:10.1016/S0165-0173(97)00011-8.

Appay, V., and Rowland-Jones, S. L. (2001). RANTES: A versatile and controversial chemokine. *Trends Immunol.* 22, 83–87. doi:10.1016/S1471-4906(00)01812-3.

Appelt-Menzel, A., Cubukova, A., Günther, K., Edenhofer, F., Piontek, J., Krause, G., et al. (2017). Establishment of a Human Blood-Brain Barrier Co-culture Model Mimicking the Neurovascular Unit Using Induced Pluri- and Multipotent Stem Cells. *Stem Cell Reports* 8, 894–906. doi:10.1016/j.stemcr.2017.02.021.

Appelt-Menzel, A., Cubukova, A., and Metzger, M. (2018). Establishment of a Human Blood-Brain Barrier Co-Culture Model Mimicking the Neurovascular Unit Using Induced Pluripotent Stem Cells. *Curr. Protoc. Stem Cell Biol.* e62. doi:10.1002/cpsc.62.

Asmat, T. M., Tenenbaum, T., Jonsson, A. B., Schwerk, C., and Schroten, H. (2014). Impact of calcium signaling during infection of Neisseria Meningitidis to human brain microvascular endothelial cells. *PLoS One* 9. doi:10.1371/journal.pone.0114474.

Avraham, R., Haseley, N., Brown, D., Penaranda, C., Jijon, H. B., Trombetta, J. J., et al. (2015). Pathogen Cell-to-Cell Variability Drives Heterogeneity in Host Immune Responses. *Cell* 162, 1309–1321. doi:10.1016/j.cell.2015.08.027.

Baines, P. B., Marzouk, O., Thomson, A. P. J., Sills, J. A., Riordan, F. A. I., and Hart, C. A. (1999). Endothelial cell adhesion molecules in meningococcal disease. *Arch. Dis. Child.* 80, 74–76.

Balin, B. J., Broadwell, R. D., Salcman, M., and El-Kalliny, M. (1986). Avenues for entry of peripherally administered protein to the central nervous system in mouse, rat, and squirrel monkey. *J. Comp. Neurol.* 251, 260–280. doi:10.1002/cne.902510209.

Bauer, H. C., Krizbai, I. A., Bauer, H., and Traweger, A. (2014). "You shall not pass"-tight junctions of the blood brain barrier. *Front. Neurosci.* 8. doi:10.3389/fnins.2014.00392.

Bernard, S. C., Simpson, N., Join-Lambert, O., Federici, C., Laran-Chich, M. P., Maïssa, N., et al. (2014). Pathogenic Neisseria meningitidis utilizes CD147 for vascular colonization. *Nat.*

Med. 20, 725–731. doi:10.1038/nm.3563.

Bernas, M. J., Cardoso, F. L., Daley, S. K., Weinand, M. E., Campos, A. R., Ferreira, A. J. G., et al. (2010). Establishment of primary cultures of human brain microvascular endothelial cells to provide an in vitro cellular model of the blood-brain barrier. *Nat. Protoc.* 5, 1265–1272. doi:10.1038/nprot.2010.76.

Betz, A., Firth, J., and Goldstein, G. (1980). Polarity of the blood-brain barrier: distribution of enzymes between the luminal and antiluminal membranes of brain capillary endothelial cells. *Brain Res.* 192, 17–28.

Betz, A., and Goldstein, G. (1978). Polarity of the blood-brain barrier: neutral amino acid transport into isolated brain capillaries. *Science* 202, 225–227. doi:10.1126/science.211586.

Bongers, T. N., Emonts, M., De Maat, M. P. M., De Groot, R., Lisman, T., Hazelzet, J. A., et al. (2010). Reduced ADAMTS13 in children with severe meningococcal sepsis is associated with severity and outcome. *Thromb. Haemost.* 103, 1181–1187. doi:10.1160/TH09-06-0376.

Borkowski, J., Li, L., Steinmann, U., Quednau, N., Stump-Guthier, C., Weiss, C., et al. (2014). Neisseria meningitidis elicits a pro-inflammatory response involving IκBζ in a human blood-cerebrospinal fluid barrier model. *J. Neuroinflammation* 11. doi:10.1186/s12974-014-0163-x.

Bradley, C. J., Griffiths, N. J., Rowe, H. A., Heyderman, R. S., and Virji, M. (2005). Critical determinants of the interactions of capsule-expressing Neisseria meningitidis with host cells: The role of receptor density in increased cellular targeting via the outer membrane Opa proteins. *Cell. Microbiol.* 7, 1490–1503. doi:10.1111/j.1462-5822.2005.00572.x.

Brouwer, M. C., de Gans, J., Heckenberg, S. G., Zwinderman, A. H., van der Poll, T., and van de Beek, D. (2009). Host genetic susceptibility to pneumococcal and meningococcal disease: a systematic review and meta-analysis. *Lancet Infect. Dis.* 9, 31–44. doi:10.1016/S1473-3099(08)70261-5.

Brouwer, M. C., Read, R. C., and van de Beek, D. (2010). Host genetics and outcome in meningococcal disease: a systematic review and meta-analysis. *Lancet Infect. Dis.* 10, 262–274. doi:10.1016/S1473-3099(10)70045-1.

Butt, A. M., Jones, H. C., and Abbott, N. J. (1990). Electrical resistance across the blood-brain barrier in anaesthetized rats: a developmental study. *J. Physiol.* 429, 47–62.

Caesar, J. J. E., Lavender, H., Ward, P. N., Exley, R. M., Eaton, J., Chittock, E., et al. (2014). Competition between antagonistic complement factors for a single protein on N. meningitidis rules disease susceptibility. *Elife* 3, e04008. doi:10.7554/eLife.04008.

Calabria, A. R., and Shusta, E. V. (2008). A genomic comparison of in vivo and in vitro brain microvascular endothelial cells. *J. Cereb. Blood Flow Metab.* 28, 135–148. doi:10.1038/sj.jcbfm.9600518.

Cassella, J. P., Lawrenson, J. G., and Firth, J. A. (1997). Development of endothelial paracellular clefts and their tight junctions in the pial microvessels of the rat. *J. Neurocytol.* 26, 567–575. doi:10.1023/A:1015438624949.

Caugant, D. A., and Maiden, M. C. J. (2009). Meningococcal carriage and disease-Population

biology and evolution. *Vaccine* 27, B64–B70. doi:10.1016/j.vaccine.2009.04.061.

Chaudhuri, A., Yang, B., Gendelman, H. E., Persidsky, Y., and Kanmogne, G. D. (2008). STAT1signaling modulates HIV-1–induced inflammatory responses andleukocyte transmigration across the blood-brain barrier. *Blood* 111, 2062–2072. doi:10.1182/blood-2007-05-091207.

Chen, T., Belland, R. J., Wilson, J., and Swanson, J. (1995). Adherence of pilus- Opa+ gonococci to epithelial cells in vitro involves heparan sulfate. *J. Exp. Med.* 182, 511–517. doi:10.1084/JEM.182.2.511.

Chen, Z., Mi, L., Xu, J., Yu, J., Wang, X., Jiang, J., et al. (2005). Function of HAb18G/CD147 in Invasion of Host Cells by Severe Acute Respiratory Syndrome Coronavirus. *J. Infect. Dis.* 191, 755–760. doi:10.1086/427811.

Chevrier, N., Mertins, P., Artyomov, M. N., Shalek, A. K., Iannacone, M., Ciaccio, M. F., et al. (2011). Systematic discovery of TLR signaling components delineates viral-sensing circuits. *Cell* 147, 853–867. doi:10.1016/j.cell.2011.10.022.

Choi, W. H., Ji, K. A., Jeon, S. B., Yang, M. S., Kim, H., Min, K. J., et al. (2005). Anti-inflammatory roles of retinoic acid in rat brain astrocytes: Suppression of interferon-γ-induced JAK/STAT phosphorylation. *Biochem. Biophys. Res. Commun.* 329, 125–131. doi:10.1016/j.bbrc.2005.01.110.

Christodoulides, M., Makepeace, B. L., Partridge, K. A., Kaur, D., Fowler, M. I., Weller, R. O., et al. (2002). Interaction of Neisseria meningitidis with Human Meningeal Cells Induces the Secretion of a Distinct Group of Chemotactic, Proinflammatory, and Growth-Factor Cytokines. *Infect. Immun.* 70, 4035–4044. doi:10.1128/IAI.70.8.4035.

Clarke, T. B., Francella, N., Huegel, A., and Weiser, J. N. (2015). Invasive Bacterial Pathogens Exploit TLR-Mediated Downregulation of Tight Junction Components to Facilitate Translocation across the Epithelium. *Cell Host Microbe* 9, 404–414. doi:10.1016/j.chom.2011.04.012.

Constantin, D., Ala'Aldeen, D., and Murphy, S. (2002). Transcriptional activation of nitric oxide synthase-2, and NO-induced cell death, in mouse cerebrovascular endothelium exposed to Neisseria meningitidis. *J. Neurochem.* 81, 270–276. doi:10.1046/j.1471-4159.2002.00816.x.

Cooray, H. C., Blackmore, C. G., Maskell, L., and Barrand, M. A. (2002). Localisation of breast cancer resistance protein in microvessel endothelium of human brain. *Neuroreport* 13, 2059–2063. doi:10.1097/00001756-200211150-00014.

Cornford, E. M., Hyman, S., and Swartz, B. E. (1994). The human brain GLUT1 glucose transporter: Ultrastructural localization to the blood-brain barrier endothelia. *J. Cereb. Blood Flow Metab.* 14, 106–112. doi:10.1038/jcbfm.1994.15.

Coureuil, M., Bourdoulous, S., Marullo, S., and Nassif, X. (2014). Invasive meningococcal disease: A disease of the endothelial cells. *Trends Mol. Med.* 20, 571–578. doi:10.1016/j.molmed.2014.08.002.

Coureuil, M., Join-Lambert, O., Lécuyer, H., Bourdoulous, S., Marullo, S., and Nassif, X. (2012). Mechanism of meningeal invasion by Neisseria meningitidis. *Virulence* 3, 164–172.

doi:10.4161/viru.18639.

Coureuil, M., Join-Lambert, O., Lécuyer, H., Bourdoulous, S., Marullo, S., and Nassif, X. (2013). Pathogenesis of meningococcemia. *Cold Spring Harb. Perspect. Med.* 3, a012393. doi:10.1101/cshperspect.a012393.

Coureuil, M., Lécuyer, H., Bourdoulous, S., and Nassif, X. (2017). A journey into the brain: Insight into how bacterial pathogens cross blood-brain barriers. *Nat. Rev. Microbiol.* 15, 149–159. doi:10.1038/nrmicro.2016.178.

Coureuil, M., Lécuyer, H., Scott, M. G. H., Boularan, C., Enslen, H., Soyer, M., et al. (2010). Meningococcus hijacks a β2-adrenoceptor/β-arrestin pathway to cross brain microvasculature endothelium. *Cell* 143, 1149–1160. doi:10.1016/j.cell.2010.11.035.

Coureuil, M., Mikaty, G., Miller, F., Lécuyer, H., Bernard, C., Bourdoulous, S., et al. (2009). Meningococcal Type IV Pili Recruit the Polarity Complex to Cross the Brain Endothelium. *Science* 325, 83–87. doi:10.1126/science.1173196.

Craig, L., and Li, J. (2008). Type IV pili: paradoxes in form and function. *Curr. Opin. Struct. Biol.* 18, 267–277. doi:10.1016/j.sbi.2007.12.009.

Crone, C., and Olesen, S. P. (1982). Electrical resistance of brain microvascular endothelium. *Brain Res.* 241, 49–55. doi:10.1016/0006-8993(82)91227-6.

Cummins, P. M. (2012). Occludin: One Protein, Many Forms. *Mol. Cell. Biol.* 32, 242–250. doi:10.1128/MCB.06029-11.

Daneman, R., Agalliu, D., Zhou, L., Kuhnert, F., Kuo, C. J., and Barres, B. A. (2009). Wnt/beta-catenin signaling is required for CNS, but not non-CNS, angiogenesis. *Proc. Natl. Acad. Sci.* 106, 641–646. doi:10.1073/pnas.0805165106.

Davila, S., Wright, V. J., Khor, C. C., Sim, K. S., Binder, A., Breunis, W. B., et al. (2010). Genome-wide association study identifies variants in the CFH region associated with host susceptibility to meningococcal disease. *Nat. Genet.* 42, 772–778. doi:10.1038/ng.640.

Dejana, E., Orsenigo, F., and Lampugnani, M. G. (2008). The role of adherens junctions and VE-cadherin in the control of vascular permeability. *J. Cell Sci.* 121, 2115–2122. doi:10.1242/jcs.017897.

Denis, K., Le Bris, M., Le Guennec, L., Barnier, J. P., Faure, C., Gouge, A., et al. (2019). Targeting Type IV pili as an antivirulence strategy against invasive meningococcal disease. *Nat. Microbiol.* doi:10.1038/s41564-019-0395-8.

Dick, J., Hebling, S., Becam, J., Taha, M.-K., and Schubert-Unkmeir, A. (2017). Comparison of the inflammatory response of brain microvascular and peripheral endothelial cells following infection with Neisseria meningitidis. *Pathog. Dis.* 75, 1–11. doi:10.1093/femspd/ftx038.

Dixon, G. L. J., Heyderman, R. S., Kotovicz, K., Jack, D. L., Andersen, S. R., Vogel, U., et al. (1999). Endothelial adhesion molecule expression and its inhibition by recombinant bactericidal/permeability-increasing protein are influenced by the capsulation and Lipooligosaccharide structure of Neisseria meningitidis. *Infect. Immun.* 67, 5626–5633. doi:10.1016/j.jinorgbio.2012.07.022.

Doulet, N., Donnadieu, E., Laran-Chich, M. P., Niedergang, F., Nassif, X., Couraud, P. O., et al. (2006). Neisseria meningitidis infection of human endothelial cells interferes with leukocyte transmigration by preventing the formation of endothelial docking structures. *J. Cell Biol.* 173, 627–637. doi:10.1083/jcb.200507128.

Ehrlich, P. (1885). Das Sauerstoff-Bedürfniss des Organismus : eine farbenanalytische Studie.

Eigenmann, D. E., Xue, G., Kim, K. S., Moses, A. V, Hamburger, M., and Oufir, M. (2013). Comparative study of four immortalized human brain capillary endothelial cell lines, hCMEC/D3, hBMEC, TY10, and BB19, and optimization of culture conditions, for an in vitro blood–brain barrier model for drug permeability studies. *Fluids Barriers CNS* 10:33. doi:10.1186/2045-8118-10-33.

Eisenblätter, T., Hüwel, S., and Galla, H. J. (2003). Characterisation of the brain multidrug resistance protein (BMDP/ABCG2/BCRP) expressed at the blood-brain barrier. *Brain Res.* 971, 221–231. doi:10.1016/S0006-8993(03)02401-6.

Engelhardt, B., and Sorokin, L. (2009). The blood-brain and the blood-cerebrospinal fluid barriers: Function and dysfunction. *Semin. Immunopathol.* 31, 497–511. doi:10.1007/s00281-009-0177-0.

Eugène, E., Hoffmann, I., Pujol, C., Couraud, P.-O., Bourdoulous, S., and Nassif, X. (2002). Microvilli-like structures are associated with the internalization of virulent capsulated *Neisseria meningitidis* into vascular endothelial cells. *J. Cell Sci.* 115, 1231–1241.

Fagerholm, U. (2007). The highly permeable blood-brain barrier: an evaluation of current opinions about brain uptake capacity. *Drug Discov. Today* 12, 1076–1082. doi:10.1016/j.drudis.2007.10.005.

Farrell, C. L., and Pardridge, W. M. (1991). Blood-brain barrier glucose transporter is asymmetrically distributed on brain capillary endothelial lumenal and ablumenal membranes: an electron microscopic immunogold study. *Proc. Natl. Acad. Sci.* 88, 5779–5783. doi:10.1073/pnas.88.13.5779.

Fenstermacher, J., Gross, P., Sposito, N., Acuff, V., Pettersen, S., and Gruber, K. (1988). Structural and Functional Variations in Capillary Systems within the Brain. *Ann. N. Y. Acad. Sci.* 529, 21–30. doi:10.1111/j.1749-6632.1988.tb51416.x.

Förstner, K. U., Vogel, J., and Sharma, C. M. (2014). READemption — a tool for the computational analysis of deep-sequencing – based transcriptome data. *Bioinformatics* 30, 3421–3423. doi:10.1093/bioinformatics/btu533.

Fortier, L. a (2005). Stem Cells: Classifications, Controversies, and Clinical Applications. *Vet. Surg.* 34, 415–423. doi:10.1111/j.1532-950X.2005.00063.x.

Fowler, M. I., Ho Wang Yin, K. Y., Humphries, H. E., Heckels, J. E., and Christodoulides, M. (2006). Comparison of the inflammatory responses of human meningeal cells following challenge with Neisseria lactamica and with Neisseria meningitidis. *Infect. Immun.* 74, 6467–6478. doi:10.1128/IAI.00644-06.

Fowler, M. I., Weller, R. O., Heckels, J. E., and Christodoulides, M. (2004). Different meningitis-causing bacteria induce distinct inflammatory responses on interaction with cells of the

human meninges. *Cell. Microbiol.* 6, 555–567. doi:10.1111/j.1462-5822.2004.00382.x.

Fransen, F., Heckenberg, S. G. B., Hamstra, H. J., Feller, M., Boog, C. J. P., Van Putten, J. P. M., et al. (2009). Naturally occurring lipid a mutants in neisseria meningitidis from patients with invasive meningococcal disease are associated with reduced coagulopathy. *PLoS Pathog.* 5, e100039. doi:10.1371/journal.ppat.1000396.

Gabison, E. E., Hoang-Xuan, T., Mauviel, A., and Menashi, S. (2005). EMMPRIN/CD147, an MMP modulator in cancer, development and tissue repair. *Biochimie* 87, 361–368. doi:10.1016/j.biochi.2004.09.023.

Glimåker, M., Olcén, P., and Andersson, B. (1994). Interferon-γ in cerebrospinal fluid from patients with viral and bacterial meningitis. *Scand. J. Infect. Dis.* 26, 141–147. doi:10.3109/00365549409011777.

Goldmann, E. E. (1913). *Vitalfärbung am Zentralnervensystem*. Berlin : Königl. Akademie der Wissenschaften.

Gotschlich, E. C., Goldschneider, I., and Artenstein, M. I. (1969). Human immunity to the meningococcus. *J Exp Med* 129, 1367–1384.

Greene, C., Hanley, N., and Campbell, M. (2019). Claudin-5: gatekeeper of neurological function. *Fluids Barriers CNS* 16. doi:10.1186/s12987-019-0123-z.

Hammerschmidt, S., Müller, A., Sillmann, H., Mühlenhoff, M., Borrow, R., Fox, A., et al. (1996). Capsule phase variation in Neisseria meningitidis serogroup B by slipped-strand mispairing in the polysialyltransferase gene (siaD): Correlation with bacterial invasion and the outbreak of meningococcal disease. *Mol. Microbiol.* 20, 1211–1220. doi:10.1111/j.1365-2958.1996.tb02641.x.

Hanna, J., Wernig, M., Markoulaki, S., Sun, C. W., Meissner, A., Cassady, J. P., et al. (2007). Treatment of sickle cell anemia mouse model with iPS cells generated from autologous skin. *Science* 318, 1920–1923. doi:10.1126/science.1152092.

Hawkins, B. T. (2005). The Blood-Brain Barrier/Neurovascular Unit in Health and Disease. *Pharmacol. Rev.* 57, 173–185. doi:10.1124/pr.57.2.4.

Hélaine, S., Carbonnelle, E., Prouvensier, L., Beretti, J. L., Nassif, X., and Pelicic, V. (2005). PilX, a pilus-associated protein essential for bacterial aggregation, is a key to pilus-facilitated attachment of Neisseria meningitidis to human cells. *Mol. Microbiol.* 55, 65–77. doi:10.1111/j.1365-2958.2004.04372.x.

Helms, H. C., Abbott, N. J., Burek, M., Cecchelli, R., Couraud, P. O., Deli, M. A., et al. (2015). In vitro models of the blood-brain barrier: An overview of commonly used brain endothelial cell culture models and guidelines for their use. *J. Cereb. Blood Flow Metab.* 36, 862–890. doi:10.1177/0271678X16630991.

Hill, D. J., Griffiths, N. J., Borodina, E., and Virji, M. (2010). Cellular and molecular biology of Neisseria meningitidis colonization and invasive disease. *Clin. Sci.* 118, 547–564. doi:10.1042/CS20090513.

Hoffman, O., and Weber, J. R. (2009). Pathophysiology and treatment of bacterial meningitis. *Ther. Adv. Neurol. Disord.* 2, 401–412. doi:10.1177/1756285609337975.

Hoffmann, I., Eugène, E., Nassif, X., Couraud, P. O., and Bourdoulous, S. (2001). Activation of ErbB2 receptor tyrosine kinase supports invasion of endothelial cells by Neisseria meningitidis. *J. Cell Biol.* 155, 133–143. doi:10.1083/jcb.200106148.

Hoffmann, S., Otto, C., Kurtz, S., Sharma, C. M., Khaitovich, P., Vogel, J., et al. (2009). Fast mapping of short sequences with mismatches, insertions and deletions using index structures. *PLoS Comput. Biol.* 5. doi:10.1371/journal.pcbi.1000502.

Honda, M., Nakagawa, S., Hayashi, K., Kitagawa, N., Tsutsumi, K., Nagata, I., et al. (2006). Adrenomedullin improves the blood-brain barrier function through the expression of claudin-5. *Cell. Mol. Neurobiol.* 26, 109–118. doi:10.1007/s10571-006-9028-x.

Hou, P., Li, Y., Zhang, X., Liu, C., Guan, J., Li, H., et al. (2013). Pluripotent stem cells induced from mouse somatic cells by small-molecule compounds. *Science* 341, 651–654. doi:10.1126/science.1239278.

http://biomed.brown.edu *Div. Biol. Med. Brown Univ.* Available at: http://biomed.brown.edu/Courses/BI108/BI108_2005_Groups/07/PluripotentStemCells.jpg.

Huang, D. W., Sherman, B. T., and Lempicki, R. A. (2009). Systematic and integrative analysis of large gene lists using DAVID bioinformatics resources. *Nat. Protoc.* 4, 44–57. doi:10.1038/nprot.2008.211.

Huang, J., Kelly, C. P., Bakirtzi, K., Villafuerte Gálvez, J. A., Lyras, D., Mileto, S. J., et al. (2019). Clostridium difficile toxins induce VEGF-A and vascular permeability to promote disease pathogenesis. *Nat. Microbiol.* 4, 269–279. doi:10.1038/s41564-018-0300-x.

Huang, S. H., Stins, M. F., and Kim, K. S. (2000). Bacterial penetration across the blood-brain barrier during the development of neonatal meningitis. *Microbes Infect.* 2, 1237–1244. doi:10.1016/S1286-4579(00)01277-6.

Hui, H., Tang, Y., Hu, M., Zhao, X., Greater, V. A., Health, L. A., et al. (2011). "Stem Cells : General Features and Characteristics" in *Stem Cells in Clinic and Research*, ed. A. Gholamrezanezhad (InTech), 3–15.

Hung, M.-C., and Christodoulides, M. (2013). The Biology of Neisseria Adhesins. *Biology (Basel).* 2, 1054–1109. doi:10.3390/biology2031054.

Iadecola, C. (2004). Neurovascular regulation in the normal brain and in Alzheimer's disease. *Nat. Rev. Neurosci.* 5, 347–360. doi:10.1038/nrn1387.

Ikenouchi, J., Matsuda, M., Furuse, M., and Tsukita, S. (2003). Regulation of tight junctions during the epithelium-mesenchyme transition: direct repression of the gene expression of claudins/occludin by Snail. *J. Cell Sci.* 116, 1959–1967. doi:10.1242/jcs.00389.

Imhaus, A.-F., and Dumenil, G. (2014). The number of Neisseria meningitidis type IV pili determines host cell interaction. *EMBO J.* 33, 1767–1783. doi:10.15252/embj.201488031.

Ivarsson, M., Schollin, J., and Björkqvist, M. (2013). Staphylococcus epidermidis and Staphylococcus aureus trigger different interleukin-8 and intercellular adhesion molecule-1 in lung cells: Implications for inflammatory complications following neonatal sepsis. *Acta Paediatr. Int. J. Paediatr.* 102, 1010–1016. doi:10.1111/apa.12350.

Johansson, L., Rytkönen, A., Bergman, P., Albiger, B., Källström, H., Hökfelt, T., et al. (2003). CD46 in Meningococcal Disease. *Science* 301, 373–375. doi:10.1126/science.1086476.

Johswich, K. O., McCaw, S. E., Islam, E., Sintsova, A., Gu, A., Shively, J. E., et al. (2013). In Vivo Adaptation and Persistence of Neisseria meningitidis within the Nasopharyngeal Mucosa. *PLoS Pathog.* 9. doi:10.1371/journal.ppat.1003509.

Johswich, K. O., McCaw, S. E., Strobel, L., Frosch, M., and Gray-Owen, S. D. (2015). Sterilizing immunity elicited by Neisseria meningitidis carriage shows broader protection than predicted by serum antibody cross- reactivity in CEACAM1-humanized mice. *Infect. Immun.* 83, 354–363. doi:10.1128/IAI.02495-14.

Jones, H. E., Strid, J., Osman, M., Uronen-Hansson, H., Dixon, G., Klein, N., et al. (2008). The role of β2 integrins and lipopolysaccharide-binding protein in the phagocytosis of dead Neisseria meningitidis. *Cell. Microbiol.* 10, 1634–1645. doi:10.1111/j.1462-5822.2008.01154.x.

Källström, H., Islam, M. S., Berggren, P. O., and Jonsson, A. B. (1998). Cell signaling by the type IV pili of pathogenic Neisseria. *J. Biol. Chem.* 273, 21777–21782. doi:10.1074/jbc.273.34.21777.

Katt, M., Xu, Z., Gerecht, S., and Searson, P. (2016). Human Brain Microvascular Endothelial Cells Derived from the BC1 iPS Cell Line Exhibit a Blood-Brain Barrier Phenotype. *PLoS One* 4, e0152105. doi:10.1371/journal.pone.0152105.

Kim, B. J., Bee, O. B., Mcdonagh, M. A., Stebbins, M. J., Palecek, S. P., Doran, K. S., et al. (2017). Modeling Group B Streptococcus and Blood-Brain Barrier Interaction by Using Induced Pluripotent Stem Cell-Derived Brain Endothelial Cells. *mSphere* 2. doi:10.1128/mSphere.00398-17.

Kim, B. J., Hancock, B. M., Bermudez, A., Cid, N. Del, Reyes, E., Van Sorge, N. M., et al. (2015). Bacterial induction of Snail1 contributes to blood-brain barrier disruption. *J. Clin. Invest.* 125, 2473–2483. doi:10.1172/JCI74159.

Kim, B. J., and Schubert-Unkmeir, A. (2019). "In Vitro Models for Studying the Interaction of Neisseria meningitidis with Human Brain Endothelial Cells" in *Methods in Molecular Biology* (Humana Press, New York, NY), 135–148. doi:10.1007/978-1-4939-9202-7_10.

Kofler, S., Nickel, T., and Weis, M. (2005). Role of cytokines in cardiovascular diseases: a focus on endothelial responses to inflammation. *Clin. Sci.* 108, 205–213. doi:10.1042/cs20040174.

Kolappan, S., Coureuil, M., Yu, X., Nassif, X., Egelman, E. H., and Craig, L. (2016). Structure of the neisseria meningitidis type IV pilus. *Nat. Commun.* 7. doi:10.1038/ncomms13015.

Kornelisse, R. F., Hack, C. E., Savelkoul, H. F. J., Van der Pouw Kraan, T. C. T. M., Hop, W. C. J., Van Mierlo, G., et al. (1997). Intrathecal production of interleukin-12 and gamma interferon in patients with bacterial meningitis. *Infect. Immun.* 65, 877–881. doi:10.1128/AEM.68.12.6256.

Korthuis, R. J., Anderson, D. C., and Granger, D. N. (1994). Role of neutrophil-endothelial cell adhesion in inflammatory disorders. *J. Crit. Care* 9, 47–71.

Krause, G., Winkler, L., Mueller, S. L., Haseloff, R. F., Piontek, J., and Blasig, I. E. (2008).

Structure and function of claudins. *Biochim. Biophys. Acta - Biomembr.* 1778, 631–645. doi:10.1016/j.bbamem.2007.10.018.

Krisch, B., Leonhardt, H., and Buchheim, W. (1978). The functional and structural border of the neurohemal region of the median eminence. *Cell Tissue Res.* 192, 327–339. doi:10.1007/BF00220750.

Krishnaswamy, G., Kelley, J., Yerra, L., Smith, J. K., and Chi, D. S. (1999). Human Endothelium as a Source of Multifunctional Cytokines: Molecular Regulation and Possible Role in Human Disease. *J. Interf. Cytokine Res.* 19, 91–104. doi:10090394.

Lacorre, D., Baekkevold, E. S., Garrido, I., Brandtzaeg, P., Haraldsen, G., Amalric, F., et al. (2004). Plasticity of endothelial cells: rapid dedifferentiation of freshly isolated high endothelial venule endothelial cells outside the lymphoid tissue microenvironment. *Blood* 103, 4164–4172. doi:10.1182/blood-2003-10-3537.

Lambotin, M. (2005). Invasion of endothelial cells by Neisseria meningitidis requires cortactin recruitment by a phosphoinositide-3-kinase/Rac1 signalling pathway triggered by the lipo-oligosaccharide. *J. Cell Sci.* 118, 3805–3816. doi:10.1242/jcs.02514.

Lambotin, M., Hoffmann, I., Laran-Chich, M., Nassif, X., Couraud, P., and Bourdoulous, S. (2005). Invasion of endothelial cells by Neisseria meningitidis requires cortactin recruitment by a phosphoinositide-3-kinase/Rac1 signalling pathway triggered by the lipo-oligosaccharide. *J. Cell Sci.* 118, 3805–3816. doi:10.1242/jcs.02514.

Langeggen, H., Berge, K. E., Johnson, E., and Hetland, G. (2002). Human Umbilical Vein Endothelial Cells Express Complement Receptor 1 (CD35) and Complement Receptor 4 (CD11c/ CD18) in vitro. *Inflammation* 26, 103–110. doi:10.1023/A:1015585530204.

Lappann, M., Haagensen, J. A. J., Claus, H., Vogel, U., and Molin, S. (2006). Meningococcal biofilm formation: Structure, development and phenotypes in a standardized continuous flow system. *Mol. Microbiol.* 62, 1292–1309. doi:10.1111/j.1365-2958.2006.05448.x.

Lécuyer, H., Borgel, D., Nassif, X., and Coureuil, M. (2017). Pathogenesis of meningococcal purpura fulminans. *Pathog. Dis.* 75. doi:10.1093/femspd/ftx027.

Lécuyer, H., Nassif, X., and Coureuil, M. (2012). Two strikingly different signaling pathways are induced by meningococcal type IV pili on endothelial and epithelial cells. *Infect. Immun.* 80, 175–186. doi:10.1128/IAI.05837-11.

Lécuyer, H., Virion, Z., Barnier, J. P., Matczak, S., Bourdoulous, S., Bianchini, E., et al. (2018). An ADAM-10 dependent EPCR shedding links meningococcal interaction with endothelial cells to purpura fulminans. *PLoS Pathog.* 14, e1006981. doi:10.1371/journal.ppat.1006981.

Lee, S. H., Lee, J. H., Han, Y. S., Ryu, J. M., Yoon, Y. M., and Han, H. J. (2015). Hypoxia accelerates vascular repair of endothelial colony-forming cells on ischemic injury via STAT3-BCL3 axis. *Stem Cell Res. Ther.* 6. doi:10.1186/s13287-015-0128-8.

Leslie, E. M., Deeley, R. G., and Cole, S. P. C. (2005). Multidrug resistance proteins: Role of P-glycoprotein, MRP1, MRP2, and BCRP (ABCG2) in tissue defense. *Toxicol. Appl. Pharmacol.* 204, 216–237. doi:10.1016/j.taap.2004.10.012.

Lim, R. G., Quan, C., Reyes-Ortiz, A. M., Lutz, S. E., Kedaigle, A. J., Gipson, T. A., et al.

(2017). Huntington's Disease iPSC-Derived Brain Microvascular Endothelial Cells Reveal WNT-Mediated Angiogenic and Blood-Brain Barrier Deficits. *Cell Rep.* 19, 1365–1377. doi:10.1016/j.celrep.2017.04.021.

Linhartova, I., Basler, M., Ichikawa, J., Pelicic, V., Osicka, R., Lory, S., et al. (2006). Meningococcal adhesion suppresses proapoptotic gene expression and promotes expression of genes supporting early embryonic and cytoprotective signaling of human endothelial cells. *FEMS Microbiol. Lett.* 263, 109–118. doi:10.1111/j.1574-6968.2006.00407.x.

Lippmann, E. S., Al-Ahmad, A., Azarin, S. M., Palecek, S. P., and Shusta, E. V. (2014). A retinoic acid-enhanced, multicellular human blood-brain barrier model derived from stem cell sources. *Sci. Rep.* 4, 1–10. doi:10.1038/srep04160.

Lippmann, E. S., Azarin, S. M., Kay, J. E., Nessler, R. A., Wilson, H. K., Al-Ahmad, A., et al. (2012). Derivation of blood-brain barrier endothelial cells from human pluripotent stem cells. *Nat. Biotechnol.* 30, 783–791. doi:10.1038/nbt.2247.

Loh, E., Kugelberg, E., Tracy, A., Zhang, Q., Gollan, B., Ewles, H., et al. (2013a). Temperature triggers immune evasion by Neisseria meningitidis. *Nature* 502, 237–240. doi:10.1038/nature12616.

Loh, E., Kugelberg, E., Tracy, A., Zhang, Q., Gollan, B., Ewles, H., et al. (2013b). Temperature triggers immune evasion by Neisseria meningitidis. *Nature* 502, 237–240. doi:10.1038/nature12616.

López-Cortés, L. F., Cruz-Ruiz, M., Gómez-Mateos, J., Viciana-Fernandez, P., Martinez-Marcos, F. J., and Pachón, A. (1995). Interleukin-8 in cerebrospinal fluid from patients with meningitis of different etiologies: Its possible role as neutrophil chemotactic factor. *J. Infect. Dis.* 172, 581–584. doi:10.1093/infdis/172.2.581.

Love, M. I., Huber, W., and Anders, S. (2014). Moderated estimation of fold change and dispersion for RNA-seq data with DESeq2. *Genome Biol.* 15. doi:10.1186/s13059-014-0550-8.

Lüttge, M., Fulde, M., Talay, S. R., Nerlich, A., Rohde, M., Preissner, K. T., et al. (2012). Streptococcus pneumoniae induces exocytosis of Weibel-Palade bodies in pulmonary endothelial cells. *Cell. Microbiol.* 14, 210–225. doi:10.1111/j.1462-5822.2011.01712.x.

Maherali, N., Sridharan, R., Xie, W., Utikal, J., Eminli, S., Arnold, K., et al. (2007). Directly Reprogrammed Fibroblasts Show Global Epigenetic Remodeling and Widespread Tissue Contribution. *Cell Stem Cell* 1, 55–70. doi:10.1016/j.stem.2007.05.014.

Mairey, E., Genovesio, A., Donnadieu, E., Bernard, C., Jaubert, F., Pinard, E., et al. (2006). Cerebral microcirculation shear stress levels determine *Neisseria meningitidis* attachment sites along the blood–brain barrier. *J. Exp. Med.* 203, 1939–1950. doi:10.1084/jem.20060482.

Maïssa, N., Covarelli, V., Janel, S., Durel, B., Simpson, N., Bernard, S. C., et al. (2017). Strength of Neisseria meningitidis binding to endothelial cells requires highly-ordered CD147/β 2-Adrenoceptor clusters assembled by alpha-Actinin-4. *Nat. Commun.* 8. doi:10.1038/ncomms15764.

Mandrell, R. E., McLeod Griffiss, J., and Macher, B. A. (1988). Lipooligosaccharides (LOS) of Neisseria gonorrhoeae and Neisseria meningitidis have components that are immunochemically similar to precursors of human blood group antigens. Carbohydrate sequence specificity of the mouse monoclonal antibodies that recogni. *J. Exp. Med.* 168, 107–126. doi:10.1084/jem.168.1.107.

Martin, M. (2011). Cutadapt removes adapter sequences from high-throughput sequencing reads. *EMBnet.journal* 17, 10–12. doi:10.14806/ej.17.1.200.

Martin, U. (2017). Therapeutic Application of Pluripotent Stem Cells: Challenges and Risks. *Front. Med.* 4. doi:10.3389/fmed.2017.00229.

Martins Gomes, S. F., Westermann, A. J., Sauerwein, T., Hertlein, T., Förstner, K. U., Ohlsen, K., et al. (2019). Induced Pluripotent Stem Cell-Derived Brain Endothelial Cells as a Cellular Model to Study Neisseria meningitidis Infection. *Front. Microbiol.* 10, 1–13. doi:10.3389/fmicb.2019.01181.

Matsuzono, Y., Narita, M., Akutsu, Y., and Togashi, T. (1995). Interleukin-6 in cerebrospinal fluid of patients with central nervous system infections. *Acta Paediatr.* 84, 879–883. doi:10.1111/j.1651-2227.1995.tb13784.x.

Mattick, J. S. (2002). Type IV Pili and Twitching Motility. *Annu. Rev. Microbiol.* 56, 289–314. doi:10.1146/annurev.micro.56.012302.160938.

McGuinness, B. T., Clarke, I. N., Lambden, P. R., Barlow, A. K., Heckels, J. E., Poolman, J. T., et al. (1991). Point mutation in meningococcal por A gene associated with increased endemic disease. *Lancet* 337, 514–517. doi:10.1016/0140-6736(91)91297-8.

Melican, K., Aubey, F., and Duménil, G. (2014). Humanized Mouse Model to Study Bacterial Infections Targeting the Microvasculature. *J. Vis. Exp.*, e51134. doi:10.3791/51134.

Melican, K., Michea Veloso, P., Martin, T., Bruneval, P., and Duménil, G. (2013). Adhesion of Neisseria meningitidis to Dermal Vessels Leads to Local Vascular Damage and Purpura in a Humanized Mouse Model. *PLoS Pathog.* 9. doi:10.1371/journal.ppat.1003139.

Mercier, F., Kitasako, J. T., and Hatton, G. I. (2002). Anatomy of the brain neurogenic zones revisited: Fractones and the fibroblast/macrophage network. *J. Comp. Neurol.* 451, 170–188. doi:10.1002/cne.10342.

Merz, A. J., Enns, C. A., and So, M. (1999). Type IV pili of pathogenic Neisseriae elicit cortical plaque formation in epithelial cells. *Mol. Microbiol.* 32, 1316–1332. doi:10.1046/j.1365-2958.1999.01459.x.

Mikaty, G., Soyer, M., Mairey, E., Henry, N., Dyer, D., Forest, K. T., et al. (2009). Extracellular bacterial pathogen induces host cell surface reorganization to resist shear stress. *PLoS Pathog.* 5, 1000314. doi:10.1371/journal.ppat.1000314.

Mizee, M. R., Wooldrik, D., Lakeman, K. A. M., van het Hof, B., Drexhage, J. A. R., Geerts, D., et al. (2013). Retinoic Acid Induces Blood-Brain Barrier Development. *J. Neurosci.* 33, 1660–1671. doi:10.1523/jneurosci.1338-12.2013.

Møllgård, K., Balslev, Y., Lauritzen, B., and Saunders, N. R. (1987). Cell junctions and membrane specializations in the ventricular zone (germinal matrix) of the developing sheep

brain: A CSF-brain barrier. *J. Neurocytol.* 16, 433–444. doi:10.1007/BF01668498.

Møllgård, K., Dziegielewska, K. M., Holst, C. B., Habgood, M. D., and Saunders, N. R. (2017). Brain barriers and functional interfaces with sequential appearance of ABC efflux transporters during human development. *Sci. Rep.* 7. doi:10.1038/s41598-017-11596-0.

Mook-Kanamori, B. B., Geldhoff, M., van der Poll, T., and van de Beek, D. (2011). Pathogenesis and pathophysiology of pneumococcal meningitis. *Clin. Microbiol. Rev.* 24, 557–591. doi:10.1016/S1473-3099(02)00450-4.

Morand, P. C., Bille, E., Morelle, S., Eugène, E., Beretti, J. L., Wolfgang, M., et al. (2004). Type IV pilus retraction in pathogenic Neisseria is regulated by the PilC proteins. *EMBO J.* 23, 2009–2017. doi:10.1038/sj.emboj.7600200.

Müller-Redetzky, H. C., Will, D., Hellwig, K., Kummer, W., Tschernig, T., Pfeil, U., et al. (2014). Mechanical ventilation drives pneumococcal pneumonia into lung injury and sepsis in mice: Protection by adrenomedullin. *Crit. Care* 18. doi:10.1186/cc13830.

Munford, R. S., and Varley, A. W. (2006). Shield as Signal: Lipopolysaccharides and the Evolution of Immunity to Gram-Negative Bacteria. *PLoS Pathog.* 2, e67. doi:10.1371/journal.ppat.0020067.

Nabeshima, S., Reese, T. S., Landis, D. M. D., and Brightman, M. W. (1975). Junctions in the meninges and marginal glia. *J. Comp. Neurol.* 164, 127–169. doi:10.1002/cne.901640202.

Nassif, X., Beretti, J. L., J Lowy, P. S., O'Gaora, P., Pfeifer, J., Normark, S., et al. (1994). Roles of pilin and PilC in adhesion of Neisseria meningitidis to human epithelial and endothelial cells. *Proc Natl Acad Sci U S A* 91, 3769–3773.

Nassif, X., Bourdoulous, S., Eugène, E., and Couraud, P.-O. (2002). How do extracellular pathogens cross the blood-brain barrier? *Trends Microbiol.* 10, 227–232. Available at: http://www.ncbi.nlm.nih.gov/pubmed/11973156.

Nassif, X., Lowy, J., Stenberg, P., O'Gaora, P., Ganji, A., and So, M. (1993). Antigenic variation of pilin regulates adhesion of Neisseria meningitidis to human epithelial cells. *Mol. Microbiol.* 8, 719–725. doi:10.1111/j.1365-2958.1993.tb01615.x.

Ni, Y., Teng, T., Li, R., Simonyi, A., Sun, G. Y., and Lee, J. C. (2017). TNFα alters occludin and cerebral endothelial permeability: Role of p38MAPK. *PLoS One* 12, 1–20. doi:10.1371/journal.pone.0170346.

Nikulin, J., Panzner, U., Frosch, M., and Schubert-Unkmeir, A. (2006). Intracellular survival and replication of Neisseria meningitidis in human brain microvascular endothelial cells. *Int. J. Med. Microbiol.* 296, 553–558. doi:10.1016/j.ijmm.2006.06.006.

Ohkubo, T., and Ozawa, M. (2004). The transcription factor Snail downregulates the tight junction components independently of E-cadherin downregulation. *J. Cell Sci.* 117, 1675–1685. doi:10.1242/jcs.01004.

Okita, K., Ichisaka, T., and Yamanaka, S. (2007). Generation of germline-competent induced pluripotent stem cells. *Nature* 448, 313–317. doi:10.1038/nature05934.

Oldendorf, W. H., Cornford, M. E., and Brown, W. J. (1977). The large apparent work capability

of the blood-brain barrier: A study of the mitochondrial content of capillary endothelial cells in brain and other tissues of the rat. *Ann. Neurol.* 1, 409–417. doi:10.1002/ana.410010502.

Omole, A. E., and Fakoya, A. O. J. (2018). Ten years of progress and promise of induced pluripotent stem cells: historical origins, characteristics, mechanisms, limitations, and potential applications. *PeerJ* 6, e4370. doi:10.7717/peerj.4370.

Oosthuysen, W. F., Mueller, T., Dittrich, M. T., and Schubert-Unkmeir, A. (2016). Neisseria meningitidis causes cell cycle arrest of human brain microvascular endothelial cells at S phase via p21 and cyclin G2. *Cell. Microbiol.* 18, 46–65. doi:10.1111/cmi.12482.

Otto, C., Stadler, P. F., and Hoffmann, S. (2014). Lacking alignments? The next-generation sequencing mapper segemehl revisited. *Bioinformatics* 30, 1837–1843. doi:10.1093/bioinformatics/btu146.

Pace, D., and Pollard, A. J. (2007). Meningococcal A, C, Y and W-135 polysaccharide-protein conjugate vaccines. *Arch. Dis. Child.* 92, 909–915. doi:10.1136/adc.2006.111500.

Pardridge, W. (2001). *Brain drug targeting: the future of brain drug development.* Cambridge, UK: Cambridge University Press.

Pardridge, W. M. (2002). Drug and gene targeting to the brain with molecular Trojan horses. *Nat. Rev. Drug Discov.* 1, 131–139. doi:10.1038/nrd725.

Parkhill, J., Achtman, M., James, K. D., Bentley, S. D., Churcher, C., Klee, S. R., et al. (2000). Complete DNA sequence of a serogroup A strain of Neisseria meningitidis 79491. *Nature* 404, 502–506. doi:10.1038/35006655.

Pashenkov, M., Teleshova, N., Kouwenhoven, M., Smirnova, T., Jin, Y. P., Kostulas, V., et al. (2002). Recruitment of dendritic cells to the cerebrospinal fluid in bacterial neuroinfections. *J. Neuroimmunol.* 122, 106–116. doi:10.1016/S0165-5728(01)00451-9.

Peters, S., Schlegel, J., Becam, J., Avota, E., Sauer, M., and Schubert-Unkmeir, A. (2019). *Neisseria meningitidis* type IV pili trigger Ca^{2+} -dependent lysosomal trafficking of the acid sphingomyelinase to enhance surface ceramide levels. *Infect. Immun.* doi:10.1128/IAI.00410-19.

Peyssonnaux, C., Cejudo-Martin, P., Doedens, A., Zinkernagel, A. S., Johnson, R. S., and Nizet, V. (2007). Cutting Edge: Essential Role of Hypoxia Inducible Factor-1 in Development of Lipopolysaccharide-Induced Sepsis. *J. Immunol.* 178, 7516–7519. doi:10.4049/jimmunol.178.12.7516.

Pong, A., and Bradley, J. S. (1999). Bacterial meningitis and the newborn infant. *Infect. Dis. Clin. North Am.* 13, 711–733. doi:10.1016/S0891-5520(05)70102-1.

Pripuzova, N. S., Getie-Kebtie, M., Grunseich, C., Sweeney, C., Malech, H., and Alterman, M. A. (2015). Development of a protein marker panel for characterization of human induced pluripotent stem cells (hiPSCs) using global quantitative proteome analysis. *Stem Cell Res.* 14, 323–338. doi:10.1016/j.scr.2015.01.009.

Pron, B., Taha, M., Rambaud, C., Fournet, J., Pattey, N., Monnet, J., et al. (1997). Interaction of Neisseria meningitidis with the Components of the Blood-Brain Barrier Correlates with an Increased Expression of PilC. *J. Infect. Dis.* 176, 1285–1292. doi:10.1086/514124.

Protasoni, M., Sangiorgi, S., Cividini, A., Culuvaris, G. T., Tomei, G., Dell'Orbo, C., et al. (2011). The collagenic architecture of human dura mater. *J. Neurosurg.* 114, 1723–1730. doi:10.3171/2010.12.jns101732.

Pujol, C., Eugene, E., Marceau, M., and Nassif, X. (1999). The meningococcal PilT protein is required for induction of intimate attachment to epithelial cells following pilus-mediated adhesion. *Proc. Natl. Acad. Sci.* 96, 4017–4022. doi:10.1073/pnas.96.7.4017.

Pushkarsky, T., Zybarth, G., Dubrovsky, L., Yurchenko, V., Tang, H., Guo, H., et al. (2002). CD147 facilitates HIV-1 infection by interacting with virus-associated cyclophilin A. *Proc. Natl. Acad. Sci.* 98, 6360–6365. doi:10.1073/pnas.111583198.

Qian, T., Maguire, S. E., Canfield, S. G., Bao, X., Olson, W. R., Shusta, E. V., et al. (2017). Directed differentiation of human pluripotent stem cells to blood-brain barrier endothelial cells. *Sci. Adv.* 3, e1701679.

Quagliarello, V., and Scheld, W. (1992). Bacterial meningitis: pathogenesis, pathophysiology, and progress. *N. Engl. J. Med.* 327, 864–872. doi:10.1056/NEJM199209173271208.

Read, R. C. (2014). Neisseria meningitidis; clones, carriage, and disease. *Clin. Microbiol. Infect.* 20, 391–395. doi:10.1111/1469-0691.12647.

Reese, T. S., and Karnovsky, M. J. (1967). Fine Structural Localization of a Blood-Brain Barrier To Exogenous Peroxidase. *J. Cell Biol.* 34, 207–217. doi:10.1083/jcb.34.1.207.

Regina, A., Koman, A., Piciotti, M., El Hafny, B., Center, M. S., Bergmann, R., et al. (2010). Mrp1 Multidrug Resistance-Associated Protein and P-Glycoprotein Expression in Rat Brain Microvessel Endothelial Cells. *J. Neurochem.* 71, 705–715. doi:10.1046/j.1471-4159.1998.71020705.x.

Ricci, S., Grandgirard, D., Wenzel, M., Braccini, T., Salvatore, P., Oggioni, M. R., et al. (2014). Inhibition of matrix metalloproteinases attenuates brain damage in experimental meningococcal meningitis. *BMC Infect. Dis.* 14, 1–10. doi:10.1186/s12879-014-0726-6.

Robinson, K., Taraktsoglou, M., Rowe, K. S. J., Wooldridge, K. G., and Ala'Aldeen, D. A. A. (2004). Secreted proteins from Neisseria meningitidis mediate differential human gene expression and immune activation. *Cell. Microbiol.* 6, 927–938. doi:10.1111/j.1462-5822.2004.00410.x.

Rosenstein, N., Perkins, B., Stephens, D., Popovic, T., and Hughes, J. (2001). Meningococcal disease. *N. Engl. J. Med.* 344, 1378–1388. doi:10.12968/prma.2018.28.8.22.

Rouphael, N. G., and Stephens, D. S. (2012). Neisseria meningitidis: Biology, Microbiology, and Epidemiology. *Methods Mol Biol.* 799, 1–20. doi:10.1016/B978-0-12-397169-2.00098-6.

Rua, R., and McGavern, D. B. (2018). Advances in Meningeal Immunity. *Trends Mol. Med.* 24, 542–559. doi:10.1016/j.molmed.2018.04.003.

Rudel, T., Scheurerpflug, I., and Meyer, T. F. (1995). Neisseria PilC protein identified as type-4 pilus tip-located adhesin. *Nature* 373, 357–359. doi:10.1038/378592a0.

Saliba, A. E., Westermann, A. J., Gorski, S. A., and Vogel, J. (2014). Single-cell RNA-seq: Advances and future challenges. *Nucleic Acids Res.* 42, 8845–8860.

doi:10.1093/nar/gku555.

Sanchez-Ramos, J. R. (2002). Neural cells derived from adult bone marrow and umbilical cord blood. *J. Neurosci. Res.* 69, 880–893. doi:10.1002/jnr.10337.

Saunders, N. R., Habgood, M. D., Møllgård, K., and Dziegielewska, K. M. (2016). The biological significance of brain barrier mechanisms: help or hindrance in drug delivery to the central nervous system? *F1000Research* 5, 313. doi:10.12688/f1000research.7378.1.

Schryvers, A. B., and Stojiljkovic, I. (1999). Iron acquisition systems in the pathogenic Neisseria. *Mol. Microbiol.* 32, 1117–1123. doi:10.1046/j.1365-2958.1999.01411.x.

Schubert-Unkmeir, A. (2017). Molecular mechanisms involved in the interaction of Neisseria meningitidis with cells of the human blood-cerebrospinal fluid barrier. *Pathog. Dis.* 75. doi:10.1093/femspd/ftx023.

Schubert-Unkmeir, A., Konrad, C., Slanina, H., Czapek, F., Hebling, S., and Frosch, M. (2010). Neisseria meningitidis Induces Brain Microvascular Endothelial Cell Detachment from the Matrix and Cleavage of Occludin: A Role for MMP-8. *PLoS Pathog.* 6, e1000874. doi:10.1088/1757-899X/201/1/012018.

Schubert-Unkmeir, A., Slanina, H., and Frosch, M. (2009). Mammalian cell transcriptome in response to meningitis-causing pathogens. *Expert Rev. Mol. Diagn.* 9, 833–842. doi:10.1586/erm.09.68.

Schubert-Unkmeir, A., Sokolova, O., Panzner, U., Eigenthaler, M., and Frosch, M. (2007). Gene expression pattern in human brain endothelial cells in response to Neisseria meningitidis. *Infect. Immun.* 75, 899–914. doi:10.1128/IAI.01508-06.

Schweitzer, K. M., Vicart, P., Delouis, C., Paulin, D., Drager, A. M., Langenhuijsen, M. M., et al. (1997). Characterization of a newly established human bone marrow endothelial cell line: distinct adhesive properties for hematopoietic progenitors compared with human umbilical vein endothelial cells. *Lab. Investig.* 76, 25–36.

Sedlakova, R., Shivers, R., and Del Maestro, R. (1999). Ultrastructure of the blood-brain barrier in the rabbit. *J Submicrosc Cytol Pathol.* 31, 149–161.

Segal, E., Hagblom, P., Seifert, H. S., and So, M. (1986). Antigenic variation of gonococcal pilus involves assembly of separated silent gene segments. *Proc. Natl. Acad. Sci. U. S. A.* 83, 2177–81.

Seifert, H. S., Ajioka, R. S., Marchal, C., Sparling, P. F., and So, M. (1988). DNA transformation leads to pilin antigenic variation in Neisseria gonorrhoeae. *Nature* 336, 392–395. doi:10.1038/336392a0.

Serruto, D., Bottomley, M. J., Ram, S., Giuliani, M. M., and Rappuoli, R. (2012a). The new multicomponent vaccine against meningococcal serogroup B, 4CMenB: Immunological, functional and structural characterization of the antigens. *Vaccine* 30, B87–B97. doi:10.1016/j.vaccine.2012.01.033.

Serruto, D., Bottomley, M. J., Ram, S., Giuliani, M. M., and Rappuoli, R. (2012b). The new multicomponent vaccine against meningococcal serogroup B, 4CMenB: Immunological, functional and structural characterization of the antigens. *Vaccine* 30, B87–B97.

doi:10.1016/j.vaccine.2012.01.033.

Sharma, A., Marceau, C., Hamaguchi, R., Burridge, P. W., Rajarajan, K., Churko, J. M., et al. (2014). Human induced pluripotent stem cell-derived cardiomyocytes as an in vitro model for coxsackievirus B3-induced myocarditis and antiviral drug screening platform. *Circ. Res.* 115, 556–566. doi:10.1161/CIRCRESAHA.115.303810.

Shukaliak, J. A., and Dorovini-Zis, K. (2000). Expression of the β-chemokines RANTES and MIP-1β by human brain microvessel endothelial cells in primary culture. *J. Neuropathol. Exp. Neurol.* 59, 339–352. doi:10.1093/jnen/59.5.339.

Simonis, A., Hebling, S., Gulbins, E., Schneider-Schaulies, S., and Schubert-Unkmeir, A. (2014). Differential Activation of Acid Sphingomyelinase and Ceramide Release Determines Invasiveness of Neisseria meningitidis into Brain Endothelial Cells. *PLoS Pathog.* 10, e1004160. doi:10.1371/journal.ppat.1004160.

Slanina, H., Hebling, S., Hauck, C. R., and Schubert-Unkmeir, A. (2012). Cell invasion by neisseria meningitidis requires a functional interplay between the focal adhesion kinase, Src and cortactin. *PLoS One* 7, e39613. doi:10.1371/journal.pone.0039613.

Sosa-Hernández, J. E., Villalba-Rodríguez, A. M., Romero-Castillo, K. D., Aguilar-Aguila-Isaías, M. A., García-Reyes, I. E., Hernández-Antonio, A., et al. (2018). Organs-on-a-Chip Module: A Review from the Development and Applications Perspective. *Micromachines* 9, 536. doi:10.3390/mi9100536.

Sprenger, H., Rösler, A., Tonn, P., Braune, H. J., Huffmann, G., and Gemsa, D. (1996). Chemokines in the cerebrospinal fluid of patients with meningitis. *Clin. Immunol. Immunopathol.* 80, 155–161. doi:10.1006/clin.1996.0109.

Sprong, T., Stikkelbroeck, N., van der Ley, P., Steeghs, L., van Alphen, L., Klein, N., et al. (2001). Contributions of Neisseria meningitidis LPS and non-LPS to proinflammatory cytokine response. *J. Leukoc. Biol.* 70, 283–288. Available at: http://www.ncbi.nlm.nih.gov/pubmed/11493621.

Stebbins, M. J., Wilson, H. K., Canfield, S. G., Qian, T., Palecek, S. P., and Shusta, E. V. (2016). Differentiation and characterization of human pluripotent stem cell-derived brain microvascular endothelial cells. *Methods* 101, 93–102. doi:10.1016/j.ymeth.2015.10.016.

Stenman, J., Rajagopal, J., Carroll, T., Ishibashi, M., Mcmahon, J., and Mcmahon, A. P. (2008). Canonical Wnt signaling regulates organ-specific assembly and differentiation of CNS vasculature. *Science* 322, 1247–1250.

Stephens, D., LH, H., and ZA, M. (1983). Interaction of Neisseria meningitidis with human nasopharyngeal mucosa: attachment and entry into columnar epithelial cells. *J Infect Dis.* 148, 369–376.

Stern, A., Brown, M., Nickel, P., and Meyer, T. F. (1986). Opacity genes in Neisseria gonorrhoeae: Control of phase and antigenic variation. *Cell* 47, 61–71. doi:10.1016/0092-8674(86)90366-1.

Stern, A., and Meyer, T. F. (1987). Common mechanism controlling phase and antigenic variation in pathogenic Neisseriae. *Mol. Microbiol.* 1, 5–12. doi:10.1111/j.1365-

2958.1987.tb00520.x.

Stern, L., and Gautier, R. (1921). Recherches sur le liquide céphalo-rachidien. 1. Les rapports entre le liquide céphalo-rachidien et la circulation sanguine. *Arch Int Physiol.* 17, 138–192.

Stins, M. F., Badger, J., and Sik Kim, K. (2001). Bacterial invasion and transcytosis in transfected human brain microvascular endothelial cells. *Microb. Pathog.* 30, 19–28. doi:10.1006/mpat.2000.0406.

Stins, M. F., Gilles, F., and Kim, K. S. (1997). Selective expression of adhesion molecules on human brain microvascular endothelial cells. *J. Neuroimmunol.* 76, 81–90. doi:10.1016/S0165-5728(97)00036-2.

Suh, W. (2017). A new era of disease modeling and drug discovery using induced pluripotent stem cells. *Arch. Pharm. Res.* 40. doi:10.1007/s12272-016-0871-0.

Sutherland, T. C., Quattroni, P., Exley, R. M., and Tang, C. M. (2010). Transcellular passage of Neisseria meningitidis across a polarized respiratory epithelium. *Infect. Immun.* 78, 3832–3847. doi:10.1128/IAI.01377-09.

Taha, M. K. (2000). Neisseria meningitidis induces the expression of the TNF-α gene in endothelial cells. *Cytokine* 12, 21–25. doi:10.1006/cyto.1999.0506.

Taha, M. K., Morand, P. C., Pereira, Y., Eugène, E., Giorgini, D., Larribe, M., et al. (1998). Pilus-mediated adhesion of Neisseria meningitidis: The essential role of cell contact-dependent transcriptional upregulation of the PilC1 protein. *Mol. Microbiol.* 28, 1153–1163. doi:10.1046/j.1365-2958.1998.00876.x.

Tang, T., Frenette, P. S., Hynes, R. O., Wagner, D. D., and Mayadas, T. N. (1996). Cytokine-induced meningitis is dramatically attenuated in mice deficient in endothelial selectins. *J. Clin. Invest.* 97, 2485–2490. doi:10.1172/JCI118695.

Tettelin, H., Saunders, N. J., Heidelberg, J., Jeffries, A. C., Karen, E., Eisen, J. A., et al. (2000). Complete genome sequence of Neisseria meningitidis serogroup B strain MC58. *Science* 287, 1809–1815.

Textoris, J., Beaufils, N., Quintana, G., Lassoud, A. B., Zieleskiewicz, L., Wiramus, S., et al. (2012). Hypoxia-inducible factor (HIF1α) gene expression in human shock states. *Crit. Care* 16, R120. doi:10.1186/cc11414.

Thair, S. A., Topchiy, E., Boyd, J. H., Cirstea, M., Wang, C., Nakada, T. A., et al. (2016). TNFAIP2 Inhibits Early TNFα-Induced NF-κB Signaling and Decreases Survival in Septic Shock Patients. *J. Innate Immun.* 8, 57–66. doi:10.1159/000437330.

Till, A., Rosenstiel, P., Bräutigam, K., Sina, C., Jacobs, G., Oberg, H.-H., et al. (2008). A role for membrane-bound CD147 in NOD2-mediated recognition of bacterial cytoinvasion. *J. Cell Sci.* 121, 487–495. doi:10.1242/jcs.016980.

Tsuji, A., Terasaki, T., Takabatake, Y., Tenda, Y., Tamai, I., Yamashima, T., et al. (1992). P-glycoprotein as the drug efflux pump in primary cultured bovine brain capillary endothelial cells. *Life Sci.* 51, 1427–1437. doi:10.1016/0024-3205(92)90537-Y.

Tunkel, A. R., and Scheld, W. M. (1993). Pathogenesis and pathophysiology of bacterial

meningitis. *Clin. Microbiol. Rev.* 6, 118–136. doi:10.1128/CMR.6.2.118.

Unkmeir, A., Latsch, K., Dietrich, G., Wintermeyer, E., Schinke, B., Schwender, S., et al. (2002). Fibronectin mediates Opc-dependent internalization of Neisseria meningitidis in human brain microvascular endothelial cells. *Mol. Microbiol.* 46, 933–946. doi:10.1046/j.1365-2958.2002.03222.x.

Uruno, T., Liu, J., Zhang, P., Fan, Y., Egile, C., Li, R., et al. (2001). Mediated Actin Polymerization By Cortactin. *Nat. Cell Biol.* 3, 259–266.

Vadeboncoeur, N., Segura, M., Al-Numani, D., Vanier, G., and Gottschalk, M. (2003). Pro-inflammatory cytokine and chemokine release by human brain microvascular endothelial cells stimulated by Streptococcus suis serotype 2. *FEMS Immunol. Med. Microbiol.* 35, 49–58. doi:10.1016/S0928-8244(02)00440-6.

van de Beek, D., de Gans, J., Tunkel, A., and Wijdicks, E. (2006). Community-Acquired Bacterial Meningitis in Adults. *N Engl J Med.* 354, 44–53. doi:10.1056/NEJMra052116.

Van Deuren, M., Brandtzaeg, P., and Van Der Meer, J. W. M. (2000). Update on meningococcal disease with emphasis on pathogenesis and clinical management. *Clin. Microbiol. Rev.* 13, 144–166. doi:10.1128/CMR.13.1.144-166.2000.

van Neerven, S., Nemes, A., Imholz, P., Regen, T., Denecke, B., Johann, S., et al. (2010). Inflammatory cytokine release of astrocytes in vitro is reduced by all-trans retinoic acid. *J. Neuroimmunol.* 229, 169–179. doi:10.1016/j.jneuroim.2010.08.005.

van Sorge, N. M., and Doran, K. S. (2012). Defense at the border: the blood–brain barrier versus bacterial foreigners. *Futur. Microbiol.* 7, 383–394. doi:10.2217/fmb.12.1.Defense.

Van Sorge, N. M., Zialcita, P. A., Browne, S. H., Quach, D., Guiney, D. G., and Doran, K. S. (2011). Penetration and activation of brain endothelium by Salmonella enterica serovar typhimurium. *J. Infect. Dis.* 203, 401–405. doi:10.1093/infdis/jiq048.

Vanarsdall, A. L., Pritchard, S. R., Wisner, T. W., Liu, J., Jardetzky, T. S., and Johnson, D. C. (2018). CD147 Promotes Entry of Pentamer-Expressing Human Cytomegalovirus into Epithelial and Endothelial Cells. *MBio* 9, e00781-18. doi:10.1128/mbio.00781-18.

Vatine, G. D., Al-Ahmad, A., Barriga, B. K., Svendsen, S., Salim, A., Garcia, L., et al. (2017). Modeling Psychomotor Retardation using iPSCs from MCT8-Deficient Patients Indicates a Prominent Role for the Blood-Brain Barrier. *Cell Stem Cell* 20, 831-843.e5. doi:10.1016/j.stem.2017.04.002.

Verma, S., Nakaoke, R., Dohgu, S., and Banks, W. A. (2006). Release of cytokines by brain endothelial cells: A polarized response to lipopolysaccharide. *Brain. Behav. Immun.* 20, 449–455. doi:10.1016/j.bbi.2005.10.005.

Vieusseux, M. (1805). Mémoire sur la maladie qui a regné a Genêve au printemps de 1805. *J Med Chir Pharmacol* 11, 163–182.

Virji, M. (2009). Pathogenic neisseriae: Surface modulation, pathogenesis and infection control. *Nat. Rev. Microbiol.* 7, 274–286. doi:10.1038/nrmicro2097.

Virji, M., Makepeace, K., Ferguson, D. J. P., Achtman, M., and Moxon, E. R. (1993).

Meningococcal Opa and Opc proteins: their role in colonization and invasion of human epithelial and endothelial cells. *Mol. Microbiol.* 10, 499–510. doi:10.1111/j.1365-2958.1993.tb00922.x.

Vogel, U., and Frosch, M. (1999). Mechanisms of neisserial serum resistance. *Mol. Microbiol.* 32, 1133–1139. doi:10.1046/j.1365-2958.1999.01469.x.

Watanabe, A., Yoneda, M., Ikeda, F., Terao-Muto, Y., Sato, H., and Kai, C. (2010). CD147/EMMPRIN Acts as a Functional Entry Receptor for Measles Virus on Epithelial Cells. *J. Virol.* 84, 4183–4193. doi:10.1128/jvi.02168-09.

Wei, Y.-P., Kita, M., Shinmura, K., Yan, X.-Q., Fukuyama, R., Fushiki, S., et al. (2002). Expression of IFN-gamma in Cerebrovascular Endothelial Cells from Aged Mice. *J. Interf. Cytokine Res.* 20, 403–409. doi:10.1089/107999000312342.

Weichselbaum, A. (1887). Ueber die Aetiologie der akuten Meningitis cerebrospinalis. *Fortschr Med* 5, 573–583.

Weiss, N., Miller, F., Cazaubon, S., and Couraud, P. O. (2009). The blood-brain barrier in brain homeostasis and neurological diseases. *Biochim. Biophys. Acta - Biomembr.* 1788, 842–857. doi:10.1016/j.bbamem.2008.10.022.

Weksler, B. B., Subileau, E. A., Perrière, N., Charneau, P., Holloway, K., Leveque, M., et al. (2005). Blood-brain barrier-specific properties of a human adult brain endothelial cell line. *FASEB J.* 19. doi:10.1096/fj.04-3458fje.

Weller, R. O., Sharp, M. M., Christodoulides, M., Carare, R. O., and Møllgård, K. (2018). The meninges as barriers and facilitators for the movement of fluid, cells and pathogens related to the rodent and human CNS. *Acta Neuropathol.* 135, 363–385. doi:10.1007/s00401-018-1809-z.

Welsch, J. A., and Ram, S. (2008). Factor H and Neisserial pathogenesis. *Vaccine* 26, 40–45. doi:10.1016/j.vaccine.2008.11.060.

Werth, N., Beerlage, C., Rosenberger, C., Yazdi, A. S., Edelmann, M., Amr, A., et al. (2010). Activation of hypoxia inducible factor 1 is a general phenomenon in infections with human pathogens. *PLoS One* 5. doi:10.1371/journal.pone.0011576.

West, S. E. H., and Sparling, P. F. (1985). Response of Neisseria gonorrhoeae to iron limitation: Alterations in expression of membrane proteins without apparent siderophore production. *Infect. Immun.* 47, 388–394.

Westermann, A. J., Barquist, L., and Vogel, J. (2017). Resolving host-pathogen interactions by dual RNA-seq. *PLoS Pathog.* 13, e1006033. doi:10.1371/journal.ppat.1006033.

Westermann, A. J., Förstner, K. U., Amman, F., Barquist, L., Chao, Y., Schulte, L. N., et al. (2016). Dual RNA-seq unveils noncoding RNA functions in host-pathogen interactions. *Nature* 529, 496–501. doi:10.1038/nature16547.

Wilson, H. K., Canfield, S. G., Hjortness, M. K., Palecek, S. P., and Shusta, E. V. (2015). Exploring the effects of cell seeding density on the differentiation of human pluripotent stem cells to brain microvascular endothelial cells. *Fluids Barriers CNS* 12, 1–12. doi:10.1186/s12987-015-0007-9.

Wise, K. (2006). Preparing Spread Plates Protocols. *Am. Soc. Microbiol. Microbe Libr.*

Wolfgang, M., Park, H.-S., Hayes, S. F., van Putten, J. P. M., and Koomey, M. (1998). Suppression of an absolute defect in Type IV pilus biogenesis by loss-of-function mutations in pilT, a twitching motility gene in Neisseria gonorrhoeae. *Proc. Natl. Acad. Sci.* 95, 14973–14978. doi:10.1073/pnas.95.25.14973.

Wolfgang, M., Van Putten, J. P. M., Hayes, S. F., and Koomey, M. (1999). The comP locus of Neisseria gonorrhoeae encodes a type IV prepilin that is dispensable for pilus biogenesis but essential for natural transformation. *Mol. Microbiol.* 31, 1345–1357. doi:10.1046/j.1365-2958.1999.01269.x.

Yang, R. C., Liu, W. T., Miao, L., Yang, X. P., Fu, J. Y., Dou, B. B., et al. (2016). Induction of VEGFA and Snail-1 by meningitic Escherichia coli mediates disruption of the blood-brain barrier. *Oncotarget* 7, 63839–63855. doi:10.18632/oncotarget.11696.

Yasukawa, K., Martin, P., Tinsley, C. R., and Nassif, X. (2006). Pilus-mediated adhesion of Neisseria meningitidis is negatively controlled by the pilus-retraction machinery. *Mol. Microbiol.* 59, 579–589. doi:10.1111/j.1365-2958.2005.04954.x.

Yeung, A. T. Y., Hale, C., Lee, A. H., Gill, E. E., Bushell, W., Parry-Smith, D., et al. (2017). Exploiting induced pluripotent stem cell-derived macrophages to unravel host factors influencing Chlamydia trachomatis pathogenesis. *Nat. Commun.* 8, 1–12. doi:10.1038/ncomms15013.

Yu, J., Vodyanik, M. A., Smuga-Otto, K., Antosiewicz-Bourget, J., Frane, J. L., Tian, S., et al. (2007). Induced Pluripotent Stem Cell Lines Derived from Human Somatic Cells. *Science* 318, 1917–1920. doi:10.1126/science.1151526.

Zhang, Y., Han, H., Elmquist, W. F., and Miller, D. W. (2000). Expression of various multidrug resistance-associated protein (MRP) homologues in brain microvessel endothelial cells. *Brain Res.* 876, 148–153. doi:10.1016/S0006-8993(00)02628-7.

Zhu, P., Morelli, G., and Achtman, M. (1999). The opcA and ψopcB regions in Neisseria: Genes, pseudogenes, deletions, insertion elements and DNA islands. *Mol. Microbiol.* 33, 635–650. doi:10.1046/j.1365-2958.1999.01514.x.

Zovein, A. C., Luque, A., Turlo, K. A., Hofmann, J. J., Yee, K. M., Becker, M. S., et al. (2010). β1 Integrin Establishes Endothelial Cell Polarity and Arteriolar Lumen Formation via a Par3-Dependent Mechanism. *Dev. Cell* 18, 39–51. doi:10.1016/j.devcel.2009.12.006.

Appendix

Appendix

Acknowledgments

I would like to thank the supervisors of this project, Prof. Dr. Alexandra Schubert-Unkmeir, Dr. Brandon Kim, Dr. rer. nat. Antje Appelt-Menzel and PD Dr. Marco Metzger, for all the guidance and mentorship. Additionally, I thank Prof. Dr. Thomas Rudel and Prof. Dr. Heike Walles for gathering the funding for the Research Training Group 2157 (3D Tissue Models for Studying Microbial Infections by Human Pathogens) that made this collaboration and project possible.

I am thankful to the members of my Thesis Committee, Prof. Dr. Roy Gross, Dr. Maria Steinke and Dr. rer. nat. Kay Johswich, for being available to discuss the data since the beginning of the project and for their helpful input during our meetings.

I thank the iPSC lab (Chair Tissue Engineering and Regenerative Medicine, University Hospital Würzburg), especially Alevtina Cubukova and Sophia Wilhelm, for all their technical assistance with cell culture during the first 2 years of the project. Additionally, I thank Jun. Prof. Dr. Alexander Westermann and Till Sauerwein for their work and assistance with the RNA-Seq data, and Dr. Nora Müller for her help with confocal microscopy.

I am grateful to have been part of a PhD Program with such an amazing network of international students, and I am glad to have met my colleagues, especially Maria V. (Mavi), Sara S., David K., Tao, Manli, and Mota. A special hug to my office buddy Saskia. Thanks for all the good times we shared!

I thank the Graduate School of Life Sciences (GSLS) of the University of Würzburg, in particular Gabriele, for being helpful and supportive, and for contributing to the development of the student´s careers by providing valuable workshops and travel awards.

Thank you to my family, especially my brother who was always there for me, giving support, advice, and (tough) love throughout this rollercoaster ride.

Thank you to Adam for everything!!

Affidativ/ Eidesstattliche Erklärung

Affidavit

I hereby declare that my thesis entitled: "Induced Pluripotent Stem Cell-derived Brain Endothelial Cells as a Cellular Model to Study *Neisseria meningitidis* Infection" is the result of my own work. I did not receive any help or support from commercial consultants. All sources and/or materials applied are listed and specified in the thesis.

Furthermore I verify that the thesis has not been submitted as part of another examination process neither in identical nor in similar form.

Würzburg, **Signature**

Eidesstattliche Erklärung

Hiermit erkläre ich an Eides statt, die Dissertation: "Induzierte pluripotente Stammzellen- basierte Hirnendothelzellen als zelluläres Modell zur Untersuchung der Infektion mit *Neisseria meningitidis*", eigenständig, d. h. insbesondere selbständig und ohne Hilfe eines kommerziellen Promotionsberaters, angefertigt und keine anderen, als die von mir angegebenen Quellen und Hilfsmittel verwendet zu haben.
Ich erkläre außerdem, dass die Dissertation weder in gleicher noch in ähnlicher Form bereits in einem anderen Prüfungsverfahren vorgelegen hat.

Würzburg, **Unterschrift**